The Impact of Supermassive Black Hole Feedback on Star Formation in Galaxies

by

Bryan Alejandro Terrazas

A dissertation submitted in partial fulfillment
of the requirements for the degree of
Doctor of Philosophy
(Astronomy and Astrophysics)
in The University of Michigan
2019

Doctoral Committee:

Professor Eric F. Bell, Chair
Professor August E. Evrard
Associate Professor Elena Gallo
Assistant Professor Kayhan Gültekin
Associate Professor Brian W. O'Shea
Professor Rachel S. Somerville

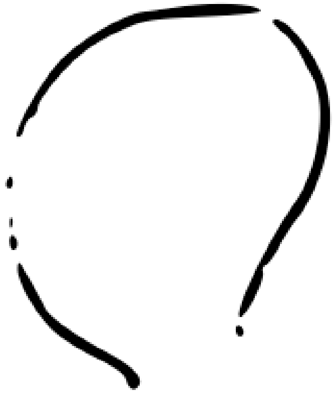

Henri Matisse

Bryan Alejandro Terrazas

bterraza@umich.edu

ORCID iD: 0000-0001-5529-7305

Dedico esta obra a mis padres.

ACKNOWLEDGEMENTS

I acknowledge that the work described in this dissertation has been done on the traditional territory of the Ojibwe, Odawa, and Bodéwadmi, and more recently the Potawatomi, Miami, and Wendat Nations. We must be mindful of our present participation in the ongoing occupation of these lands and advocate for Indigenous sovereignty whenever possible.

This dissertation and the degree that accompanies it would have been incredibly difficult without the love and support of various people in my life. I would first and foremost like to thank my parents. From buying me my first astronomy-related books and magazines in elementary school to traveling to Ann Arbor for the second time in a month to attend my defense, your constant support throughout the years has been incredible. This dissertation, my degrees, and all that I have accomplished - son tuyos también, because the love you've shown me has motivated me every step of the way. Even apart from astronomy, you have always been cheering me on whether it had to do with music, school, or my personal life. No hay palabras para describir mi agradecimiento a ustedes. Te amo con todo mi alma, gracias por todo lo que han hecho y sacrificado para darme esta vida.

I would also like to thank all the friends I met in Ann Arbor. Moving from New York City to a college town in Michigan was incredibly difficult for me during my first couple of years. The people I met here have meant the world to me and have helped make Ann Arbor a very special place. It took a few years for this sentiment to build up so I'd like to extend a special thank you to Jordan Fricks who went through the very first part of this transition with me during my first few years here.

I'd also like to extend an enormous thank you to Taïna Jean-Louis. The friendship and love we built throughout the last half of my time in Michigan has been one of the most special and unique connections I've ever made. Together we helped each other learn about life, self-care, self-awareness, how to be a good friend, and so much more. I'm incredibly happy we met and were able to connect on such a beautiful level. I will never forget the time we spent together not only in Ann Arbor but also in Paris, Chicago, Toronto, New York, Virginia/DC, and the cornfields of Illinois on our way to and from Carbondale. Also, thank you for your help with that coding problem where I mistakenly indexed with i twice!

I also want to thank Kenzo Esquivel who I met relatively recently yet has become one of my closest friends. Thank you for sitting through disastrous practice runs for talks late at night, for being present when I felt hopeless about my progress in research, and for motivating me to take care of myself when stressing out about grad school. Your friendship has made my last two years in Ann Arbor incredibly special. Also, thank you for pushing me to become a better cook, go to the gym more often, enjoy outdoor activities, and listen to more Ariana Grande.

I'd also like to give a special thank you to all the graduate students I met in the astronomy program at Michigan. From the senior students who graduated shortly after I started to the current first year cohort, so many of you have been wonderful friends and colleagues. Thank you for making the space within astronomy so special. A particularly special thank you goes out to two members of my cohort: Tom Rice and Alejo Stark. We went through so much together, especially during those first two years of classes. Both of you have shaped my entire graduate school experience. We became incredibly close through it all and the resulting friendships we built have and always will hold a special place in my heart.

I also want to thank the historically marginalized and underrepresented people who are or have ever been a part of the astronomy community. Your struggles through this historically and predominantly white, patriarchal, and heterocentric space has paved the way for people like me to be able to learn about the universe.

Throughout the last four years, my dissertation committee members have been incredible mentors. I want to extend a warm thank you to Gus, Elena, Kayhan, Brian, and Rachel for providing immense support for me during my candidacy. Your guidance and feedback with regards to my progress throughout my studies have been incredibly helpful.

Finally, I would like to thank my advisor, Eric Bell. You have been the most important part of my graduate school experience. Your support as an advisor and mentor has been instrumental in building my identity as a scientist during these past six years. Your office has been a safe space for me during the toughest of times in graduate school. Being able to talk and work through problems that I encountered throughout my time here has been incredibly important for learning how to navigate and succeed in academia. Thank you for your investment in my success, for treating me with respect, for your guidance, and for your kindness.

Your office was also a space where the ideas detailed in this dissertation flourished. The frontispiece of this dissertation is a collection of four line drawings by Henri Matisse. There was an exhibition on Matisse's line drawings at the University of Michigan Museum of Art a few years back that I visited a number of times before the exhibition was eventually closed. I was fascinated by the way a few simple lines could be combined to form a complex representation of a scene. Our approach to science these past six years has focused on taking the incredibly complex phenomena involved in galaxy formation and evolution and trying to distill it into its most understandable and intuitive form. These line drawings are no more than one to five lines, and yet the human mind interprets them to represent dance, body, and movement. They are distilled representations of complex phenomena and yet they are a few lines on a page drawn in rapid succession. Despite this, Matisse's incredible artistic ability was absolutely essential in the creation of these line drawings. In his words, "It is in order to liberate grace and character that I study so intensely before making a pen drawing." Our collaboration has aimed at forming and communicating a simple and intuitive way of thinking about galaxies. This is only possible after digging through and understanding the immense complexities of galaxy formation in order to illuminate its foundational physical drivers. I believe this is an immensely powerful approach that we have taken and, while it has its limitations, it has shaped the way I think about and do science. Thank you for your guidance in my exploration of galaxy evolution, thank you for working with me to liberate the grace and character that emerges from that exploration, and thank you for your advice and mentorship during these past six years. I look forward to seeing what we can do in the future.

TABLE OF CONTENTS

CHAPTER

LIST OF FIGURES

Figure

ABSTRACT

Observations have revealed the significant growth of a population of 'quiescent' galaxies with reduced star formation activity since z $\sim$ 2. Mounting evidence from across the electromagnetic spectrum indicates that supermassive black hole feedback plays a critical role in suppressing the ability of gas to cool and condense to form fuel for star formation in massive galaxies. However, the link between the galaxy-scale suppression of star formation and relatively small-scale black hole physics is not well understood. In order to explore this link, my dissertation work focuses on the question: *How can observable correlations between black holes and the properties of their host galaxies reveal the underlying mechanism behind quiescence?* In my work, I find that the latest version of the L-Galaxies semi-analytic model features a black hole mass threshold above which galaxies are quiescent due to the heating rate from black hole feedback overcoming the cooling rate of the gaseous atmosphere (Terrazas et al., 2016a). I find similar behavior in the real universe using a diverse sample of 91 local galaxies with dynamical black hole masses (Terrazas et al., 2016b, 2017). In particular, galaxies with more massive black holes at a given stellar mass exhibit progressively less star formation. Using five galaxy formation models, I find that variations between implementations of black hole growth, accretion physics, and feedback prescriptions predict systematically different joint distributions of stellar mass, black hole mass, and star formation rate. Only models that continuously suppress the cooling of gas onto the galaxy via low accretion rate black hole feedback are able to qualitatively reproduce the trends seen in the observations at z = 0. When quantitatively comparing the distributions of stellar mass, black hole mass, and star formation rate, none of the models agree with one another or with the observations. This largely results from differences in how black hole feedback affects gas as well as differences in how black hole and stellar mass couple to one another. These results indicate the importance of taking into account the scattered relationship between black hole and stellar mass and its dependence on star formation activity in order to adequately model black holes and the relationship to their host galaxies.

CHAPTER I

Introduction

1.1 Towards a statistical understanding of galaxy populations

The birth of extragalactic astronomy began in the 1910s, when astronomers were actively debating whether spiral 'nebulae' resided within or outside of our own Milky Way Galaxy (Crommelin, 1918; Shapley, 1919; Curtis, 1920; Shapley & Curtis, 1921). Using the fact that Cepheid variable stars could be used as distance estimators (Leavitt, 1908; Leavitt & Pickering, 1912), M31 and M33 were measured to be several times farther than the furthest galactic star (Hubble, 1925). Shortly after, distances to other 'nebulae' were similarly measured and the existence of external galaxies revolutionized the field of astronomy.

Since their discovery, a major goal of extragalactic astronomy has been to statistically characterize the population of galaxies. One early approach was to characterize the shapes of galaxies across a sequence from early-type, elliptical galaxies to late-type, spiral galaxies (Hubble, 1926). Another fundamental and more quantitative approach was to count the number of galaxies as a function of their luminosity in a particular wavelength band (Hubble, 1936; Zwicky, 1948). This was important not only for understanding the characteristics of galaxies, but also for understanding cosmology by quantifying the distribution of matter in the universe. The first modern measurements of luminosity functions contained ∼200 galaxies (van den Bergh, 1961; Kiang, 1961; Arakelyan & Kalloglyan, 1970; Shapiro, 1971; Huchra & Sargent, 1973; Christensen, 1975; Schechter, 1976; Gott & Turner, 1976). These seminal works established that faint galaxies are much more numerous than the brightest galaxies, whose numbers decrease exponentially with brightness.

Since then, major advances have been made through the efforts of surveys where photometric and/or spectroscopic observations are obtained for hundreds of thousands of galaxies (e.g., CFRS: Lilly et al., 1995, SDSS: York et al., 2000; 2dFGRS: Colless et al., 2001; 6dFGS: Jones et al., 2004; GALEX: Martin et al., 2005; 2MASS: Skrutskie et al., 2006; UKIDSS: Dye et al., 2006; COSMOS: Scoville et al., 2007; GAMA: Driver et al., 2009; CANDELS: Koekemoer et al., 2011; Grogin et al., 2011; UltraVISTA: McCracken et al., 2012, DEEP2: Newman et al., 2013). The increasing sensitivity of telescopes and detectors have also allowed for the characterization of galaxies at progressively higher redshifts. The collection of data for galaxies at different epochs presents the opportunity for understanding galaxy evolution throughout the history of the universe by studying the differences between these populations.

In addition to technological improvements, advancements have also been made for translating observed measurements into more physically meaningful quantities. For example, stellar masses were derived from photometric or spectroscopic measurements using either a constant or varying mass-to-light ratio or stellar population synthesis models (e.g., Rix & Rieke, 1993; Brinchmann & Ellis, 2000; Bell & de Jong, 2001; Blanton & Roweis, 2007). Thus, luminosity functions could be turned into stellar mass functions (Cole et al., 2001; Bell et al., 2003; Li & White, 2009; Marchesini et al., 2009; Ilbert et al., 2010; Mortlock et al., 2011; Ilbert et al., 2013; Muzzin et al., 2013; Moustakas et al., 2013; Tomczak et al., 2014), which became a key diagnostic tool for understanding galaxy formation in terms of stellar mass assembly.

Another physically meaningful quantity is star formation rate, the first calculations of which came from advances in star formation theory in the local volume within the Milky Way (Schmidt, 1959). Theoretical calculations of the evolution of stellar populations found that the colors of galaxies should correlate with star formation rate (Tinsley, 1968; Searle et al., 1973; Larson & Tinsley, 1978). These studies found important differences in star formation histories as a function of galaxy type. Since then, measurements across the electromagnetic spectrum have been calibrated and used as star formation rate indicators (for reviews, see Kennicutt, 1998; Kennicutt & Evans, 2012).

Today, it is well established that galaxies are bimodal in their colors (Strateva et al., 2001; Kauffmann et al., 2003), indicating major differences in the star formation properties of galaxies. The population of brighter, more massive, and less numerous galaxies have redder colors and therefore less star formation activity on average. Studies of the evolution in the number density of these 'quiescent' galaxies - i.e., galaxies exhibiting reduced amounts of star formation - show a pronounced growth from the early universe to the present day (e.g., Bell et al., 2004; Brown et al., 2007; Muzzin et al., 2013; Mortlock et al., 2015). Current estimates state that quiescent galaxies constitute $\sim$50% of the $z = 0$ mass density, declining steadily to $\lesssim$10% at $z \gtrsim 2$ (Lapi et al., 2017).

While it is impossible for humans to observe the changes individual galaxies undergo throughout their lifetimes across billions of years, several attempts have been made to link galaxy populations at different redshifts and infer their evolutionary pathways. Some of the first attempts of this exercise used galaxy scaling relations (e.g., the color-magnitude relation, fundamental plane, mass-color-size relation, etc.) to infer changes in galaxy properties through cosmic time (van Dokkum & Franx, 1996; Gladders et al., 1998; Stanford et al., 1998; Holden et al., 2004; Franx et al., 2008b). Recently, several studies have assumed a constant (e.g., van Dokkum et al., 2010, 2013) or evolving (e.g., Torrey et al., 2015) spatial number density for a given population of galaxies to trace their evolution. All of these studies largely support the idea that massive quiescent galaxies were once actively star-forming at earlier epochs and at some point in time became passively evolving with little continuing star formation. Determining the physical processes necessary for galaxies to become quiescent and produce the observed demographics of the galaxy population has become a central goal of modern extragalactic astronomy.

1.2 The physics of galactic quiescence

In order to understand how quiescence may occur within the galaxy population, it is important to outline the cosmological context within which galaxies form and evolve (White & Rees, 1978; White & Frenk, 1991). Within the cold dark matter (CDM) paradigm (for a review, see Blumenthal et al., 1984), small primordial perturbations in the density of matter in the early universe grew hierarchically to form gravitationally bound structures (e.g., Peebles, 1982). The majority of the matter content in the universe and thus of these structures was in the form of CDM, a type of matter that was first detected indirectly through its gravitational interactions with matter made up of atoms, i.e. baryons (Zwicky, 1933; Rubin et al., 1978, 1980). Baryonic matter concurrently fell into the gravitational potential wells of dark matter halos as they grew. Dissipative processes caused baryonic material in the form of gas to lose energy and cool (Silk, 1977; Rees & Ostriker, 1977; Binney, 1977) while largely conserving angular momentum. These cooling processes formed disks of cold gas at the centers of large, extended dark matter halos (Fall & Efstathiou, 1980). Instabilities in the gas as it cooled cause fragmentation into dense clumps and cores (Toomre, 1964) that eventually formed stars, allowing galaxies to grow and evolve.

Thus, the natural tendency for matter to seek a lower energy state within this cosmological context drives the formation of galaxies via gas cooling and subsequent star formation. The growth of a population of galaxies exhibiting quiescence, or a state of reduced or absent star formation activity in galaxies, indicates that there are other physical processes at work that either deplete the amount of cold gas available or prevent the cooling and collapse of gas into star forming regions.

One important factor in exploring possible physical mechanisms for quiescence relies on the fact that the hierarchical growth of structures predicts the merging of both dark matter halos and the galaxies within them. Halo merging does not necessarily result in the merging of galaxies, since smaller halos are able to live within larger ones to create substructure (Bond et al., 1991; Bower, 1991; Moore et al., 1999). As such, galaxies can be classified as central and satellite galaxies, where satellites belong to 'subhalos' that have fallen into the potential well of a larger halo with its own central galaxy. Satellites are observed to have redder colors, early-type morphologies, and less star formation (Oemler, 1974; Dressler, 1980; Balogh et al., 1997; Baldry et al., 2006). Due to their positions within larger halos, there are various environmental processes that are thought to deplete or remove cold gas, such as ram pressure forces (Gunn & Gott, 1972) or tidal interactions (Icke, 1985).

When galaxies do merge as a result of hierarchical assembly, the stellar and gaseous structures of galaxies can be significantly affected. Observations of irregular galaxy morphologies (Hubble, 1926) were eventually understood to be a result of galaxy merging (Toomre & Toomre, 1972; Ostriker & Tremaine, 1975; White, 1983). Mergers are thought to disrupt disk-like morphologies, producing tails and shells of tidal debris and eventually contributing to the formation of the spheroidal components of galaxies (e.g., Toomre, 1977; Hernquist & Quinn, 1988; Barnes & Hernquist, 1992; Hernquist & Spergel, 1992). These disruptions can also induce star formation (e.g., Joseph & Wright, 1985; Sanders et al., 1988), potentially causing the depletion of star forming gas (e.g., Gao & Solomon, 1999). These studies as well as the correlation between bulge-dominated morphologies and quiescence (e.g., Bell et al., 2012; Bluck et al., 2014b) have led to the idea that merging plays an important role in the growth of the quiescent population.

Another mechanism that might limit star formation comes from star formation itself. Star formation transfers energy into gas, reducing the amount of gas cooling. This feedback energy primarily comes from the stellar winds of massive stars or the deaths of these stars in supernova explosions (McKee & Ostriker, 1977). The energy from this feedback is thought to eject and heat star forming material in the galaxy, thus contributing to quiescence in galaxies (Hoyle et al., 1968; Reddish, 1969; Mathews & Baker, 1971; Sanders, 1981; Tang & Wang, 2005; Conroy et al., 2015).

Some of the first observational evidence of stellar feedback came from observations of radio emission external to galaxies such as the Milky Way, Andromeda, and M33 (Baldwin, 1954, 1955; Brown & Hazard, 1959). One postulation was that radio halos were a consequence of ejective feedback from star formation (Burbidge & Hoyle, 1963). The existence of gas halos was also an indication that primordial gas from the intergalactic medium was continuing to accrete into the dark matter halos that host significantly evolved central galaxies. These first indications of gas existing outside of galactic disks in extended 'coronae' (Spitzer, 1956) were also corroborated by absorption lines in the spectra of quasars that indicated the existence of intervening gas at distances far from the galactic plane of a foreground galaxy (e.g., Bahcall & Spitzer, 1969). Since then, these multiphase gaseous halos have been extensively studied through absorption line studies (e.g., Morris et al., 1993; Lanzetta et al., 1995; Prochaska et al., 2004; Tumlinson et al., 2011; Werk et al., 2014) and, for systems with enough hot gas to be detectable, X-ray imaging (e.g., Gursky et al., 1971; Forman et al., 1972; Lin et al., 2003; Vikhlinin et al., 2006). These lines of evidence strongly suggested that most if not all galaxies host an extended, gas halo, indicating that a complete absence of gas through gas depletion is not an adequate explanation for quiescence.

The existence of a massive gaseous halo makes the production of quiescent galaxies much more difficult. Not only does the mechanism need to prevent the interstellar medium from cooling, but it must also prevent cooling and accretion from the much more massive and extended circumgalactic medium. Thus, a few proposed mechanisms for quiescence become inconceivable for galaxies with gas halos. One such mechanism is morphological quenching, where a disk of gas can be stable against fragmentation into star forming clumps (Martig et al., 2009). The accretion of gas from a halo will inevitably prevent the stability of disks through the buildup of gas.

One proposed mechanism behind quiescence that takes into account the importance of the circumgalactic medium is the decrease in the efficiency of cooling for halo gas within progressively more massive halos (Birnboim & Dekel, 2003; Dekel & Birnboim, 2006; Cattaneo et al., 2006a; Birnboim et al., 2007). The physical basis for this is a change in the accretion mode of gas onto a galaxy's halo from the intergalactic medium. Gas can accrete onto a less massive halo at the free fall time since the virial temperature of the halo will be lower or comparable to the temperature of the gas. If the virial temperature of the halo is higher than the temperature of the gas, as is the case for more massive halos, then accreted gas is shock heated near the virial radius of the halo (Binney, 1977; Rees & Ostriker, 1977; White & Frenk, 1991). This forms a hot gas atmosphere that is less efficient at cooling to provide star forming material to the galaxy. Studies have shown that the halo mass at which cooling becomes less efficient ($\sim 10^{12}$ M$_\odot$) coincides with the stellar mass at which galaxies are predominantly quiescent (Kereš et al., 2005).

All of these proposed mechanisms for inducing quiescence likely occur within galaxies in one form or another, affecting the physics of gas cooling and star formation in galaxies. However, recent studies have argued that many of these cannot adequately suppress star formation to reproduce the quiescent population at stellar masses larger than $\sim 10^{10}$ M$_\odot$ (e.g., Su et al., 2018). For example, stellar feedback serves to regulate the rate of star formation, not suppress it (Cox, 1983; Dopita, 1985; Dutton et al., 2010; Hopkins et al., 2011; Hayward & Hopkins, 2017). This is due to the fact that stellar feedback cannot produce enough energy to evacuate the entire gas halo. Therefore, reaccretion of gas from the circumgalactic medium will provide continued fuel for star formation. Similarly, shock heating of accreted material in massive halos will render cooling onto the galaxy less efficient but it will not suppress it completely. X-ray observations show cooling luminosities around quiescent galaxies that predict much higher levels of cold gas deposition and much bluer colors than are observed (e.g., Fabian et al., 1982; Johnstone et al., 1987; Fabian, 1994; Donahue et al., 2000; Böhringer et al., 2002). This indicates that some form of energetic feedback must be acting to counteract the cooling that is happening in the gas (O'Dea et al., 2004). Finally, while environmental processes that affect satellite galaxies may be efficient at halting star formation, the physics that governs this does not extend to the majority of the high mass systems that exist as central galaxies.

1.3 Feedback from supermassive black holes

One proposed mechanism for quiescence that has received particular attention in the past few decades has been energetic feedback from the accretion onto supermassive black holes at the centers of galaxies. The idea that black holes may exist in galaxies began as a theoretical explanation for the presence of active galactic nuclei (AGN) observed in the universe (Salpeter, 1964; Soltan, 1982; Lynden-Bell, 1969; Lynden-Bell & Rees, 1971). The intrinsic brightness of these sources was enormous, often outshining the host galaxy (Schmidt, 1963). This strongly suggested that accretion onto a massive, compact object such as a black hole was the cause since events such as these are some of the only mechanisms that could produce energies of this magnitude.

The most direct search for black holes in galaxies first came in the form of dynamical mass estimates from the movements of stars and gas within the black hole's gravitational sphere of influence (for an early review, see Kormendy & Richstone, 1995). The sphere of influence for supermassive black holes can range between a few to a few hundred parsecs, making the search limited to galaxies close enough to resolve stellar or gas dynamics within the inner parsecs of a galaxy. The first measurements were made for M87 (Sargent et al., 1978), M32 (Tonry, 1984, 1987; Dressler & Richstone, 1988), M31 (Dressler, 1984; Dressler & Richstone, 1988), NGC 4594 (the Sombrero Galaxy, Kormendy, 1988), and our own Milky Way (Sellgren et al., 1987; Rieke & Rieke, 1988). Since then, measurement techniques and technologies have greatly improved, offering higher spatial resolution for the measurements of black holes (e.g. for the Milky Way, Ghez et al., 1998, 2008), and a wider search area throughout the local universe.

The major dynamical mass estimation methods for black holes are through stellar dynamics, gas dynamics, masers (Dos Santos & Lepine, 1979; Miyoshi et al., 1995; Greene et al., 2010), and reverberation mapping (Blandford & McKee, 1982; Wandel et al., 1999; Bentz & Katz, 2015). Stellar and gas dynamics attempt to trace the sphere of influence by measuring the radial velocity dispersion within the gravitational sphere of influence. Stellar dynamics are generally more reliable than gas dynamics since gas can undergo non-gravitational interactions that could affect its motions in the disk. Masers are stimulated emission lines that are used to trace the velocities within accretion disks. Reverberation mapping measures the motion of gas in the broad line region around the black hole, requiring time delay measurements between the variation in the accretion disk and the variation in the emission lines coming from the broad line regions in order to estimate the distance from the black hole. Using the broad line region's velocities along with the distance measured from this time delay results in a dynamical black hole mass measurement. Recently, the Event Horizon Telescope used very long baseline interferometry in order to resolve the radio emission from the event horizon of M87, providing the first direct imaging capabilities of the gas immediately surrounding a black hole and the first black hole mass estimate using this technique (Event Horizon Telescope Collaboration et al., 2019). Apart from this latest result, these techniques have increased the sample of dynamical black hole mass measurements to a few hundred (e.g., van den Bosch, 2016). It is now generally believed that most galaxies, at least with stellar masses greater than $\sim 10^{10}$ $M_\odot$, host a supermassive black hole.

With the growth of the number of dynamical black hole mass measurements, correlations between black holes and their host galaxies' properties such as spheroidal bulge mass, velocity dispersion, galaxy mass, light concentration, and other properties came into view (e.g., Ferrarese & Merritt, 2000; Gebhardt et al., 2000; Graham et al., 2001; Häring & Rix, 2004; Gültekin et al., 2009; McConnell & Ma, 2013; Kormendy & Ho, 2013; Saglia et al., 2016). These correlations have implied a coevolution between black holes and the intragalactic environment surrounding them (Silk & Rees, 1998; Kauffmann & Haehnelt, 2000; King, 2003). Additionally, these galaxy properties correlate closely not only with black hole mass but also with quiescence (e.g., Kauffmann et al., 2003; Bell, 2008; Bell et al., 2012), further implying a connection between black holes and their host galaxies for massive systems and, more recently, for less massive galaxies as well (Gallo et al., 2008; Baldassare et al., 2015; Dickey et al., 2019).

Studies of AGN have also long supported the idea that black holes affect their host galaxies since these objects indicate the existence of highly energetic activity in the nuclear regions of galaxies. One version of this came from luminous point-like sources visible at many wavelengths that were quasi-stellar in appearance (Burbidge & Burbidge, 1969; Burbidge & O'dell, 1972). These quasi-stellar objects, now referred to as quasars, are the most extreme cases of AGN where black holes are thought to be accreting at or close to the Eddington limit (Lynden-Bell, 1969).

Ionized outflows from AGN have been observed, indicating the bulk movement of material outwards from the interstellar medium (Heckman et al., 1981; Crenshaw et al., 2010; Villar-Martín et al., 2011; Harrison et al., 2014; Cicone et al., 2014; Woo et al., 2016). Ejective feedback is thought to come from the radiation pressure exerted (Begelman et al., 1983; Shlosman et al., 1985) from thin disk accretion around a black hole (Shakura & Sunyaev, 1973). Several studies have attempted to understand whether this form of AGN activity can cause quiescence its host galaxy (Sanders et al., 1988; Di Matteo et al., 2005; Hopkins et al., 2006; Zubovas & King, 2012). The issue with this form of feedback with regards to quiescence is that high accretion rate activity is presumably short lived, meaning that the gas that is ejected into the circumgalactic medium through this mechanism would likely be able to return once high accretion rates subside. Additionally, some studies indicate that this form of feedback does very little to affect the cold gas inside the galaxy since it is too dense to be significantly moved by radiation pressure (Roos et al., 2015; Balmaverde et al., 2016).

Another version of AGN has been observed in cluster studies that identified the existence of radio emission emanating up to several hundred kiloparsecs from the central galaxies in clusters in two semi-symmetric lobes (Jennison & Das Gupta, 1953; Maltby & Moffet, 1962; Miley, 1980; Begelman et al., 1984). These observations led to theoretical arguments that inefficient, low accretion rate black hole feedback (Ichimaru, 1977) could produce winds or jets (Blandford & Begelman, 1999; Blandford & Znajek, 1977) that inflated buoyant, radio-emitting bubbles into the intracluster medium surrounding galaxies (Gull & Northover, 1973; Churazov et al., 2001; Brüggen et al., 2002). Since then, observations of clusters have shown strong evidence that radio lobes from black hole activity create cavities in X-ray emitting cluster atmospheres (Boehringer et al., 1993; Bîrzan et al., 2004; Rafferty et al., 2006; Bîrzan et al., 2008; Hlavacek-Larrondo et al., 2015). These signatures are thought to provide a solution the 'cooling flow' problem, describing the fact that the gas in clusters and around massive ellipticals was observed to have cooling luminosities and mass deposition rates that greatly exceeded the observed amount of cold gas in these galaxies (Fabian, 1994). The enormous impact of these jets on the central regions of galaxy and cluster atmospheres could potentially offset the energy that supports the cooling flows seen in many cluster and group environments (Tabor & Binney, 1993; Ciotti & Ostriker, 2001; Mathews & Brighenti, 2003; McNamara & Nulsen, 2007; McDonald et al., 2018). This would offer an explanation for how black hole feedback may halt the flow of star-forming material into massive galaxies and produce quiescence. The exact form of this energy continues to be an active topic of debate (e.g., Zhuravleva et al., 2014; Zhang et al., 2018).

Recent work indicates that X-ray cavities are just as common in group and isolated environments as they are in clusters (Shin et al., 2016), lending support to the idea that this form of black hole feedback may be important for galaxies at masses similar to that of the Milky Way. However, these X-ray cavities are more easily observable in the most massive systems. Group or isolated galaxies in less massive halos with less hot, X-ray emitting gas are also less likely to be detected by X-ray telescopes like Chandra without better sensitivity. Thus, the current technological capabilities make the study of intermediate mass galaxies and their gaseous atmospheres difficult. In terms of radio emission, LOFAR (van Haarlem et al., 2013) may make significant strides towards detecting radio sources around these systems.

1.4 Testing theories of galaxy formation and evolution

Models and simulations provide tools with which to test the fundamental physical theories that govern our understanding of astrophysical processes. Any physical interpretation coming from the analysis of astronomical observations must be tested in order to assess the theory. These tests are limited by the lack of capabilities that humans have, technological and otherwise, for simulating the immense complexities of Nature and the spatial and temporal scales within which they operate. While this necessarily limits the ability for models to perfectly reproduce Nature's behavior, it also encourages the development of simple and intuitive theories that encapsulate complex phenomena.

The field of extragalactic astronomy has relied on models and simulations to test much of the established paradigms of galaxy formation and evolution. The first computer simulations of galaxies were limited by computer power and thus began by focusing on gravity alone. Collisionless, N-body simulations that simulated gravitational forces in, for example, galaxy clusters (von Hoerner, 1960; Aarseth, 1963; Peebles, 1970; White, 1976; McGlynn, 1984; Frenk et al., 1990) or galaxy interactions (Gerhard, 1981; Negroponte & White, 1983; Barnes, 1988; Hernquist, 1992) were run to test whether the resulting structures would reproduce what was observed in the universe. The need to simulate dissipative processes of gas led to the development of Lagrangian smoothed particle hydrodynamical (SPH, Gingold & Monaghan, 1977) and Eulerian grid-based (with or without adaptive mesh refinement) hydrodynamical (Norman et al., 1980; Berger & Colella, 1989) codes. Additional advances were made by simulating dark matter N-body interactions alongside the hydrodynamics of gas interactions with the P3MSPH (Evrard, 1988, 1990; Evrard et al., 1994) and the TREESPH (Hernquist & Katz, 1989; Katz et al., 1992, 1996) codes. Currently, a multitude of hydrodynamical codes exist for both SPH-based (GADGET - Springel et al., 2001b; GADGET-2 - Springel, 2005) and grid-based (ART - Kravtsov et al., 1997; FLASH - Fryxell et al., 2000; RAMSES - Teyssier, 2002; ENZO - O'Shea et al., 2004; Bryan et al., 2014) approaches. More recently, hybrid approaches that combine the advantages of both SPH- and grid-based codes have also been developed (AREPO - Springel, 2010; GIZMO - Hopkins, 2015, 2017).

Modeling the complex phenomena in gas hydrodynamics alongside the gravitational interactions of dark matter is an important step forward in attempting to simulate galaxies. However, a major limiting factor to these simulations is the finite temporal and spatial resolution that models can obtain with a reasonable, cost-efficient, and time-efficient amount of computing power. Thus, ‘subgrid’ prescriptions of physical processes thought to be important for galaxy formation need to be implemented. For example, individual giant molecular clouds and the substructures that form individual stars within them cannot be feasibly resolved if an entire galaxy or cosmological volume is simulated. Therefore, the formation of star particles or cells that represent multiple stars must be assumed following the thermodynamic state of the gas and, for example, an equation of state. Similar semi-analytic methods must be implemented to model the energetic feedback from the deaths or winds of individual stars, where they must be assumed to act in a uniform fashion across a large volume of space that could amount to a few kiloparsecs (e.g., Katz et al., 1996; Yepes et al., 1997; Springel & Hernquist, 2003; Schaye & Dalla Vecchia, 2008). Similarly, gas cooling can be modeled semi-analytically using the standard pre-calculated cooling curves of gas at different temperatures and metallicities (Sutherland & Dopita, 1993). Several large-volume cosmological hydrodynamical simulations have been run by various groups (OWLS and EAGLE - Schaye et al., 2010, 2015; Illustris and IllustrisTNG - Vogelsberger et al., 2014a; Pillepich et al., 2018; BAHAMAS - McCarthy et al., 2017; MassiveBlack-I and -II - Di Matteo et al., 2012; Khandai et al., 2015; HorizonAGN - Dubois et al., 2016).

Another approach to simulating galaxy formation and evolution that was being developed concurrently was semi-analytic modeling (SAMs, e.g. White & Rees, 1978; White & Frenk, 1991). These simulations related the properties of galaxies to the underlying dark matter framework developed through the CDM paradigm. Using N-body gravity-only simulations for dark matter structure formation, semi-analytic models placed galaxies on top of dark matter halos and simulated their growth. Since the details of gas hydrodynamics were not modeled using fluid equations, SAMs used simplified, physically-motivated prescriptions of mechanisms that are thought to be important for galaxy formation such as halo and galaxy merging, gas cooling, disk and bulge formation, star formation, and stellar feedback. This way, SAMs remained relatively less expensive and much faster to run compared to hydrodynamical simulations. In addition, a larger volume could be simulated, thereby allowing a robust study of the model's population statistics. As SAMs developed, Monte Carlo Markov Chain methods became useful for running the model several times and adjusting the free parameters so that galaxy populations agree with various observational constraints. Several groups have contributed to the development of SAMs (e.g., Santa Cruz - Somerville & Primack, 1999; Somerville et al., 2008; Porter et al., 2014; Durham - Baugh et al., 1998; Helly et al., 2003; Croton et al., 2006; Bower et al., 2006; Munich - Kauffmann et al., 1999; Springel et al., 2005; Guo et al., 2011; Henriques et al., 2015; GALICS - Hatton et al., 2003; Cattaneo et al., 2006a).

Since SAMs are faster models to run and the physical prescriptions governing galaxy formation are more simple, the theories that are implemented within SAMs can be tested much more readily than in hydrodynamical simulations. For example, it was through SAMs that black hole feedback became a widely popular idea for causing quiescence in relatively massive galaxies (Benson et al., 2003; Bower et al., 2006). More specifically, high accretion rate black hole feedback is much more effective at higher redshifts in SAMs. If this form of feedback was implemented to suppress star formation in galaxies, then the number of massive galaxies at high redshifts were severely underestimated even if the local luminosity function were reproduced (Baugh et al., 1998; Somerville et al., 2001). However, producing the correct distributions of galaxies at high redshifts caused the overproduction of massive galaxies at low redshift (Kauffmann et al., 1999). As such, low-accretion rate black hole feedback was implemented to suppress the growth of galaxies at late times (Croton et al., 2006).

These breakthroughs helped cosmological hydrodynamical simulations address similar issues that SAMs were having. Early simulations of clusters have been shown to cool a large amount of gas onto the galaxy (e.g., Katz & White, 1993; Suginohara & Ostriker, 1998), resulting in high star formation rates. This is in contradiction to observations where the central galaxies of clusters exhibit much less star formation activity than what is theoretically calculated (see Balogh et al., 2001, for a discussion of the 'cooling crisis'). Currently, all large-volume hydrodynamical models since the mid-2000s have relied on some form of black hole feedback in order to suppress star formation in massive galaxies (OWLS, EAGLE, Illustris, IllustrisTNG, BAHAMAS, MassiveBlack-I and -II, and HorizonAGN).

1.5 The goals and aims of this work

While black hole feedback provides promising results in terms of reproducing the broad characteristics of quiescence, it is important to remain skeptical based on the current state of the field. Models that include black hole feedback use subgrid, semi-analytic implementations that vary with respect to how they grow black holes, produce their energetic feedback, and couple this feedback to the surrounding gas (Croton et al., 2006; Sijacki et al., 2007; Booth & Schaye, 2009; Weinberger et al., 2017). Despite being physically motivated based on observed forms of black hole feedback, a comprehensive theory on the black hole-galaxy connection has not been made.

Additionally, the observations of black hole activity and feedback for less massive galaxies such as the Milky Way are scarce compared to observations of this phenomena for clusters. The difficulty in detecting the same ubiquity of black hole feedback signatures in intermediate mass galaxies (with stellar masses between 10^{10-11} $\mathrm{M}_{\odot}$) as in their higher mass counterparts (with stellar masses greater than 10^{12} $\mathrm{M}_{\odot}$) has led to much skepticism in prescribing its importance to intermediate mass galaxies that host a significant fraction of quiescent central galaxies.

As such, this work aims to explore the cause and mechanism of quiescence by addressing the question: *How can observable correlations between black holes and the properties of their host galaxies reveal the underlying mechanism behind quiescence?*

Specifically, this work will analyze the correlations between stellar mass, black hole mass, and star formation rate. Stellar mass is thought to correlate with dark matter halo mass and thus with total halo gas mass (for a review, see Wechsler & Tinker, 2018). More massive galaxies would thus have a larger amount of gas to cool and condense onto the galaxy. Therefore, stellar mass can act as a proxy for the amount of cooling that would happen in the absence of feedback processes.

The energy from black hole feedback is often assumed to be related to the accretion rate onto the black hole, $\mathrm{E_{BH}} \propto \dot{\mathrm{M}}_{\mathrm{BH}}$, where the accretion rate is often assumed to be following Bondi-Hoyle-Lyttleton formalism (Hoyle & Lyttleton, 1939; Bondi & Hoyle, 1944; Bondi, 1952) with $\dot{\mathrm{M}}_{\mathrm{BH}} \propto \mathrm{M}_{\mathrm{BH}}^2$, and so $\mathrm{E_{BH}} \propto \mathrm{M}_{\mathrm{BH}}^2$. Similar arguments relating the energy from black hole feedback to the binding energy of the black hole also result in $\mathrm{E_{BH}} \propto \mathrm{M}_{\mathrm{BH}}^2$. Therefore, black hole mass can be used as a proxy for the amount of black hole-driven feedback energy released.

The distribution of galaxies on the star formation rate-stellar mass plane shows a fairly tight positive correlation with a slope on the order of $\sim$1. This has been called the star-forming main sequence where galaxies that fall below this sequence are classified as quiescent (Brinchmann et al., 2004; Salim et al., 2007). Thus, dividing the star formation rate by stellar mass to obtain a specific star formation rate can be used to indicate a galaxy's distance from the star forming main sequence, i.e. a galaxy's degree of quiescence.

The location of galaxies on this three-dimensional space should then be sensitive to the physics underlying gas cooling, black hole feedback energy injection, and star formation. Following this simple framework, an exploration of this parameter space in the context of models and observations may provide clues to whether these processes are linked and how the physics that governs their possible connection operates.

Chapter 2 will discuss a study on the diversity of growth histories for Milky Way-mass central galaxies in the L-Galaxies semi-analytic model. This work aims to address whether the many pathways for stellar mass growth are indicative of systematic physical processes related to quiescence. This chapter will show that the L-Galaxies model predicts a strong correlation between black hole mass and star formation rate. Chapter 3 will present results that confirm that this correlation is qualitatively reproduced in the real Universe for a sample of central galaxies with dynamical black hole mass measurements. Chapter 4 will present, for the first time, an empirical correlation between black hole mass and the star formation activity within its host galaxy. Chapter 5 will contain an analysis of quiescence in the IllustrisTNG hydrodynamical simulation suite. This last work, not yet published, aims to use the results from Chapters 3 and 4 in order to characterize and assess the black hole feedback model used in a state-of-the-art galaxy formation simulation. Chapter 6 will contain a summary of the work presented in this dissertation and the outlook for future work related to the topics discussed here.

CHAPTER II

The diversity of growth histories of Milky Way-mass galaxies

2.1 Abstract

We use the semi-analytic model developed by Henriques et al. (2015) to explore the origin of star formation history diversity for galaxies that lie at the centre of their dark matter haloes and have present-day stellar masses in the range $5 - 8 \times 10^{10}$ $M_{\odot}$, similar to that of the Milky Way. In this model, quenching is the dominant physical mechanism for introducing scatter in the growth histories of these galaxies. We find that present-day quiescent galaxies have a larger variety of growth histories than star-formers since they underwent 'staggered quenching' – a term describing the correlation between the time of quenching and present-day halo mass. While halo mass correlates broadly with quiescence, we find that quiescence is primarily a function of black hole mass, where galaxies quench when heating from their active galactic nuclei becomes sufficient to offset the redshift-dependent cooling rate. In this model, the emergence of a prominent quiescent population is the main process that flattens the stellar mass–halo mass relation at mass scales at or above that of the Milky Way.

2.2 Introduction

One of the primary goals of galaxy formation theory is to better understand the evolution of galaxy stellar mass in relation to their dark matter haloes. Tight constraints on the parameters of the ΛCDM cosmological framework from observations have allowed detailed N-body simulations to characterize the distribution of dark matter at the present day and its evolution with cosmic time (Springel et al., 2005; Boylan-Kolchin et al., 2009; Klypin et al., 2011). In conjunction, observational surveys of hundreds of thousands of galaxies have also begun to allow a statistical understanding of observed galaxy properties over about 10 Gyrs (e.g., SDSS: York et al., 2000; 2dFGRS: Colless et al., 2001; 6dFGRS: Jones et al., 2004; GALEX: Martin et al., 2005; 2MASS: Skrutskie et al., 2006; COSMOS: Scoville et al., 2007; CANDELS: Koekemoer et al., 2011; Grogin et al., 2011; UltraVISTA: McCracken et al., 2012, DEEP2: Newman et al., 2013). These studies have provided the foundation for understanding the evolution of galaxy number density as a function of stellar mass – the stellar mass function – from $z = 0-8$ (Cole et al., 2001; Li & White, 2009; Marchesini et al., 2009; Ilbert et al., 2010; Mortlock et al., 2011; Ilbert et al., 2013; Muzzin et al., 2013; Moustakas et al., 2013; Tomczak et al., 2014). As a result, understanding how the dark matter halo mass function from N-body simulations and the stellar mass functions from observational surveys map onto one another at different epochs has recently been a subject of intense study.

In this chapter, we use the semi-analytic model developed by Henriques et al. (2015) to characterize the growth histories of galaxies at the centres of their dark matter haloes with present-day stellar masses $5 - 8 \times 10^{10}$ $M_{\odot}$ since $z \sim 2.07$. We explore what drives the diversity of pathways that could lead to galaxies with the same stellar mass yet different galactic properties at the present day in the context of this model. Understanding this fundamental behavior of galaxy growth has important implications for the way stellar mass is generally linked with halo mass in a variety of models and observational studies.

A powerful approach for building intuition on how the observable properties of galaxies relate to the dark matter framework is the use of galaxy formation models. The goal of such models is to accurately simulate the gravitationally-driven evolution of dark matter haloes, the infall, cooling, and heating of gas in this dark matter framework, the formation of stars at the centres of potential wells, the formation of rotationally-supported discs and dispersion-supported spheroids, and feedback from stars and black holes. Realistically reproducing these processes is essential to understanding the underlying physics of observed phenomena at extragalactic scales.

One such approach to simulating galaxy formation, and the approach we choose to use in our study, is semi-analytic modeling (Kauffmann et al., 1999; Springel et al., 2001a; Helly et al., 2003; Hatton et al., 2003; Kang et al., 2005; Croton et al., 2006; Somerville et al., 2008; Bower et al., 2006; Guo et al., 2011; Porter et al., 2014; Henriques et al., 2015). These models use simplified analytic parameterizations to model complex baryonic physics on top of dark matter simulations. This method has the advantage of being relatively computationally inexpensive and therefore more easily able to simulate large cosmological volumes. In addition, searching through parameter space in semi-analytic models is straightforward, especially compared to hydrodynamic simulations. A caveat is that these models incorporate many free parameters, leading to considerable degeneracies in their results. Even so, they have included progressively more nuanced prescriptions for the physical drivers of galaxy evolution, and advanced statistical procedures such as Monte Carlo Markov Chain (MCMC) methods which aim to more comprehensively constrain model parameters using observational data. The development of MCMC methods in semi-analytic models began with the work of Kampakoglou et al. (2008) and Henriques et al. (2009) and has since been extended to a wide range of simulations and sampling methods (Benson & Bower, 2010; Bower et al., 2010; Henriques & Thomas, 2010; Lu et al., 2011, 2012; Henriques et al., 2013; Mutch et al., 2013; Benson, 2014; Ruiz et al., 2015). As a result, these models have developed into powerful tools to study the mapping of stellar mass onto dark matter haloes.

Models such as these provide tools with which to test and explore physical and statistical recipes for galaxy evolution using large-scale observational datasets. In the past decade, studies attempting to track the ancestry of galaxies by linking galaxy populations in these datasets at different redshifts have flourished (De Lucia & Blaizot, 2007a; van Dokkum et al., 2010; Brammer et al., 2011; Papovich et al., 2011; Leja et al., 2013; van Dokkum et al., 2013; Barro et al., 2013; Patel et al., 2013a; Barro et al., 2014; Williams et al., 2014). While it is not possible to observe how individual systems evolve, a combination of models and observations can be used to develop methods by which one can attempt to identify the progenitors of present-day galaxies.

Many of these progenitor studies have used stellar mass to characterize the growth histories of galaxies. Such studies suggest that galaxies grow significantly in size but without much gain in mass for the most massive galaxies (van Dokkum et al., 2010; Morishita et al., 2015), whereas lower mass galaxies grow significantly in both mass and size (Patel et al., 2013b; Papovich et al., 2015). These studies depend on strong assumptions, such as a constant comoving number density or a stellar mass growth inferred from the evolution of the star forming main sequence. Yet, galaxy growth may involve a considerable degree of stochastic variation as a result of many different halo parameters and assembly histories, leading to a diversity of galaxy growth histories (Smethurst et al., 2015; Henriques et al., 2015; Contreras et al., 2015; Torrey et al., 2015). A concern is that the degree of growth history diversity may be large enough to undermine any insight gained by studying the average or median growth histories of galaxy populations.

Intuitively, intrinsic scatter in growth histories is a natural consequence of the suppression of star formation in galaxies. A relatively massive galaxy that halts its production of stars by $z = 1$ may end up having the same stellar mass at the present day as a low mass galaxy at high redshift that has continually formed stars. Observational surveys have shown that the quiescent population of galaxies has grown substantially since $z \sim 2$ (Bell et al., 2004; Faber et al., 2007; Brammer et al., 2009; Muzzin et al., 2013). While quenched central galaxies are possible at stellar masses above 10^9 $M_\odot$ (Geha et al., 2012), they become increasingly more common at high stellar masses (Kauffmann et al., 2003). Detailed studies of these quenched galaxies have revealed concentrated light distributions and high velocity dispersions (Bell, 2008; Franx et al., 2008b; Cheung et al., 2012; Bell et al., 2012; Lang et al., 2014), pointing to the likely existence of relatively large central black holes.

For this reason, one of the most popular explanations for the quenching of galaxies at high stellar mass is feedback from active galactic nuclei (AGN) since heating from this mechanism is thought to correlate with black hole mass. This mechanism works first via quasar-mode then radio-mode feedback (Kauffmann & Haehnelt, 2000; Croton et al., 2006; Sijacki et al., 2007). Quasar-mode feedback occurs as a result of mergers and drives cold gas into the central regions of the galaxy. This causes rapid growth of the black hole and high accretion disc luminosities (Kauffmann & Haehnelt, 2000; Di Matteo et al., 2005), as well as massive outflows of gas (Sturm et al., 2011; Cicone et al., 2014). After this phase, radio-mode feedback begins where gas from the hot halo is fed into the black hole inefficiently, producing a jet which heats the surrounding gaseous atmosphere (Page et al., 2012; Gaspari et al., 2012; Dubois et al., 2013; Man et al., 2016).

Inclusion of AGN heating in galaxy formation models has significantly improved the agreement between the high-mass ends of the simulated and observed stellar mass functions by reducing the amount of star formation in high mass galaxies (Croton et al., 2006; Bower et al., 2006). Other less important quenching mechanisms that affect central galaxies are mergers which could deplete the amount of cold gas available in the galaxy by triggering star formation (Mihos & Hernquist, 1996; Lambas et al., 2003; Woods et al., 2006; Bridge et al., 2007), secular processes such as morphological quenching (Kormendy & Kennicutt, 2004; Martig et al., 2009; Cisternas et al., 2011), and halo or mass quenching which ties quenching together with hot gas mass (Dekel & Birnboim, 2006; Cattaneo et al., 2006b; Birnboim et al., 2007; Dekel et al., 2009; Gabor & Davé, 2015).

As a result, the focus of this chapter is twofold: (1) to understand the most important parameters that determine how quenching operates in a particular galaxy formation model, and (2) to understand how this quenching adds scatter to stellar mass growth histories for galaxies with present-day stellar masses similar to that of the Milky Way. We will use the semi-analytic model developed by Henriques et al. (2015) in order to obtain galaxy growth histories of Milky Way-mass galaxies. We choose to analyse this model as it matches the stellar mass functions and the star-forming/quiescent fractions out to $z \sim 3$ by design (See their Figures 2 and 5, respectively). Agreement with these two observations is essential since our study focuses on stellar mass buildup within the star-forming and quiescent populations.

For this study, we define Milky Way-mass galaxies as *central* galaxies with stellar masses, $M_* = 5\text{–}8\times10^{10}$ $\mathrm{M}_\odot$ (Flynn et al., 2006; McMillan, 2011). In this model, central galaxies are defined as those which are located at the minimum of the potential of the main halo. Milky Way-mass galaxies are ideal for studying the many pathways of galaxy evolution since they contain a large diversity of morphologies and star formation histories (e.g. Kauffmann et al., 2003; Borch et al., 2006; Moustakas et al., 2013; Tomczak et al., 2014). The study of Milky Way-mass galaxies therefore allows us to better understand the physical mechanisms that differentiate those galaxies that become star-forming from those that become quiescent within the same stellar mass range at the present day. We choose to focus on central galaxies since satellites are affected by additional processes such as ram pressure stripping, tidal forces, and a loss of hot gas mass when plunging into the tidal field and diffuse gaseous halo of the main galaxy/group/cluster potential.

The organization of this chapter is as follows. After introducing the Henriques et al. (2015) semi-analytic model (Section 2.3), we describe their physically-motivated model parameterization of quiescence (Section 2.4). We then highlight general trends observed in the stellar mass-halo mass (SMHM) relation of central galaxies and describe the evolutionary pathways of the main progenitors of Milky Way-mass galaxies in the model since $z = 2.07$ (Section 2.5). Splitting the present-day Milky Way-mass galaxy population into star-forming and quiescent galaxies, we then examine sources of scatter in the growth histories of each group (Section 2.6). A discussion of how the growth of the black hole contributes to the scatter in Milky Way-mass growth histories (Section 2.7) then leads to a possible way to relate our analysis to the entire central galaxy population in terms of the SMHM relation (Section 2.8). We then focus on how our results may be useful for observational studies by comparing model values of stellar mass, halo mass, and black hole mass as potential observational signatures of the relevant quenching mechanism at work (Section 2.9). Finally, we discuss some important implications and conclusions from our study on the scatter in the growth histories of Milky Way-mass galaxies (Sections 2.10 and 5.9).

2.3 The Henriques et al. 2015 Semi-Analytic Model

2.3.1 Model Description

Henriques et al. (2015), hereafter referred to as H15, produced a semi-analytic model of baryonic processes overlaid on the Millennium Simulation (MS, Springel et al., 2005). A second simulation, the Millennium-II Simulation (MS-II, Boylan-Kolchin et al., 2009), was run with 125 times better mass resolution, 5 times better force resolution, and 5 times smaller box length than the MS in order to better model the behavior of smaller structures. Combined, the MS and MS-II provide a way to study the formation of galaxies ranging from faint dwarfs to the most massive cD galaxies. The H15 data was downloaded from the Millennium Databases[1].

The H15 model is a descendant of the semi-analytic model produced by Guo et al. (2011) and includes significant improvements in terms of its agreement with observational data. With regards to the dark matter structure, the Guo et al. (2011) model adopts a ΛCDM cosmology with cosmological parameters based on results from 2dFGRS (Colless et al., 2001) and WMAP1 (Spergel et al., 2003). H15 also adopts a ΛCDM cosmology but with more recently published cosmological parameters from the *Planck* Collaboration (Planck Collaboration et al., 2014). The new parameters based on *Planck* data are $\Omega_{\mathrm{M}} = 0.315$, $\Omega_{\Lambda} = 0.685$, $\Omega_{\mathrm{b}} = 0.0487$ ($f_{\mathrm{b}} = 0.155$), $n = 0.96$, $\sigma_8 = 0.829$, and $H_0 = 67.3$ km s^{-1} Mpc^{-1}. The Millennium Simulation was scaled to this cosmology according to the technique detailed in Angulo & White (2010) and Angulo & Hilbert (2015). With this new cosmology, the MS has a resolution of 2160^3 particles in a periodic box of side length $480.279h^{-1}$ Mpc with a particle mass of $9.6 \times 10^8 h^{-1}$ M$_{\odot}$. Despite this difference, the change in cosmology does not significantly change the outcome of the model since the uncertainties are dominated by galaxy formation physics rather than cosmology.

The following description details the general physical mechanisms that affect the evolution of central galaxies since these are the focus of our work. In this model, there are six main baryonic components that are followed as galaxies evolve in time – a hot gas atmosphere, cold interstellar gas, a reservoir of gas which has been ejected by winds, stars in the bulge, disc, and intracluster light components, central supermassive black holes, and diffuse primordial gas associated with dark matter that does not yet

---

[1] To access the Millennium databases: http://gavo.mpa-garching.mpg.de/Millennium. For a description of the Munich Galaxy Formation Model: http://galformod.mpa-garching.mpg.de/public/LGalaxies.

belong to any halo. These components are functions of the dark matter merger trees on top of which they are built. Primordial gas is fed into the halo in one of two ways: (1) Rapidly infalling at the free-fall time, or (2) forming a cooling flow after the gas has been initially shock heated to the virial temperature (White & Rees, 1978; White & Frenk, 1991; Birnboim & Dekel, 2003). These two regimes depend on whether the cooling time is shorter or longer than the halo sound crossing time.

The angular momentum of the gas that cools to the bottom of the potential well leads to the formation of a disc (Fall & Efstathiou, 1980). Once the gas is in the disc, stars can form at a rate that depends on the angular momentum of the disc, the amount of cold gas available, and the maximum circular velocity of the halo. As stars reach the end of their lives, supernovae provide an important source of feedback which can eject gas out of the galaxy and into a reservoir (White & Rees, 1978; Dekel & Silk, 1986; Heckman et al., 1990; Cole, 1991; White & Frenk, 1991). This heated gas remains in the reservoir until it is able to join the hot halo and possibly cool back onto the central galaxy depending on whether there are any other heating mechanisms at play (Benson et al., 2003; De Lucia et al., 2004; Birrer et al., 2014; Henriques et al., 2013). The cooling of this gas would allow for future star formation.

Mergers add stellar mass to the galaxy by forming a spheroid or bulge of merged stars and creating a short-lived starburst phase in the disc (Toomre, 1977; Barnes, 1988; van den Bergh, 1990; Somerville et al., 2001; Naab & Burkert, 2003; Bournaud et al., 2007). In addition, the supermassive black hole grows significantly during a merger due to the accretion of cold gas as well as the satellite's black hole merging with that of the central (Kauffmann & Haehnelt, 2000). After this short-lived quasar-mode AGN feedback phase, radio-mode AGN feedback begins, where slow accretion from the hot gas atmosphere onto the supermassive black hole provides a heating source which affects the cooling of hot gas onto the disc (McNamara & Nulsen, 2007). We expand on the AGN feedback prescription in greater detail in Section 2.4.

It is important to note particular differences in the prescriptions for galaxy formation physics between the H15 model and its predecessors. These changes were motivated by H15's use of Monte Carlo Markov Chain (MCMC) methods, which allowed a thorough exploration of model parameter space. They found that there were no combination of parameters in the Guo et al. (2011) model which would result in reasonable agreement with the observed stellar mass functions over the redshift range $0 \leq z \leq 3$ (Henriques et al., 2013). This motivated significant modifications being made to the model in order to better match observations.

The most significant change was with respect to the reincorporation of supernovae-ejected gas into the galaxy. In both Guo et al. (2011) and H15, gas is ejected into a reservoir which is eventually reincorporated into the hot halo and can then cool and condense onto the galaxy. For the Guo et al. (2011) model, the time it takes to be reincorporated into the hot halo is dependent on the halo mass and redshift. In the H15 model, however, the reincorporation time depends only on the halo mass and does not directly depend on redshift. These changes cause the reincorporation time to be longer for lower mass systems and shorter for higher mass systems in the H15 model than is the case in the Guo et al. (2011) model. See Fig. S2 in H15 for a visual representation of this effect. The new prescription produces behavior similar to that found in hydrodynamic studies by Oppenheimer & Davé (2008) and Oppenheimer et al. (2010). This causes the abundance evolution of lower mass systems to be significantly different in H15. Whereas there was very little late-time abundance evolution at low stellar masses in Guo et al. (2011), there is a more significant change in H15 that better matches the observations.

In order to build intuition about how to interpret observational datasets, H15 also incorporates a redshift-dependent error which models the observational errors in measuring stellar mass. This effect is included when comparing the model to the observational stellar mass functions used in their MCMC methods. The error is modeled by a Gaussian with a dispersion $0.08(1+z)$ centred on the log of stellar mass, $\log_{10} M_*$. In this work, we impose this scatter on all stellar masses used unless otherwise noted. We do this in order to visualize how we might observe galaxy growth in the real universe with observational errors included. We note that this introduces some unphysical effects where the stellar mass of some galaxies appears to decrease from one redshift to the next. This effect is small, however, and affects a minority of galaxies in our study.

Other changes to the model include a lower gas surface density threshold for star formation, the elimination of ram pressure stripping effects on satellites that fall into haloes with $M_{\rm h} < 10^{14}$ $\rm M_{\odot}$, and an AGN feedback model that heats gas and suppresses cooling more effectively at low redshifts. For a more detailed explanation of these changes see Henriques et al. (2015) and Henriques et al. (2013).

In this work, we extensively use dark matter halo mass as an important parameter for characterizing the stellar mass growth history of central galaxies. The H15 model provides both the virial mass, $M_{\rm vir}$, and the maximum rotational velocity of the halo, $\rm v_{max}$, each of which can characterize the halo. In H15, the virial mass is defined as the mass within the virial radius which encloses a mean overdensity 200 times the critical value for the universe. In contrast, $\rm v_{max}$ is the maximum rotational velocity of the halo. In order to allow comparison with earlier work (Behroozi et al., 2013; Moster et al., 2013), we will characterize haloes using $M_{\rm vir}$ rather than $\rm v_{max}$ while noting that qualitatively our results do not change for the other choice.

We also note that for this analysis, we use only the MS and not the MS-II. The two give similar results for Milky Way-mass galaxies, but we use the former since it allows us to probe a larger number of galaxies than its smaller volume counterpart. This results in some resolution effects at low masses but does not greatly affect our results. We take note of this in the relevant sections.

In addition, the plots in this work at times show the full central galaxy population rather than just Milky Way-mass galaxies. We note that in such cases we display a randomly selected, representative 0.2% of the full simulation data in H15. For all plots showing Milky Way-mass galaxies, we show 2.5% of this population where we choose the main (most massive) progenitors of these galaxies. For all statistical exercises, such as calculating medians and 68 percentile distributions, we use 100% of the simulation data.

Finally, we note that H15 is currently the most successful semi-analytic model with regards to matching both the observed stellar mass functions and the star-forming/quiescent fractions out to $z \sim 2$. In terms of our goals for this work, matching the stellar mass function is essential in understanding how the distribution of stellar mass throughout the universe changes as a function of redshift. H15 builds up the low mass end of the stellar mass function in a more realistic way than previous models. Since all galaxies by necessity pass through a stage where they were lower mass, agreement with the observed stellar mass functions should result in more realistic galaxy growth histories. Agreement with the observed star-forming/quiescent fraction of galaxies is also important since we focus on the cessation of star-forming galaxies and the growth of the quiescent fraction for main progenitors of Milky Way-mass galaxies. H15 therefore broadly reproduces the effect of quenching and quiescence on the evolution of the stellar mass function, even if the specific mechanism invoked is incorrect in detail. As a result, this model provides a strong foundation for our study of how quenching produces the scatter in the growth histories of central galaxies with stellar masses similar to that of the Milky Way.

2.3.2 Star-formation Selection

A main goal of this work is to understand how differences between the pathways to star-forming and quiescent populations produce scatter in the growth histories of Milky Way-mass galaxies. We thus need a selection method to differentiate these two groups. In our analysis, we split the star-forming and quiescent populations in this model with a sSFR cut described by:

$$\mathrm{sSFR} = \frac{(1+\mathrm{z})}{2\mathrm{t_H}}, \tag{2.1}$$

where sSFR is the specific star formation rate (SFR/M_*) in years^{-1}, z is the redshift, and $\mathrm{t_H}$ is the present-day Hubble time in years. Quiescent galaxies with sSFR $< 10^{-12}$ yr^{-1} were assigned an artificial value by H15 designed to approximately match observationally derived sSFR measurements (e.g. Brinchmann et al., 2004; Salim et al., 2007; Schiminovich et al., 2010). These low sSFRs signify either low-level star formation not well modeled by H15, or a contribution of older stellar populations and/or low-level AGN activity to observational sSFR estimates (see Section 5.2 in H15). Using this selection will allow us to identify and analyse the growth histories of these two groups.

2.4 The Physics of Quenching in H15

Simulated galaxies in this model quench their star formation when heating energy from accretion onto a supermassive black hole offsets the radiation from cooling and infalling gas in a given halo. The general physical picture is that galaxy mergers result in the growth of the supermassive black hole by a combination of black hole mergers and the rapid feeding of cold gas into the black hole. Afterwards, the hot gas from the atmosphere around the galaxy is fed into the black hole through radio-mode accretion. The galaxy heats up its atmosphere via jets from the accretion onto the black hole.

There are many theories that attempt to explain the exact mechanism by which the atmosphere is heated, whether it be shocks due to an AGN jet injecting energy into the atmosphere (Fabian et al., 2005; Blanton et al., 2009; Randall et al., 2011), cosmic ray heating from the jet (Sijacki et al., 2008; Guo & Oh, 2008), or effervescent heating from buoyant bubbles in the ICM (Begelman, 2001; Brüggen et al., 2002; Roychowdhury et al., 2004; Voit & Donahue, 2005; Brüggen & Kaiser, 2002), but the current status of these studies is inconclusive. In H15, AGN heating is simplified where the AGN provides a heating rate which depends on the hot gas mass and the mass of the black hole. The heating counteracts halo gas cooling and hot gas is prevented from condensing into star-forming material and falling onto the central galaxy.

In order to explore H15's AGN feedback model quantitatively, we will follow the formulation of heating and cooling rates detailed in H15 (See their Sections S1.4 and S1.10). We will first describe how the heating rate is calculated followed by a description of how the cooling rate is calculated in the two different regimes that the model takes into account. Finally, we will show that these rates can be approximately defined using only black hole mass and halo mass as variables. As a result, we will be able to calculate a rough boundary where heating exactly balances cooling on a $M_{\rm BH}$-$M_{\rm h}$ plot. We will show that this boundary coincides with the boundary between star-forming and quiescent galaxies, effectively building intuition for how galaxies quench in this model.

H15 accounts for AGN heating in Equation S26 of their supplementary material where,

$$\dot{M}_{\rm heat} \propto \frac{\dot{E}_{\rm radio}}{V_{\rm vir}^2}, \tag{2.2}$$

and, following their Equations S24 and S25,

$$\dot{E}_{\rm radio} \propto \dot{M}_{\rm BH} \propto M_{\rm hot} M_{\rm BH}. \tag{2.3}$$

Here, $\dot{M}_{\rm heat}$ is the heating rate from radio-mode feedback, $\dot{E}_{\rm radio}$ is the energy output rate due to radio-mode accretion onto the black hole, $V_{\rm vir}$ is the virial velocity of the dark matter halo, $M_{\rm BH}$ is the black hole mass, $\dot{M}_{\rm BH}$ is the mass accretion onto the black hole from radio-mode accretion, and $M_{\rm hot}$ is the hot gas mass. This formula is taken from Equation 10 in Croton et al. (2006) except with the Hubble parameter divided out to provide more effective heating at later times. Inserting Equation 2.3 into Equation 2.2 gives:

$$\dot{M}_{\rm heat} \propto \frac{M_{\rm hot} M_{\rm BH}}{V_{\rm vir}^2}. \tag{2.4}$$

In order to model cooling, the H15 model follows two modes by which cool gas can reach the central galaxy: the rapid infall regime and the cooling flow regime. The rapid infall regime generally describes lower mass and higher redshift haloes that experience the free fall of cool gas onto their central galaxy without a stand-off shock. At higher halo masses, cool gas flowing into the virial radius of the halo is shock heated to the virial temperature, contributing to a hot gaseous halo around the galaxy. The cooling flow regime describes the mode where the inner regions of the gaseous halo can eventually cool onto the central galaxy by radiating away their energy.

In the cooling flow regime, the cooling rate is described by Equation S6 in H15,

$$\dot{M}_{\rm cool} \propto M_{\rm hot} \frac{r_{\rm cool}}{R_{\rm vir}}, \tag{2.5}$$

where, following Equation S5,on

$$r_{\rm cool} \propto \left[\frac{M_{\rm hot} \Lambda}{T_{\rm vir} R_{\rm vir}} \right]^{1/2}. \tag{2.6}$$

Plugging Equation 2.6 into Equation 2.5 results in:

$$\dot{M}_{\rm cool} \propto \left(\frac{M_{\rm hot}}{R_{\rm vir}} \right)^{3/2} \left(\frac{\Lambda}{T_{\rm vir}} \right)^{1/2}. \tag{2.7}$$

Here, $\dot{M}_{\rm cool}$ is the cooling rate of the hot gas atmosphere, $r_{\rm cool}$ is the cooling radius at which the cooling time equals the halo dynamical time, $R_{\rm vir}$ is the virial radius, Λ is the cooling function that describes how gas cools, and $\mathrm{T}_{\rm vir}$ is the virial temperature of the halo. We note here that the dynamical time of the halo, $t_{\rm dyn}$, depends only on $H(z)$ and therefore is constant for all haloes at a specified redshift, which is why we drop this term as a constant. This dependence on $H(z)$ has important consequences which we describe more fully in Section 2.7.

To simplify these expressions, we assume $T_{\rm hot} \propto T_{\rm vir}$ and $M_{\rm hot} \propto M_{\rm vir}$. In addition we can use the fact that $M_{\rm vir} \propto V_{\rm vir}^3 \propto R_{\rm vir}^3$ and $T_{\rm vir} \propto V_{\rm vir}^2 \propto M_{\rm vir}^{2/3}$ in order to simplify $\dot{M}_{\rm heat}$ and $\dot{M}_{\rm cool}$ and express these quantities in terms of $M_{\rm vir}$ and $M_{\rm BH}$,

$$\dot{M}_{\rm heat} \propto M_{\rm vir}^{1/3} M_{\rm BH} \tag{2.8}$$

$$\dot{M}_{\rm cool} \propto M_{\rm vir}^{2/3} \Lambda^{1/2}. \tag{2.9}$$

Here, $\Lambda = \Lambda(T_{\rm hot}, Z_{\rm hot})$ where the cooling function is defined by Sutherland & Dopita (1993). Taking the rough estimate that $\Lambda \propto T_{\rm vir}^{-0.7}$ in this temperature regime, we find that,

$$\dot{M}_{\rm cool} \propto M_{\rm vir}^{0.43} \tag{2.10}$$

We can then find a relation between $M_{\rm vir}$ and $M_{\rm BH}$ in the case where $\dot{M}_{\rm heat} = \dot{M}_{\rm cool}$ at the boundary where heating offsets cooling for the cooling flow regime,

$$\frac{\dot{M}_{\rm heat}}{\dot{M}_{\rm cool}} \propto \frac{M_{\rm vir}^{1/3} M_{\rm BH}}{M_{\rm vir}^{0.43}} \tag{2.11}$$

$$\frac{\dot{M}_{\rm heat}}{\dot{M}_{\rm cool}} \propto M_{\rm vir}^{-0.097} M_{\rm BH} \propto \mathrm{const.} \tag{2.12}$$

The resulting expression is:

$$M_{\rm BH} \propto M_{\rm vir}^{0.097} \tag{2.13}$$

for haloes in the cooling flow regime.

In the rapid infall regime, the cooling rate is described by Equation S7 in H15:

$$\dot{M}_{\rm cool} \propto M_{\rm hot} \propto M_{\rm vir}. \tag{2.14}$$

Doing a similar exercise as with the cooling flow regime, we can find the relation between the black hole mass and the virial mass where $\dot{M}_{\rm heat} = \dot{M}_{\rm cool}$,

$$\frac{\dot{M}_{\rm heat}}{\dot{M}_{\rm cool}} \propto M_{\rm vir}^{-2/3} M_{\rm BH} \propto {\rm const} \tag{2.15}$$

$$M_{\rm BH} \propto M_{\rm vir}^{2/3}. \tag{2.16}$$

Equations 2.13 and 2.16 represent the slopes of the approximate boundaries between galaxies that are dominated by heating via AGN radio-mode feedback and galaxies that are dominated by cooling in one of two regimes on a $M_{\rm BH}$-$M_{\rm h}$ plot.

In Figure 2.1 we show the $M_{\rm BH}$-$M_{\rm h}$ plot for a randomly-selected, representative 0.2% of the entire central galaxy population at $z = 0$ in H15. Using the selection criteria described in Section 2.3.2, we show the star-forming and quiescent populations in blue and red dots, respectively. The black arrow points to the black hole mass below which the MS's black hole mass function begins to differ from that of the MS-II due to resolution effects. The dotted vertical line represents the approximate boundary between the rapid infall regime at low halo masses and the cooling flow regime at high halo masses. Finally, we include the slopes we analytically derived above with the black dashed lines for the two different regimes. This line represents the area

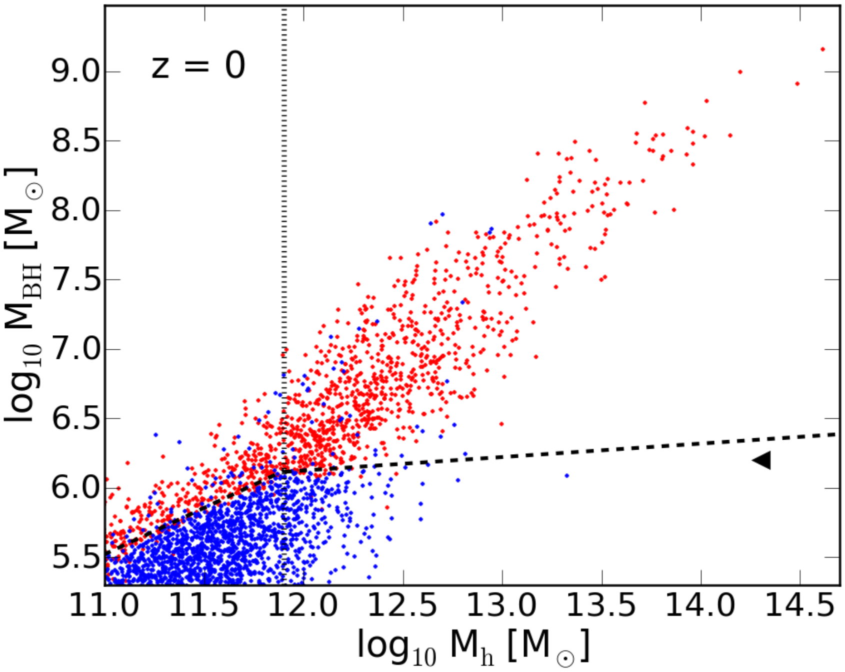

Figure 2.1: Black hole mass as a function of halo mass for 0.2% of all central galaxies at $z = 0$ in H15. Each point represents a galaxy where blue and red indicate star-forming and quiescent galaxies, respectively. The dashed lines represents the *heating-cooling equilibrium boundary* described in Section 2.4. The vertical dotted line represents the approximate transition between two modes of gas cooling: a rapid infall and a cooling flow regime. The black arrow points to the black hole mass below which resolution effects begin to show up as differences between the black hole mass functions in the MS (shown here) and MS-II.

where AGN heating balances the cooling of hot gas onto the central galaxy, or what we will call the *heating-cooling equilibrium boundary.*

We note that black hole mass and halo mass are broadly correlated. In addition, we see a fairly clear boundary between those that are star-forming and those that are quiescent. This boundary between blue and red dots is described well by our analytic approximation of the slopes shown with dashed lines. We note that the boundary is in the same location whether we use the MS or MS-II, regardless of the resolution effects below black hole masses $\sim 10^{6.2}$ $M_{\odot}$. It is clear that, to a good approximation, a galaxy is quenched once heating via AGN feedback dominates over gas cooling.

This behavior is characteristic of the H15 model, but we assert that any model which simulates the cessation of star formation by balancing AGN energy input against cooling will result in a qualitatively similar behavior. In these models the cessation of star formation should be a function of black hole mass and halo mass, similar to H15's formulation.

While the populations of quiescent and star-forming galaxies are quite distinct, there is a small number of star-forming galaxies that lie above the heating-cooling equilibrium boundary. These galaxies account for about 1.3% of the star-forming galaxy population. This scatter is a result of the time-scale in which AGN feedback effectively quenches a galaxy. These galaxies have either recently grown their black hole by a large amount or were already quiescent with a large black hole but were 'revived' briefly in terms of star formation activity as a result of a merger with a gas-rich companion. The fact that so few data points overlap between the two populations in this plot demonstrates that quenching via AGN heating occurs on fairly short time-scales. It takes ∼0.5–1.5 Gyr for most Milky Way-mass galaxies to quench to a sSFR an order of magnitude below our sSFR cut (See Section 2.3.2). Additional scatter is introduced since we made several simplifying assumptions in the above formulation of these boundaries that may fail in significant ways for individual galaxies.

Even with this scatter, there is excellent agreement between our analytic approximation of the slopes for the equilibrium boundary and the actual boundary between star-forming and non-star forming galaxies. As a result, we see that halo mass and black hole mass work together on relatively short time-scales in order to prevent hot gas from cooling onto the galaxy and forming stars. We note that in H15 AGN feedback does not fundamentally depend on stellar mass. Therefore, unless there is a unique mapping between stellar mass and either halo mass or black hole mass, a galaxy's stellar mass may not provide a good characterization of its star formation properties. This has the potential to introduce a significant amount of variation in the growth histories of quenched galaxies. In the following sections, we will address specifically how the stellar mass growth is parametrized first in terms of the halo mass and finally in terms of the black hole mass.

2.5 Scatter in Milky Way-mass Galaxy Growth Histories

Now that we have described the physical drivers of galaxy growth and quenching in H15, we turn to how Milky Way-mass galaxies grow. We begin by exploring the evolution of the relation between the stellar masses of these systems and their halo masses. An increasingly popular tool in this respect has been the stellar mass-halo mass (SMHM) relation which maps these two parameters onto one another (Yang et al., 2009; Conroy & Wechsler, 2009; Guo et al., 2010; Moster et al., 2010; Behroozi et al., 2010; Leauthaud et al., 2012; Behroozi et al., 2013). The amount of scatter in this relation quantifies the variety of stellar masses that can be contained within a halo of a given mass or the variety of halo masses which can host a central galaxy of a certain stellar mass. Halo occupation techniques that link these two parameters in order to create empirical models for the galaxy distribution have relied on the assumption that this mapping is simple. In this section, we begin to explore and challenge this assumption by analysing in detail the scatter in this relation within the H15 model. In addition, we will use Milky Way-mass galaxy growth histories in the context of this model as a case study to further explore how individual galaxies evolve with respect to the SMHM relation.

2.5.1 The Stellar Mass-Halo Mass Relation

The top two panels on the left of Figure 2.2 show the stellar mass plotted against the halo mass of 0.2% of all central galaxies in the H15 simulation for $z = 0$ and $z = 2.07$, where gray dots denote individual central galaxies in H15. The purple lines represent the median (solid) and 68 percentile scatter (dashed) of these data, calculated using 100% of the entire central galaxy population to have accurate values for the median and the scatter. We note that this plot includes observational errors in the stellar masses as described in Section 2.3.

First we note the emergence of a nearly constant stellar mass population towards high halo masses at $z = 0$. We find that while the scatter in stellar mass is relatively uniform for all halo masses, the scatter in halo mass increases strongly with increasing stellar mass. This signals a change in stellar mass build-up for central galaxies as they move into different mass regimes. The significant scatter in this relation is important to note when performing studies of galaxy growth since it likely originates from physical mechanisms, such as quenching, which can affect stellar mass growth within dark matter haloes.

In order to visualize the efficiency of stellar mass build-up of different sized haloes, we plot the stellar mass-halo mass ratio against the halo mass at $z = 0$ and 2.07 in the bottom two panels on the left of Figure 2.2. At low masses, the ratio of stellar mass to halo mass grows with halo mass up to about $\sim 10^{12}$ $M_{\odot}$, at which point the ratio decreases. This turnover point has often been defined as the halo mass at which the star formation efficiency peaks. Previous studies have attempted to pinpoint a certain halo mass or stellar mass-halo mass ratio at which this peak star formation

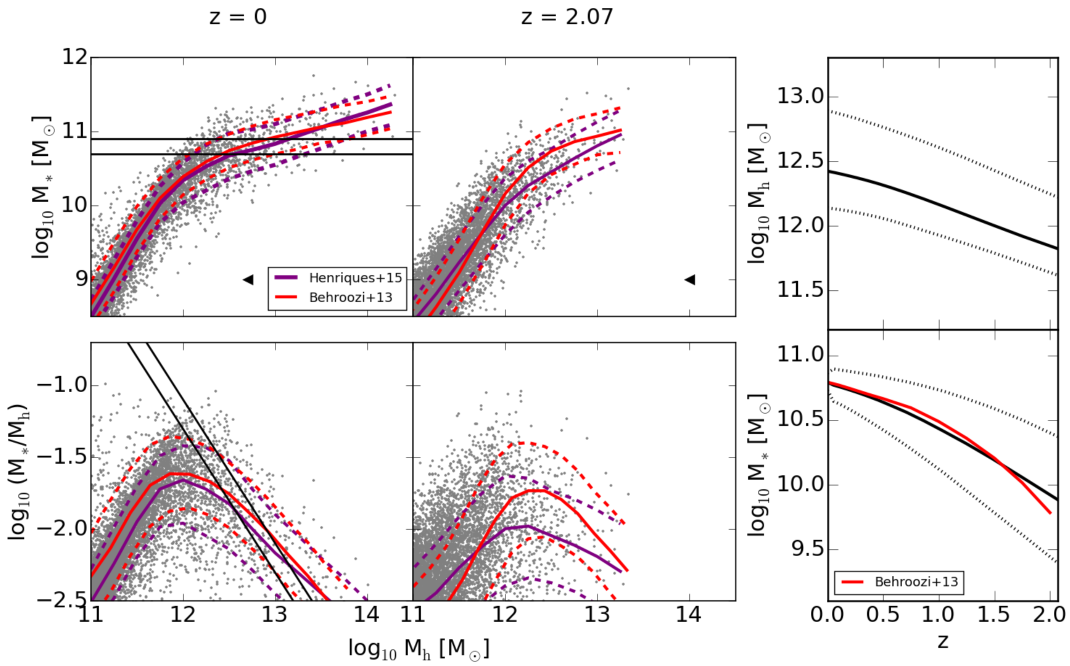

Figure 2.2: *Left*: The SMHM relation at $z = 0$ and $z = 2.07$ for 0.2% of all central galaxies in H15. The upper two plots show stellar mass, M_*, as a function of halo mass, M_h, and the bottom two plots show M_*/M_h as a function of M_h. Each gray point represents one galaxy in the H15 model. The purple lines represent the median (solid) and 68 percentile scatter (dashed) of 100% of the central galaxy population in H15, respectively. The red lines represent the median (solid) and 68 percentile scatter (dashed) of data from the Behroozi et al. (2013) model, respectively. The black solid lines represent the range of Milky Way-mass stellar masses we use in this work. The black arrows point to the stellar mass below which resolution effects begin to take place in the MS. *Right*: The upper and lower panels represent the halo and stellar mass tracks for all main progenitors of Milky Way-mass galaxies out to $z = 2.07$ for the H15 model, respectively. The solid black line in each plot shows the median at each redshift while the dotted black lines encompass 68 per cent of the tracks. The red line in the plot showing stellar mass tracks is the median progenitor track from the Behroozi et al. (2013) model.

efficiency occurs in order to better understand how it evolves (Conroy & Wechsler, 2009; Leauthaud et al., 2012; Moster et al., 2013; Behroozi et al., 2013; Durkalec et al., 2015). If we choose 10^{12} $\mathrm{M}_{\odot}$ to be the halo mass at which the relation 'turns over' at $z = 0$, we see in the bottom left panel of Figure 2.2 that while some of these mid-sized haloes have been relatively efficient at building up their stellar mass, many have low M_*/M_h ratios. At this halo mass, we find $\log_{10}(M_*/M_\mathrm{h}) = -1.66^{+0.24}_{-0.30}$. Given this large scatter, defining just one point at which the efficiency peaks is a poor characterization of galaxy assembly histories.

In order to compare the scatter in H15's SMHM relation to another model, we also show the median and 68 percentile range of the SMHM relation for the Behroozi et al. (2013) model (solid and dashed red lines, respectively) in both of these visualizations. Behroozi et al. (2013) carried out a careful, empirically-motivated analysis with the goal of estimating the SMHM relation and its scatter as a function of redshift from $z = 8$ to the present day. In addition to the intrinsic sources of scatter implemented by Behroozi et al. (2013), we add observational scatter to this model's stellar masses as per Equation 11 in Behroozi et al. (2013). Even though by $z = 2$ these models differ significantly, we find that the scatter in the empirical model is comparable to the scatter we find in the H15 model.

2.5.2 The General Population of Milky Way-mass Galaxies

We now turn to Milky Way-mass galaxies and their main progenitors as a case study to better understand the evolution of the SMHM relation, especially in the context of its scatter. This exercise will also help gain insight into the variety of pathways that result in a central galaxy with the stellar mass of the Milky Way at $z = 0$.

The solid black lines in the leftmost panels of Figure 2.2 indicate lines of constant stellar mass at 5×10^{10} and 8×10^{10} $\mathrm{M}_{\odot}$. In the rightmost panels of Figure 2.2, we

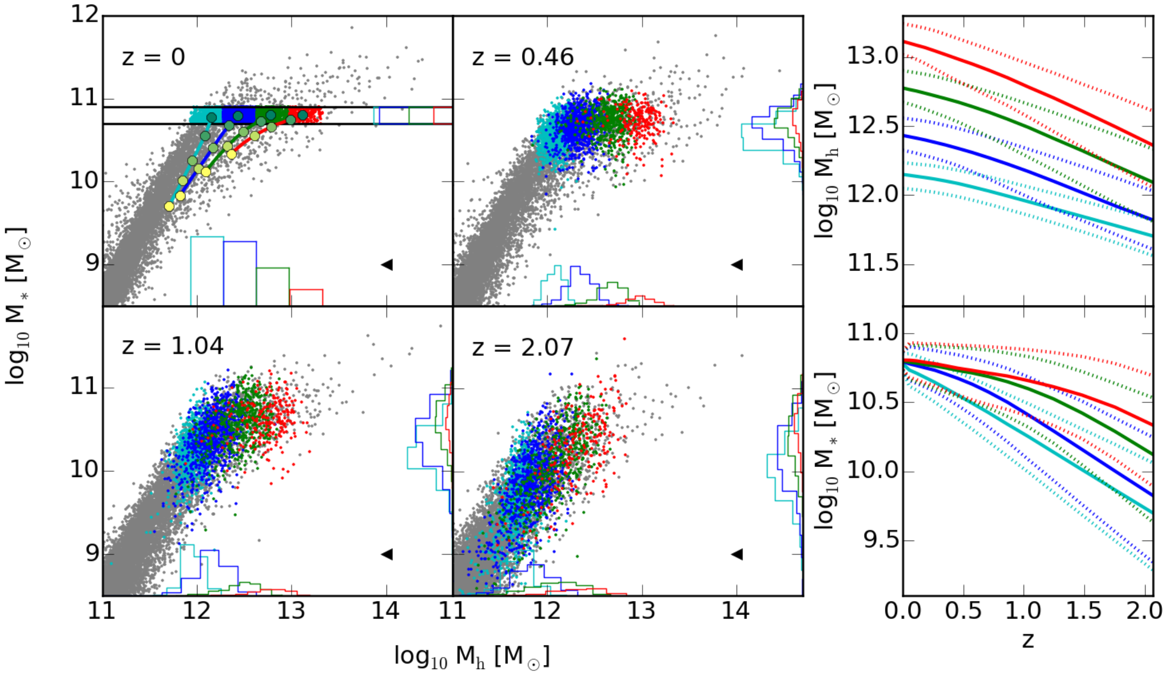

Figure 2.3: *Left*: The SMHM relation for Milky Way-mass galaxies at $z = 0$, 0.46, 1.04, and 2.07, where the gray dots represent the 0.2% of the total galaxy population in H15. The colored points represent 2.5% of all main progenitors of present-day Milky Way-mass galaxies split into four halo mass bins, where the boundaries are at $M_{\rm h} = 10^{12.5}$, $10^{12.9}$, and $10^{13.3}$ $\rm M_\odot$. Each panel also shows the histogram of the distributions for each group in stellar mass and halo mass on the right and bottom edges of the plots, respectively. These histograms are scaled with respect to the total number of Milky Way-mass galaxies. In the $z = 0$ panel, we track the evolution of the median stellar and halo mass of the main progenitors of these galaxies in time. The large colored circles represent the median values at $z = 0$, 0.46, 1.04, 1.48, and 2.07 where the circles go from green to yellow with increasing redshift. The black arrows point to the stellar mass below which resolution effects begin to take place in the MS. *Right*: The upper and lower panels represent the halo and stellar mass tracks for all main progenitors of Milky Way-mass galaxies split into four halo mass bins at $z = 0$. The solid line in each plot shows the median at each redshift while the dotted lines encompass 68 per cent of the tracks.

take all central galaxies at $z = 0$ with stellar masses in this range and trace out the median and 68 percentile range of halo and stellar masses of their main progenitors out to $z = 2.07$ in the upper and lower panels, respectively. We note that these plots include observational errors in stellar mass as described in Section 2.3.

First, we note a large range of halo masses for Milky Way-mass galaxies at all redshifts, a trend also seen in the upper leftmost panel where the scatter in the SMHM relation at Milky Way masses is quite large. While the 68 percentile range in halo masses stays roughly the same with a modest 0.15 dex decrease at high redshifts, our narrow range of present-day stellar masses increases from 0.13 to 0.98 dex by $z = 2.07$. This shows that there is a wide diversity of ways to become a Milky way-mass galaxy, where some grow more than twenty times their stellar mass while others grow very little.

One of our goals is to understand the origin of this diversity of growth histories. In Figure 2.3, we show the SMHM relation at $z = 0$, 0.46, 1.04, and 2.07. The gray dots represent 0.2% of all central galaxies and the colored dots show 2.5% of all main progenitors of Milky Way-mass galaxies at the present day. The different colors within this latter group represent Milky Way-mass galaxies within different halo mass ranges at $z = 0$. Evolving them backwards into their main progenitor stellar and halo masses results in the distributions shown both in the colored dots and in the histograms in each panel. The median evolutionary tracks of each halo mass bin are shown in the top left panel in colored lines where each circle represents the median value at $z = 2.07$, 1.48, 1.04, 0.46, and 0, color coded from yellow to green, respectively.

We note that galaxies with different present-day halo masses exhibit different median growth tracks on the SMHM relation. Galaxies with less massive haloes tend to grow rapidly in stellar mass towards the present day, whereas galaxies with more massive haloes had already formed a large fraction of their present-day stellar mass by

$z = 2.07$ and grew very little afterwards. This is more clearly shown in the rightmost panels of Figure 2.3, where we plot the halo and stellar mass evolution of these four Milky Way-mass galaxy groups split by halo mass in the upper and lower panels, respectively. As before, the solid lines indicate medians and the dotted lines indicate the 68 percentile scatter. This illustrates an important finding of our study – there is a great deal of correlation between growth history and halo mass in the H15 model, in the sense that more massive haloes tend to grow most of their stellar mass earlier. Such ‘anti-hierarchical’ behavior has long been inferred from observational datasets (e.g. Thomas et al., 2005) and emerges naturally from the H15 model.

While stellar mass at high redshift does correlate slightly with growth history for Milky Way-mass galaxies, as is shown in the vertical histograms, we also see that halo mass does a much better job at differentiating between distinct pathways of galaxy growth in the SMHM relation. These trends will provide the basis upon which we will continue our study of this galaxy population with respect to their star formation activity.

2.6 The Star-forming and Quiescent Populations of Milky Way-mass Galaxies

Now that we have quantified the scatter in the stellar and halo mass growth histories of Milky Way-mass galaxies, we use the selection criteria described in Section 2.3.2 to divide our Milky Way-mass galaxy sample into star-forming and quiescent galaxies at the present day. Complementary to the right panel of Figure 2.2, the right panel of Figure 2.4 shows the median and 68 percentile range of halo and stellar masses of the main progenitors of these groups out to $z = 2.07$ in the upper and lower panels, respectively. In our sample, 36% of galaxies are star-forming at $z = 0$ while 64% are quiescent. Although these two populations do exhibit significant differences in growth histories, we note the large overlap in stellar masses between the present-day star-forming and quiescent populations. In contrast, the growth histories of halo masses are quite distinct, where haloes that host galaxies that will quench by $z = 0$ are generally more massive at all redshifts.

A main goal of our study is to understand the scatter of stellar mass growth histories of Milky Way-mass galaxies. While splitting our sample population into star-forming and quiescent descendants does hint at the origin of much of this scatter, there is a significant amount of it still unaccounted for in the evolutionary tracks of these two groups. We first comment on the scatter in star-forming galaxies' growth histories and then focus on that of the quiescent galaxies' growth histories.

2.6.1 Scatter in Growth Histories of Star-Forming Galaxies

Figure 2.4 shows significant scatter in stellar mass growth histories of currently star-forming Milky Way-mass galaxies, albeit less so than those which are currently quiescent. A good deal of this scatter originates from 'observational error' in M_* that we impose on the 'true' stellar masses to match the observed stellar mass functions, as discussed in Section 2.3. Removing these 'observational stellar mass errors' diminishes the total range of these progenitor stellar masses from 0.78 to 0.58 dex at $z = 2.07$ and 0.49 to 0.32 dex at $z = 1.04$. While the scatter in growth histories from 'observational error' does not reflect true changes in the mass of the model galaxies, it is crucial to account for in studies attempting to connect galaxy populations at different cosmic epochs.

The remaining amount of scatter in the tracks for star-forming galaxies shown in Figure 2.4 comes from the physical prescriptions used in H15. The models for gas cooling, star formation, and feedback depend on the cold gas mass, the radius of the gas disc, and the dynamical time of the disc. The cold gas mass is largely a function of halo mass and halo growth history, the radius of the gas disc depends on

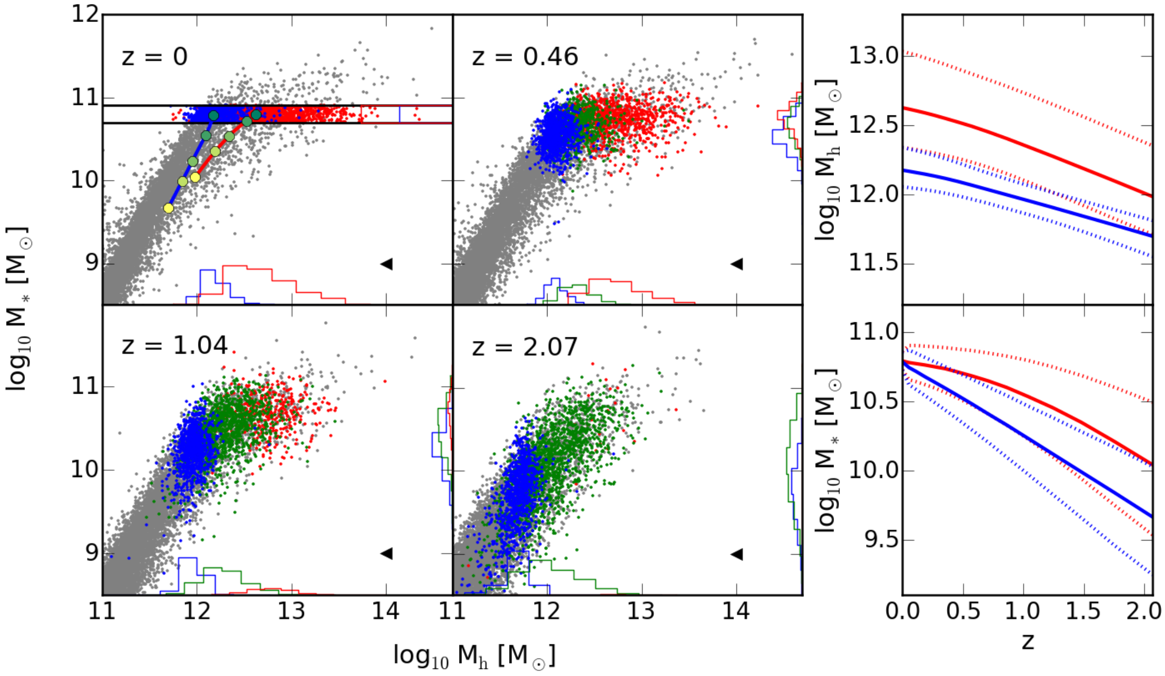

Figure 2.4: *Left*: The SMHM relation for Milky Way-mass galaxies at $z = 0$, 0.46, 1.04, and 2.07, where the gray dots represent the 0.2% of the total galaxy population in H15. The colored points represent 2.5% of all main progenitors of present-day Milky Way-mass galaxies, where blue dots represent galaxies that have remained star-forming since $z = 2.07$, green dots represent galaxies that are star-forming at the given redshift but will become quiescent by the present day, and red dots represent galaxies that have quenched and that will remain quiescent up to the present day. Each panel also shows the histogram of the distributions for each group in stellar mass and halo mass on the right and bottom edges of the plots, respectively. These histograms are scaled with respect to the total number of Milky Way-mass galaxies. In the $z = 0$ panel, we track the evolution of the median stellar and halo mass of the main progenitors of galaxies that have always been star-forming in blue and galaxies that become quiescent by the present day in red. The large colored circles represent the median values at $z = 0$, 0.46, 1.04, 1.48, and 2.07 where the circles go from green to yellow with increasing redshift. The black arrows point to the stellar mass below which resolution effects begin to take place in the MS. *Right*: The upper and lower panels represent the halo and stellar mass tracks for all main progenitors of present-day star-forming and quiescent Milky Way-mass galaxies in blue and red, respectively. The solid line in each plot shows the median at each redshift while the dotted lines encompass 68 per cent of the tracks.

the spin parameter, and the dynamical time depends on the maximum halo velocity and therefore the concentration of the halo. Consequently, an intrinsic diversity of values for these halo quantities imposes scatter in star formation histories at a given halo mass, driving the majority of the scatter in growth histories of star-forming galaxies seen in Fig 2.4. We note that this physical source of scatter affects both the star-forming and quiescent populations in the model.

2.6.2 Scatter in Growth Histories of Quiescent Galaxies: Staggered Quenching

In contrast to galaxies that have always been star-forming, the scatter in evolutionary tracks of quiescent galaxies is particularly pronounced. At one extreme, a currently quiescent galaxy could follow the evolutionary track of a star-forming galaxy up until relatively recent times, only to diverge from that track at $z < 0.5$. At the other extreme, a quiescent galaxy could follow the evolutionary track of a galaxy that grows rapidly at $z > 2.07$ and very little thereafter. This results in a large overlap region where star-forming galaxies and quiescent galaxies at the present day could have had similar stellar masses at earlier times. While star-forming galaxies do exhibit scatter, their growth histories match in the sense that they more steadily grow their stellar mass towards the present day, rather than exhibit a stunted growth. In order to understand these trends we must understand how the stellar mass growth of the quiescent population is affected by the cessation of star formation.

To illustrate, we show the SMHM relation for 2.5% of all main progenitors of present-day Milky Way-mass galaxies at $z = 0$, 0.46, 1.04, and 2.07 in the left panels of Figure 2.4. Blue dots represent galaxies that have remained star-forming since $z = 2.07$, green dots represent galaxies that are star-forming at the given redshift but will become quiescent by $z = 0$, and red dots represent galaxies that have quenched and that will remain quiescent up to the present day. In the top left panel of Figure 2.4, we

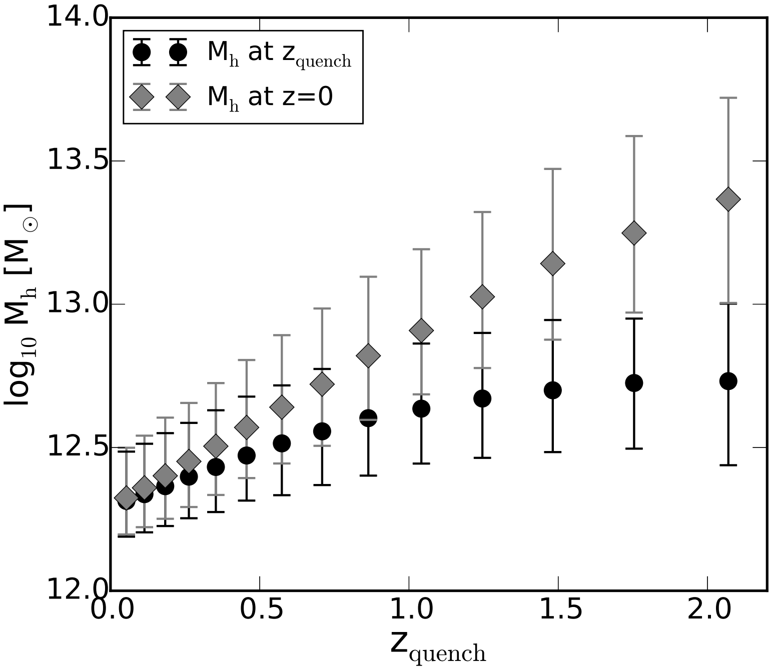

Figure 2.5: Halo mass as a function of the quenching redshift of all Milky Way-mass galaxies in the H15 model. Grey diamonds represent the median present-day halo mass, $M_{\mathrm{h}}(z = 0)$, of galaxies that quenched at each redshift while black circles represent the median halo mass of those same galaxies at the redshift they quenched, $M_{\mathrm{h}}(z = z_{\mathrm{quench}})$. The error bars represent the 68 percentile scatter in halo masses for galaxies that quenched at each respective redshift.

plot median tracks on the SMHM relation of Milky Way-mass galaxies that remain star-forming in blue and Milky Way-mass galaxies that have become quiescent by $z = 0$ in red, where each circle represents the median value at $z = 2.07$, 1.48, 1.04, 0.46, and 0 color coded from yellow to green.

Almost all Milky Way-mass galaxies were star-forming at $z = 2.07$, even those that will become quiescent by the present day. We also note that the quiescent population grows gradually, where galaxies in more massive haloes quench earlier than those in lower mass haloes.

In order to probe this behavior more directly, we evaluate the quenching redshift of all central Milky Way-mass galaxies that are quiescent at $z = 0$. In Figure 2.5, we plot the median and 68 percentile range of present-day halo masses against the redshift at which these galaxies quenched as gray diamonds. In black circles we plot the halo masses at the redshift at which the galaxy quenches against the quenching redshift. The halo mass difference between the gray diamonds and the black circles show us the median halo mass growth since the time of quenching. We see a scattered but clear correlation between the present-day halo masses of galaxies and the redshift at which these galaxies quench. We call this behavior *staggered quenching*. This demonstrates that present-day high mass haloes tend to have quenched earlier than present-day lower mass haloes, showing that galaxies have undergone different growth histories as a function of their halo masses.

This correlates well with the behavior we saw in Section 2.5.2, where a population with a large range in halo mass points to a large diversity of growth histories. In the upper right panel of Figure 2.4, we note the much larger range of halo masses for those galaxies that have become quiescent by the present day and the much narrower range of halo masses for those galaxies that have remained star-forming, where once again these ranges encompass 68 per cent of the data. The larger diversity of halo masses for today's quiescent galaxies implies they also have a larger variation of growth histories than their star-forming counterparts, at least in the context of this model.

While halo mass broadly correlates with quenching times in this model, we have already shown in Section 2.4 that black hole mass also plays a vital role in heating the atmospheres of galaxies via AGN radio-mode feedback. In order to explore this further, in Figure 2.6 we plot halo mass, stellar mass (without observational scatter), black hole mass, and specific star formation rate tracks for three representative Milky Way-mass galaxies that quenched at $z = 0.18$, 0.7, and 1.47 in solid, dashed, and dotted lines, respectively. The black dots in the sSFR tracks indicate the last redshift at which this galaxy is classified as star-forming.

In this visualization, we see the effect of staggered quenching where galaxies in larger haloes quench earlier. While this trend exists, the significant mass growth of the central black hole for two of these systems directly coincides with a significant decrease in the galaxies' sSFR. [2] This demonstrates the limits of looking only at halo mass and staggered quenching in order to explain the onset of quiescence. In the following section, we focus on how black hole mass, halo mass, and quenching are connected with regards to Milky Way-mass galaxies in H15.

2.7 Black Hole Mass Dependence

In H15's framework, mergers cause most of the black hole mass growth. A supermassive black hole is formed at the centre of a galaxy via quasar-mode feedback after a merger, whether it be major or minor. The more equal the merger ratio and the more cold gas there is in the colliding galaxies, the more massive the initial black hole. In contrast, radio-mode AGN feedback adds a negligible amount of mass onto the black hole (See Croton et al. 2006, Figure 3). A consequence of this is that black hole growth is completely determined by the merger histories of galaxies, which are largely stochastic by nature. This connection between the black hole and halo mass has important implications for how Milky Way-mass galaxies quench in H15.

In order to incorporate the importance of the central black hole within our discussion, we return to the black hole mass-halo mass relation. In Figure 2.7, we show black hole mass as a function of halo mass for 0.2% of all centrals (gray) and for 2.5% of all main progenitors of Milky Way-mass galaxies (colored) at $z = 0$, 0.46, 1.04, and 2.07. As before, blue dots represent galaxies that have remained star-forming since $z = 2.07$, green dots represent galaxies that are star-forming at the given redshift but

---

[2] We note that while the galaxies that quench at $z = 0.18$ and 0.7 grow their black hole mass by a large amount in a very short time, this is not representative of all Milky Way-mass galaxies since some do become quiescent as their central black hole grows more gradually. This is the case for the galaxy that quenches at $z = 1.47$ – its black hole is already very large and, as a result, halts its star formation early on without the need for significant black hole mass growth. We discuss this phenomenon in more detail in Section 2.7.

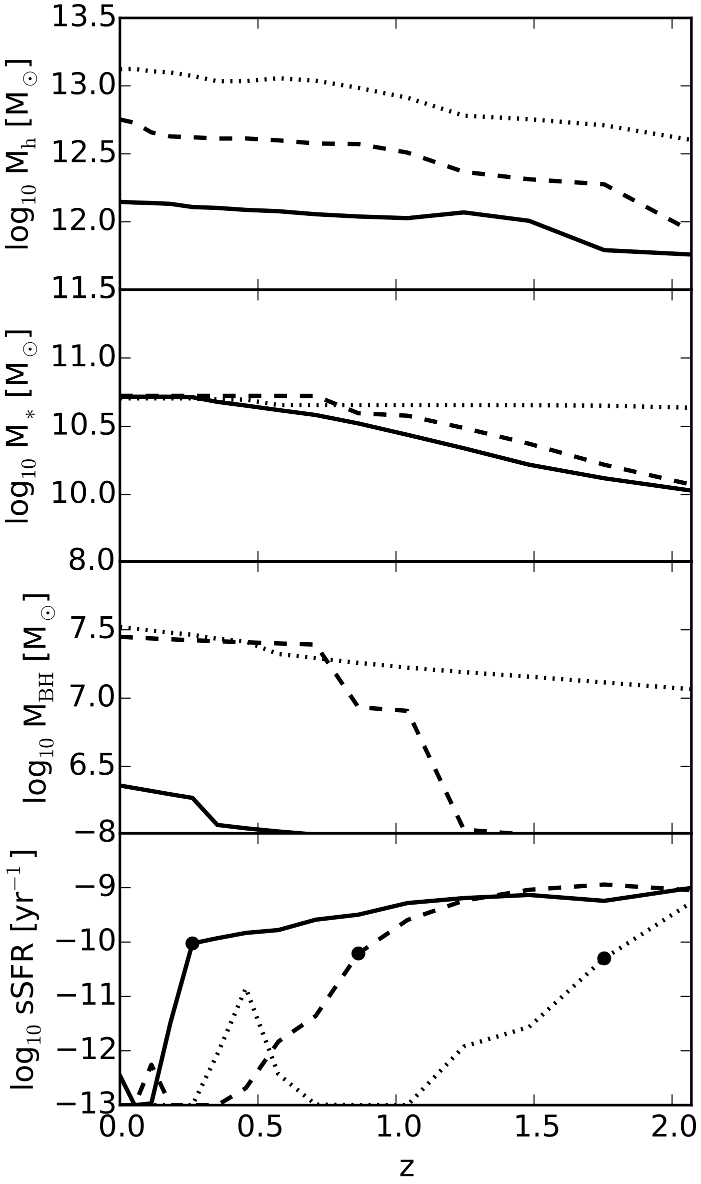

Figure 2.6: Halo mass, stellar mass, black hole mass, and specific star formation rate tracks for three representative Milky Way-mass galaxies in the H15 model. Each galaxy is denoted by either a solid, dashed, or dotted line. The black dots in the sSFR tracks represent the last redshift at which they are star-forming according to our definition (See Section 2.3.2).

will become quiescent by the present day, and red dots represent galaxies that have quenched and that will remain quiescent up to the present day. The black arrows point to the black hole mass below which the MS's black hole mass function begins to differ from that of the MS-II due to resolution effects. We note that even with this limitation, the results for Milky Way-mass galaxies in both the MS and MS-II are qualitatively similar. The histograms at each redshift represent the distribution of halo masses for those galaxies that have a black hole mass of zero in the MS[3]. We find that all central galaxies with no central black hole are star-forming, providing further evidence that the black hole is a crucial ingredient to quiescence. In addition, we note that galaxies that are star-forming but will become quiescent (green dots) occupy a region between those that will remain star-forming (blue) and those that have already become quiescent (red).

In this visualization, the heating-cooling equilibrium boundary introduced in Section 2.4 can be seen as the boundary between red and blue dots at $z = 0$ and red and green dots at higher redshifts. We note that Milky Way-mass galaxies in the H15 model quench almost exclusively in the cooling flow regime, leading to a shallow boundary between heating-dominated and cooling-dominated Milky Way-mass systems on a $M_{\rm BH}$-$M_{\rm h}$ plot. This means that, at a given redshift, quiescence is primarily a function of black hole mass. The boundary evolves in time, eventually decreasing the black hole mass thresholds for quiescence at lower redshifts. The decreasing threshold is mainly because H15 designed the model so that $\dot{M}_{\rm cool}$ is inversely proportional to the dynamical time and the virial radius of the halo, both of which depend on the Hubble parameter, $H(z)$. This dependence on $H(z)$ results in $\dot{M}_{\rm cool}$ being much larger at higher redshift while the AGN heating term stays almost constant due to its weak dependence on the virial mass. While the slope of the boundary stays the same – defined by galaxies being in the cooling flow regime at these halo masses –

---

[3] In the MS-II, such galaxies have low, non-zero black hole masses as a consequence of being able to resolve small mergers. This is not the case in the MS.

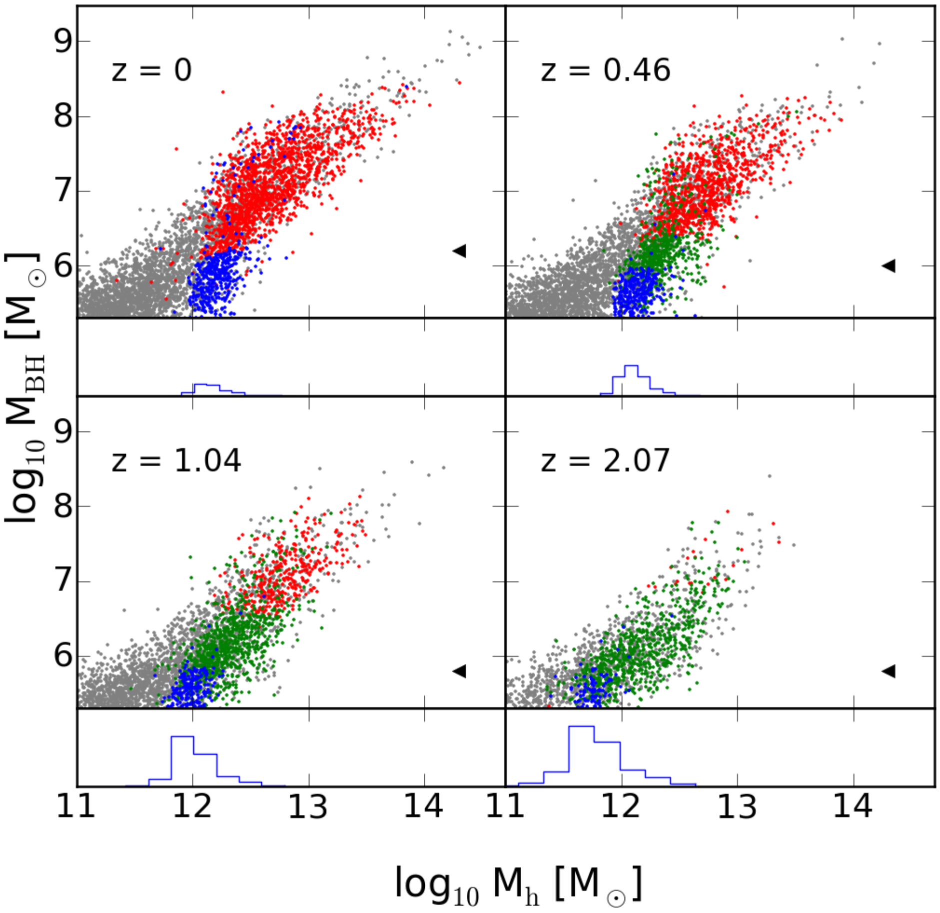

Figure 2.7: The black hole mass-halo mass relation at $z = 0$, 0.46, 1.04, and 2.07 where gray dots represent 0.2% of the whole central galaxy population in H15. The colored dots represent 2.5% of all main progenitors of Milky Way-mass galaxies; blue dots represent those that have remained star-forming since $z = 2.07$, green dots represent galaxies that are star-forming at the given redshift but will become quiescent by the present day, and red dots represent galaxies that have quenched and that will remain quiescent up to the present day. The histograms represent the distribution of halo masses for those galaxies that have a black hole mass of zero. We note that these galaxies are only star-forming; quiescent central galaxies do not have zero-mass black holes.

the normalization changes with redshift.

This has important implications for the central galaxy population at $z = 0$ since cooling becomes increasingly less effective at late times for these model galaxies. We note that the shallow equilibrium boundary derived in Equation 2.13 in Section 2.4 means halo mass growth is not the fundamental reason for quenching in this model. The reason why there is a correlation between halo mass and quiescence (see Section 2.6.2) is because of the positive correlation between halo and black hole mass. As the equilibrium boundary decreases, lower mass haloes are able to quench as a result of this positive correlation. This effectively results in the staggered quenching behavior we saw in Section 2.6.2.

In addition, this means that a galaxy does not necessarily need to drastically increase its black hole mass in order to quench since the dependence on the Hubble parameter naturally evolves the black hole mass threshold for quiescence to lower values with decreasing redshift. This results in some Milky Way-mass systems in H15 that already have black holes large enough that they do not need to grow anymore in order to quench – this is the case for the galaxy that quenches at $z = 1.47$ in Figure 2.6. Instead of the rapid black hole mass growth seen in the other two galaxies as a result of a major merger, this galaxy quenches mainly as a result of a decreasing cooling efficiency. At earlier times cooling is intense enough to offset AGN heating. As the efficiency of cooling drops, however, the heating effectively stops star formation. These galaxies may help interpret quiescent galaxies with large bulges but large or dominant disks that do not show evidence of a recent major merger. In terms of Milky Way-mass galaxies, we find that 65.9% of this population shows the onset of quiescence concurrently with a black hole growth of twofold or greater and 33.2% shows the onset of quiescence with an order of magnitude or greater growth in black hole mass. Nevertheless, for Milky Way-mass galaxies, systems which show a more gradual black hole growth into quiescence are not negligible in this model.

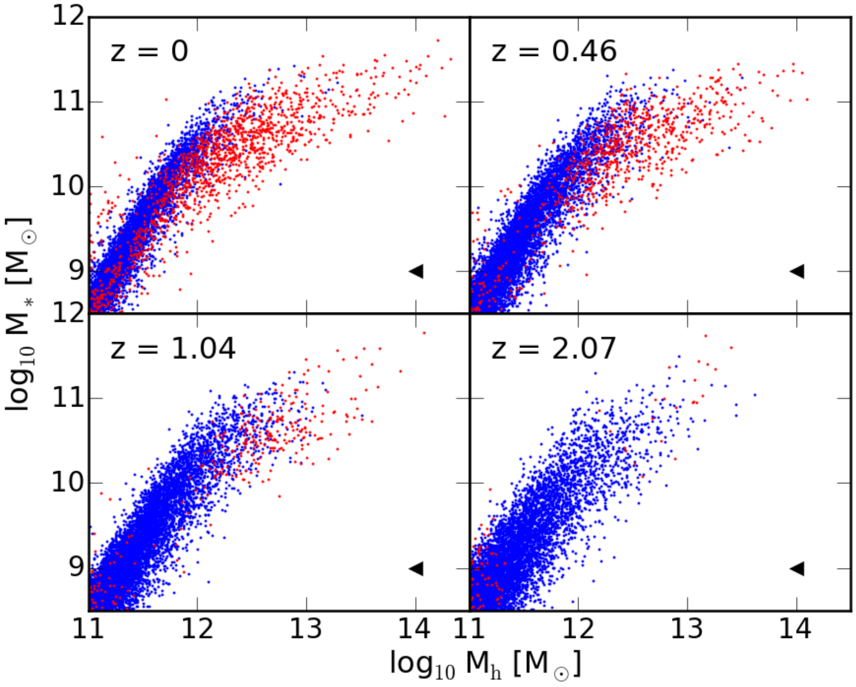

Figure 2.8: The SMHM relation for 0.2% of all central galaxies split into star-forming (blue) or quiescent (red) at $z = 0$, 0.46, 1.04, and 2.07. The black arrows point to the stellar mass below which resolution effects begin to take place in the MS.

2.8 Bimodality in the SMHM Relation

In the previous section, we discussed what causes the growth of the quiescent Milky Way-mass galaxy population in the context of this model. In this section, we move on to how this might affect the entire central galaxy population. In Figure 2.2, we showed the evolution of the SMHM relation between $z = 2.07$ and $z = 0$. In Figure 2.8, we show the evolution of the SMHM relation since $z = 2.07$ where we have split 0.2% of the whole central galaxy population into star-forming (blue dots) and quiescent (red dots) at each redshift.

Much like what we saw in Section 2.6 for the Milky Way-mass galaxy population, the majority of galaxies at $z = 2.07$ are star-forming with a gradual increase in the number of quiescent galaxies at each subsequent redshift. We can also see a familiar correlation between higher mass haloes and earlier quenching times in the whole central population. In fact, in this model, the high mass end of the SMHM relation seems to form solely as a result of quenching. If we look at only star-forming galaxies, we see a single power-law distribution with scatter. The quenched population evolves off to the right of the star-forming 'main sequence' of the SMHM relation. Although these two populations are fairly distinct, there is not a specific halo mass at which central galaxies are quenched. This reflects the importance of black hole mass in quenching. In lower mass haloes where the rapid infall regime of cooling operates, we expect halo mass growth to play a more important role in quenching since the slope of the heating-cooling equilibrium boundary causes quenching to be a stronger function of halo mass (See Section 2.4).

In addition, the emergence of a shallow distribution at the high halo mass end of the SMHM relation at late times as a result of quiescence has important implications for studies attempting to link galaxy stellar masses to their host halo masses. In H15, the star formation efficiency of galaxies as a function of halo mass increases until these galaxies become quiescent, accounting for a peak in a plot showing the stellar mass–halo mass ratio versus halo mass (See the lower left panel of Figure 2.2). Quiescence causes M_*/M_h to decrease after a certain point because stellar mass growth via star formation stops while halo mass growth continues. This differs from previous studies that model an evolving SMHM relation with a smoothly varying star formation efficiency (e.g. Behroozi et al., 2013; Moster et al., 2013). We discuss the implications of this difference in greater detail in Section 2.10.

2.9 Observational Signatures of Quiescence

In an attempt to elucidate what physical mechanisms are behind quiescence, a number of efforts have explored trends in the fraction of quenched galaxies as a function of galaxy parameters using observational datasets at $z < 2$ (Schiminovich et al., 2007; Bell et al., 2012; Bluck et al., 2014a). As in this work, some have attempted to focus on central galaxies, either explicitly (e.g. Bell, 2008), or by noting that at Milky Way masses and above, most galaxies are centrals in their own haloes (e.g. Wuyts et al., 2011). Restricting our attention to parameters directly inferred from observations, the fraction of quenched galaxies appears to vary with stellar mass, stellar surface density within the half light radius or 1 kpc, inferred velocity dispersion ($\propto$ M/R), Sersic index, and bulge to total mass (B/T) ratio (Kauffmann et al., 2003; Bell et al., 2004; Franx et al., 2008b; Bell, 2008; Cheung et al., 2012; Bell et al., 2012; Lang et al., 2014; Bluck et al., 2014b). The broad consensus is that the degree of bulge domination appears to be the parameter with which quiescence varies the most strongly (e.g. Bluck et al., 2014b; Lang et al., 2014). Lang et al. (2014) explicitly compare with the Somerville et al. (2008, 2012, with developments by Porter et al. 2014) semi-analytic models, arguing that the observed strength of the correlations of quiescence with B/T ratio could come from a strong dependence of quiescence on the black hole mass, with galaxies that have more massive black holes being substantially more likely to be quiescent. In fact, Bluck et al. (2014a) found a correlation between the quiescent fraction and their black hole mass estimate, inferred by the joint consideration of bulge mass and velocity dispersion.

In Figure 2.9 we present visualizations of the quenching behavior in H15 for central galaxies as a function of stellar mass (left), halo mass (middle), and black hole mass (right). The top panels show the distributions of 0.2% of all central galaxies where star-forming galaxies are blue dots and quiescent galaxies are red dots. The bottom panels show the same axes but we plot the distributions for 2.5% of all main progenitors of Milky Way-mass galaxies in colored dots over 0.2% of the whole central population in gray dots. In these panels, as before, blue dots represent galaxies that have remained star-forming since $z = 2.07$, green dots represent galaxies that are star-forming at the given redshift but will become quiescent by the present day, and red dots represent galaxies that have quenched and that will remain quiescent up to the present day.

In the top panels we note the growth of the quiescent population as a function of redshift which was already seen in Figure 2.4 and 2.8. In accord with observations, the models show a broad and scattered correlation between quiescence and stellar mass, where at higher stellar masses the population is more quenched. Also in accord with observations is the wide range of star formation rates, centred largely on the mass of the Milky Way, where one has both quenched and star-forming central galaxies (e.g. Kauffmann et al., 2003).

In the centre panels one can see that quiescent galaxies tend towards higher halo masses, a trend that was already seen in Figure 2.4. An important implication here is that, at least in the context of this model, quenched galaxies with similar stellar masses as star-forming galaxies are likely to live in a substantially more massive dark matter haloes. This leads to the expectation that quenched galaxies at a given stellar mass have a considerably increased number and wider velocity distribution of satellite galaxies, a higher average weak lensing signal, a higher incidence of bright satellites/companions, and if globular cluster number scales with halo mass, a larger number of globular clusters. Many of these expectations are in qualitative accord with weak lensing measurements (Velander et al., 2014; Mandelbaum et al., 2016a) and globular cluster number and specific frequency (Hudson et al., 2014). In fact, Wang & White (2012) found that central galaxies with stellar masses larger than that of the Milky Way have a significantly larger number of satellites if the central is red in color, or quiescent, than if a galaxy of the same stellar mass is blue, or star-forming. These observations strongly suggest that quenched centrals do in fact live within larger dark matter haloes.

The upper and lower sets of plots at the far right show the relationship between SFR and black hole mass, showing that quiescent galaxies are expected to have more

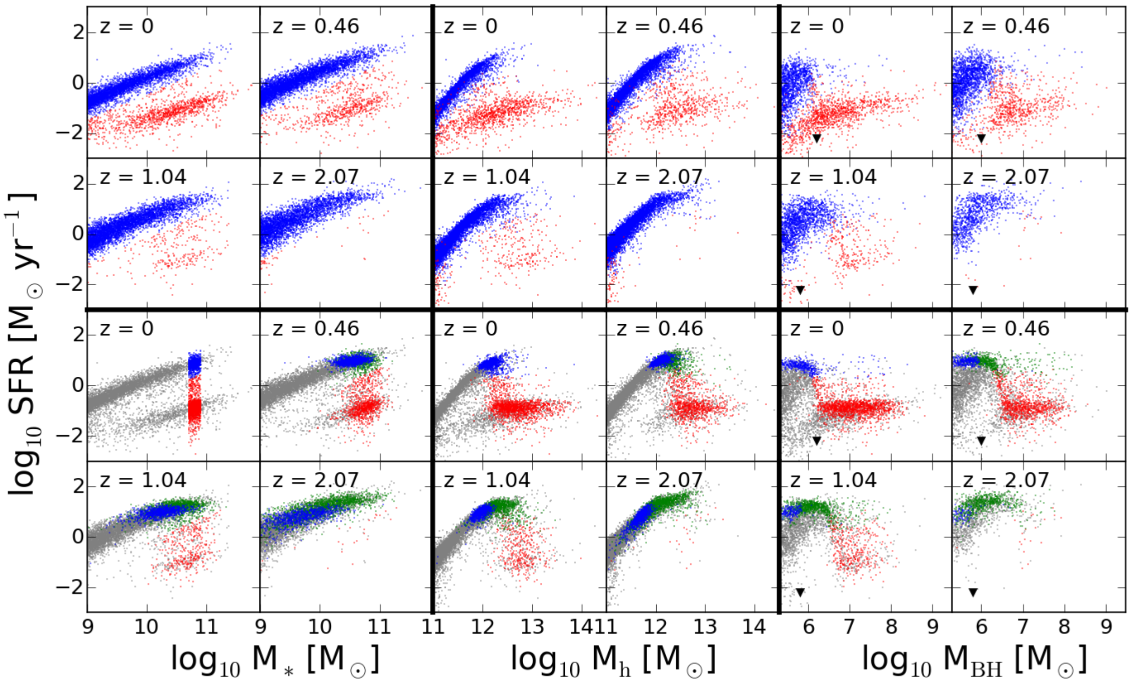

Figure 2.9: The star formation rate (SFR) as a function of stellar mass (left), halo mass (middle), and black hole mass (right) at $z = 0$, 0.46, 1.04, and 2.07. The top panels show 0.2% of the whole central population split into star-forming and quiescent galaxies at each respective redshift. The bottom panels show 0.2% of the central galaxy population in gray dots as reference and 2.5% of all main progenitors of Milky Way-mass galaxies in colored dots. Blue dots represent those Milky Way-mass galaxies that have remained star-forming since $z = 2.07$, green dots represent those that are star-forming at the given redshift but will become quiescent by the present day, and red dots represent those that have quenched and that will remain quiescent up to the present day. The black arrows point to the black hole mass below which the MS's black hole mass function begins to differ from that of the MS-II due to resolution effects.

massive black holes than star-forming galaxies, as is expected from our analysis in Section 2.4. We note that there is still some scatter between quiescence and black hole mass in the upper panel, with a tail of quenched galaxies having low black hole masses. This emphasizes one of the main messages of Figure 2.1 – that, in this model at least and likely in the universe, quiescence is a function of a number of physical parameters and joint consideration of two or more variables is likely to be important for illuminating the causes of quiescence.

In the lower panel, we present Milky Way-mass galaxies which have a narrow range in stellar mass but a large range of black hole and halo masses. For this range of halo masses, quenching is almost uniquely a function of black hole mass and there is a very narrow region of black hole masses where a galaxy's SFR plummets down to low values. This characteristic value of black hole mass reflects the shallow equilibrium boundary for galaxies in the cooling flow regime, as we explained in Section 2.7. The central galaxy population as a whole does not exhibit this behavior because it samples a much wider range of halo masses which include cooling via both the rapid infall and cooling flow regimes. While this provides a physical mechanism for quenching in this model, it is not clear whether this behavior is reflected in the observations.

2.10 Discussion

The goals of our study were (1) to understand the parameters important in quenching galaxies and (2) to analyse the way quiescence affects scatter in the growth histories of central galaxies with the stellar mass of the Milky Way. To summarize our results, we began by showing that the dominant quenching mechanism in H15 is AGN feedback, a process that primarily depends on halo mass and black hole mass. We also found that Milky Way-mass galaxies at the present day have an increasingly large range of progenitor stellar masses towards higher redshifts. This diversity in growth history is correlated with present-day halo mass, where more massive haloes tend to have built up their stars earlier than lower mass haloes. When splitting the Milky Way-mass galaxy population into star-forming and quiescent galaxies, we found that present-day quenched galaxies underwent a staggered quenching, where their present-day halo mass correlates with the redshift at which they quench. Finally, we showed that while halo mass is a useful parameter with which to characterize quenching, black hole mass is a much better indicator of quiescence at a given redshift.

We are cognizant that our analysis is likely to be affected by simplifications and model choices made in the course of developing the H15 semi-analytic model. Our results are likely to be rather sensitive to the time-scale for the reincorporation of gas into the hot halo in the H15 model (See Section 2.3). This particular part of the model is important in determining when and how much hot gas can cool back onto the galaxy. This effect causes gas to be reincorporated into lower mass systems at later times so that the galaxy stays star-forming for a longer time period. Larger systems reincorporate gas on much shorter time-scales which causes them to build most of their stellar mass at early times and cease star formation earlier. This change in the reincorporation recipe is particularly important in better matching the stellar mass function at intermediate redshifts (comparing H15 with e.g., Guo et al., 2011, see also Weinmann et al., 2012 for a more in-depth discussion of the issue). It is currently unclear if this simplified prescription for the reincorporation of gas is the most robust or physically-motivated way to delay the consumption of cold gas in low mass galaxies at intermediate and high redshift.

We also note that the internal structure of the gas disc and the stellar distribution, and their fates upon merging are modeled by H15 using highly simplified prescriptions. Choices about how to calculate the sizes, assign characteristic velocities, and estimate SFRs vary between models (Knebe et al., 2015; Pujol & Gaztañaga, 2014; Contreras et al., 2013), and in the future it would be useful to explore the importance of such choices on the inferred diversity of growth histories of Milky Way-mass galaxies.

Perhaps more importantly, the prescriptions for quenching are also highly simplified, depending primarily on the balance between the cooling rate of the hot halo gas and the heating rate of the energy input from AGN feedback, which in turn depends on the black hole mass and hot halo mass. This results in a particularly clean separation between quiescent and star-forming galaxies as a joint function of primarily black hole mass and secondarily halo mass at a given redshift. While we acknowledge that this picture is highly simplified, we also point out that it can and should be observationally tested. A census of star formation activity in central galaxies with reliable black hole and halo mass measurements may help characterize the heating-cooling equilibrium boundary, if it indeed exists, giving insight into how halo mass and black hole mass contribute to the quenching of the central galaxy. Unfortunately, halo mass measurements are not likely to be available for individual galaxies at this mass range in the near future and, as a result, reliable proxies for characterizing the depth of the potential well would need to be determined (see Chapter 3).

Since we show in Sections 2.7 and 2.9 that black hole mass correlates well with quenching, we can also posit that the way in which black holes grow at the centre of their host central galaxies is extremely important in affecting the galaxy's future stellar mass growth. Although this growth process is fully understood in this particular model as being dependent on the merger history of galaxies coupled with the amount of cold gas available for consumption (See Section 2.7), the details of how and when black holes grow in the real universe is not fully understood. Given the importance of AGN feedback to Milky Way-mass galaxy growth in H15, a better understanding of black hole growth will be important for future feedback and quenching models.

With regards to identifying progenitors of Milky Way-mass galaxies, previous studies have focused on determining their median stellar mass evolution in order to attempt to observationally understand how these galaxies grow (van Dokkum et al., 2010; Papovich et al., 2011; van Dokkum et al., 2013; Patel et al., 2013a). While we do match the median mass growth from progenitor studies that agree with the observed stellar mass function and take into account merging and other effects, very few of these have taken into account the intrinsic scatter of progenitor galaxy stellar masses characteristic of MW-mass galaxy growth in models of galaxy formation. This introduces difficulties when observationally identifying the progenitors of galaxies of a specific present-day stellar mass. Since progenitors of star-forming and quiescent galaxies are likely to be systematically different, this must be correctly accounted for when identifying progenitor populations.

Our results also point to a potentially important limitation of the abundance matching technique for linking galaxies and dark matter haloes (Vale & Ostriker, 2004; Kravtsov et al., 2004; Conroy et al., 2006; Conroy & Wechsler, 2009; Guo et al., 2010; Trujillo-Gomez et al., 2011; Behroozi et al., 2013). These models explicitly match galaxies to haloes by assuming these two properties are monotonically correlated apart from some purely statistical scatter. While this model is fairly simple and agrees with clustering measurements, the basic assumptions it relies upon are inherently uncertain due to our lack of understanding with regards to galaxy growth within haloes. By construction, halo masses do not depend on any attributes of the galaxy other than its stellar mass in most of these models, which is in strong contrast to the physical prescriptions used in semi-analytic modeling. For example, many of these studies do not differentiate between star-forming and quiescent galaxies, a necessary distinction in order to account for the emergence of the flat distribution at high halo masses in the SMHM relation according to our study (See Section 2.8). The necessity of this differentiation is also implied by observational studies which suggest quiescence correlates with halo mass estimates from satellite abundances and gravitational lensing (Wang & White, 2012; Mandelbaum et al., 2016a).

While the H15 model simulates a population that broadly follows a double power-law fitting of the SMHM relation – a fit that many others have used before – the scatter in the relation is substantial and worth noting explicitly. Such scatter has been incorporated in recent generations of models. For example, Behroozi et al. (2013) assumes a scatter in stellar mass given a halo mass following a lognormal distribution. The fact that the scatter in stellar mass at fixed halo mass is a weak function of halo mass means that abundance matching works relatively well at reproducing this scatter even with the potentially invalid assumption of a lognormal scatter (Tasitsiomi et al., 2004; Guo et al., 2015), as is seen in Figure 2.2. Even so, in the H15 model, where the scatter arises from the astrophysical modeling, we find it to be asymmetric, with long tails towards high halo masses for Milky Way-mass galaxies.

We saw in Sections 2.6 and 2.9 that not only is there a significant amount of scatter in the SMHM relation in this model, but that this scatter strongly correlates with galactic properties, such as those that are important for quenching. For example, the scatter in halo masses and growth histories systematically correlates with star formation activity, such that quiescent galaxies typically live in higher mass haloes with a variety of quenching times. This has important implications for studies attempting to explore star formation activity and histories in a halo framework (e.g. Hearin et al., 2015). For example, the opposite trend is predicted by the recent age-matching models of Watson et al. (2015, see Mandelbaum et al. 2016a) which is likely to be a serious limitation to using them to study galaxy evolution. While we acknowledge that semi-analytic models are simplified, they include prescriptions for a diversity of physical processes, and this model in particular agrees with both the observed stellar mass functions and the observed fractions of quiescent and star-forming galaxies over the range of redshifts and stellar masses relevant for this study. Accordingly, this model is a reasonable *qualitative* guide to how the real universe might differ from the assumptions underlying abundance matching analyses. As a result, studies of galaxy growth, especially when focusing on specific galaxy populations, should be aware of these caveats before relying on abundance or age matching techniques.

2.11 Conclusions

Galaxies appear to be particularly diverse at stellar mass scales similar to that of the Milky Way, where bulgeless star-forming disc galaxies coexist with centrally-concentrated quiescent galaxies. Our goal in this study was to use the semi-analytic model developed by Henriques et al. (2015) to explore the diversity of growth histories of central galaxies with stellar masses similar to that of the Milky Way, focusing particularly on how the quenching of star formation affects their growth histories.

The growth history and quenching of central galaxies in this model correlates jointly with black hole mass and halo mass, where quiescent galaxies are those in which AGN heating exceeds the halo cooling rate (Section 2.4). This results in a scattered relation between stellar mass and halo mass for central galaxies (Figure 2.2). While this scatter is quantitatively similar to values found in previous studies (e.g. Behroozi et al., 2013; Moster et al., 2013), it is strongly correlated with the physical properties of the central galaxies, a fact that has often been overlooked despite its important implications for the diversity of galaxy growth histories. Central Milky Way-mass galaxies in H15 show a wide diversity in growth histories, from galaxies that constantly form stars since $z \sim 2$ to quenched galaxies which have very little $z < 2$ star formation.

We find that the quenching of star formation is a significant source of scatter in central galaxy growth histories in H15 (Figure 2.4) since it causes the stellar mass buildup of some galaxies to significantly slow down. More specifically, the time at which these galaxies quench correlates with present-day halo mass (Figure 2.5) – a phenomenon we call staggered quenching. This creates a link between quenching and halo mass, where, at a fixed stellar mass, more massive haloes at the present day tend to have quenched earlier than lower mass haloes. While halo mass correlates better with quiescence than stellar mass, we found that the central black hole mass correlates best with the quenching of galaxies of this stellar mass (Figure 2.9). While many galaxies experience rapid black hole growth via merging prior to quenching, there do exist systems which become quiescent more gradually. In these systems, while the AGN heating rate is constant, gas cooling becomes less effective at low redshifts. This can stop star formation in galaxies close to the heating-cooling equilibrium boundary (Section 2.7). In addition, the H15 model shows a pronounced heating-cooling equilibrium boundary driven by AGN feedback. This is an observationally testable prediction of a boundary in the M_{BH}-M_{h} relation and future work should focus on searching for it (see Chapter 3).

Our results are also important for attempts at observationally identifying progenitors of Milky Way-mass galaxies. Our description of "staggered quenching" points to a correlation between halo mass and quenching time that, if at least indirectly observed in the real universe, may give clues to a galaxy's growth history. More importantly, perhaps, is a more complete understanding of the connection between quiescence and the mass of a galaxy's supermassive black hole. Our analysis showed that black hole mass is a better predictor of quiescence than halo mass in the H15 model, so understanding how black holes grow in the real universe seems to be an important factor to understanding the growth of progenitors of quenched galaxies. In terms of other models, abundance matching, age matching, and halo occupancy distribution models all make simplifying assumptions in their implementation that are in partial disagreement with our physically-motivated framework. Understanding in detail how quiescence is reflected in the SMHM relation in these models is essential to address the main question of our work in the context of other frameworks. Our results serve to show the importance of understanding the astrophysics underlying the quenching of star formation in galaxies.

Acknowledgments

This chapter is a reproduction of an article of the same title published on March 28, 2016 in the Monthly Notices of the Royal Astronomical Society in Volume 459, Issue 2, Pages 1929-1945. The co-authors of this article are Eric F. Bell, Bruno M. B. Henriques, and Simon D. M. White. The article is reproduced here under the non-exclusive right of republication granted by the Oxford Journals to the author(s) of the article.

B.A.T. is supported by the National Science Foundation Graduate Research Fellowship under Grant No. DGE 1256260. The work of BH and SW was supported by Advanced Grant 246797 "GALFORMOD" from the European Research Council. This work is partially supported by *HST* grant GO-12060. Support for Program number GO-12060 was provided by NASA through a grant from the Space Telescope Science Institute, which is operated by the Association of Universities for Research in Astronomy, Incorporated, under NASA contract NAS5-26555. This publication also made use of NASA's Astrophysics Data System Bibliographic Services. The Millennium Simulation databases used in this chapter and the web application providing online access to them were constructed as part of the activities of the German Astrophysical Virtual Observatory (GAVO, Lemson & Virgo Consortium, 2006). We appreciate fruitful conversations with Brian O'Shea, Keren Sharon, Peter Behroozi, and Casey Papovich.

CHAPTER III

Quiescence correlates strongly with directly-measured black hole mass in central galaxies

3.1 Abstract

Roughly half of all stars reside in galaxies without significant ongoing star formation. However, galaxy formation models indicate that it is energetically challenging to suppress the cooling of gas and the formation of stars in galaxies that lie at the centers of their dark matter halos. In this Letter, we show that the dependence of quiescence on black hole and stellar mass is a powerful discriminant between differing models for the mechanisms that suppress star formation. We compare these models with the observed distribution of 90 quiescent and star-forming central galaxies with directly-measured black hole masses, finding that quiescent central galaxies host more massive black holes than star-forming central galaxies with similar stellar masses. Our results show qualitative agreement between observations and models that assume that effective, more-or-less continuous AGN feedback suppresses star formation, strongly suggesting the importance of the black hole in producing quiescence in central galaxies.

3.2 Introduction

Galaxy surveys have revealed the dramatic growth of the quiescent, non-star-forming galaxy population with cosmic time (e.g., Muzzin et al., 2013). Despite the high present abundance of quiescent galaxies, the relative importance of possible physical drivers of galaxy-wide suppression of star formation remains uncertain. In a cosmological context, gas cooling and accretion into the center of a dark matter halo fuels ongoing star formation. Thus, the onset of quiescence means that gas is somehow removed from the galaxy and that gas cooling is offset by some source of heat. Unlike satellites, galaxies in the center of a halo's potential well – hereafter referred to as central galaxies – must eject and heat their gas without relying on interactions with the hot, diffuse medium present in other halos, groups, and clusters (Tinker et al., 2013). This implies stringent energetic requirements not easily met by stellar feedback (e.g. Bower et al., 2006).

Heating mechanisms proposed for central galaxies include ejected gas from supernovae Ia (SNIa) and stellar winds (e.g. Hopkins et al., 2012), virial shock heating (e.g. Birnboim et al., 2007), gravitational heating (e.g. Johansson et al., 2009), and – currently the most popular explanation – feedback from active galactic nuclei (AGN, Kauffmann & Haehnelt, 2000; Di Matteo et al., 2005; Croton et al., 2006; Cattaneo et al., 2009; Fabian, 2012).

One powerful approach towards characterizing the importance of different physical drivers of quiescence in central galaxies is to measure the correlation between quiescence and a range of galaxy properties that could affect the balance between heating and cooling. For example, cooling and gas accretion depend strongly on halo mass, and would thus be expected to correlate with stellar mass (with significant scatter; see Terrazas et al., 2016a). Heating or gas ejection could correlate with a variety of properties: halo mass due to virial shock heating or gravitational quenching, stellar mass due to SNIa and stellar feedback, or black hole mass due to AGN feedback.

With these concerns in mind, many studies have explored how quiescence correlates with a variety of quantities: for example, stellar mass, halo mass, surface density, inferred velocity dispersion, Sérsic (1963) index, and bulge mass (Kauffmann et al., 2003; Franx et al., 2008a; Bell et al., 2012; Lang et al., 2014; Bluck et al., 2014b; Woo et al., 2015; Mandelbaum et al., 2016b). The latter quantities are expected to correlate with the prominence of a supermassive black hole (Kormendy & Ho, 2013), in support of the idea that AGN feedback is an important driver of quiescence. Yet, correlating quiescence with directly-measured black hole mass would be a clearer and more critical test of AGN feedback. With the number of dynamical black hole mass measurements increasing each year, such an exercise has now become possible.

The goal of this Letter is to characterize the physical drivers of quiescence by studying the observed distribution of star-forming and quiescent central galaxies as a function of their central black hole mass and stellar mass (§4.3) and comparing those findings with the results from four galaxy formation models (Henriques et al., 2015, §3.3.2; Illustris – Vogelsberger et al., 2014a, §3.3.3; EAGLE – Schaye et al., 2015, §3.3.4; and GalICS – Cattaneo et al., 2006a, §3.3.5). We then describe (§5.6.2) and discuss (§5.8) the apparent agreement between observations and models that use effective, more-or-less continuous AGN feedback to halt star formation. We assume the standard cosmology in order to be consistent with our compiled observational distances: $\Omega_M = 0.3$, $\Omega_\Lambda = 0.7$, and $\mathrm{H}_0 = 70$ km/s/Mpc.

3.3 Data

3.3.1 Observational estimates of black hole masses, stellar masses and star formation rates

Dynamical estimates of black hole masses (M_{BH}) are heterogeneous, coming from stellar dynamics, gas dynamics, masers, and reverberation mapping techniques. We adopt the $M_{\rm BH}$ estimates compiled by Saglia et al. (2016), supplemented by van den Bosch (2016, and references therein). Our conclusions are insensitive to the particular compilation that we adopt. We select central galaxies by identifying the brightest or only members of their group within a ~1 Mpc radius in order to omit the effects of quenching unique to satellites. Finally, we choose nearby galaxies within ~150 Mpc ($z \lesssim 0.034$). Our final sample includes 91 central galaxies.

Stellar masses (M_*) were estimated using extinction-corrected 'total' $K_{\rm s}$ apparent magnitudes from the 2MASS Redshift Survey (Huchra et al., 2012). We adopt a single K-band stellar $M_*/L_{\rm K}$ ratio of 0.75, the average value for the luminous galaxies studied by Bell et al. (2003), adjusted to a Chabrier (2003) IMF. The variation in $M_*/L_{\rm K}$ is expected to be too small to significantly affect our results (Bell et al., 2003).

The chief observational novelty of our analysis is the use of star formation rates (SFRs) to characterize quiescence in conjunction with directly-detected black hole masses. We calculate far-infrared (FIR) derived SFRs using IRAS (Rice et al., 1988; Moshir & et al., 1990; Surace et al., 2004; Serjeant & Hatziminaoglou, 2009, see also corrections to Knapp et al., 1989 in NED by Knapp 1994). As discussed in Bell (2003), FIR-derived SFRs are most appropriate for relatively massive galaxies with significant dust contents, since ultraviolet (UV) or Hα fluxes are typically strongly attenuated by dust. The FIR is also less susceptible to contamination from AGN than mid-IR or radio SFR estimates. Equation A1 in Bell (2003) uses 60 and 100 μm fluxes to estimate the FIR flux. Non-detections are estimated using the ratios $f_{60}/f_{70} = 0.88$, $f_{60}/f_{100} = 0.39$, $f_{60}/f_{25} = 7.19$, $f_{60}/f_{12} = 11.0$, which are derived from a large number of local galaxies. The 70 μm measurements are from Spitzer/MIPS (Temi et al., 2009; Dale et al., 2009). We then estimate the total infrared (TIR) flux via TIR = 2 × FIR (Bell, 2003). The TIR-derived SFR is calculated using Equation 12 in Kennicutt & Evans (2012),

$$\log_{10}\mathrm{SFR}_{\mathrm{TIR}}\,(\mathrm{M}_{\odot}\,\mathrm{yr}^{-1}) = \log_{10}L_{\mathrm{TIR}} - 43.41 \tag{3.1}$$

where $\mathrm{L}_{\mathrm{TIR}}$ is the TIR luminosity calculated using our TIR flux estimates and the distances to the galaxies. Galaxies with no infrared detections or detections that result in $\mathrm{SFR}/M_* < 10^{-13}\ \mathrm{yr}^{-1}$ are taken as upper limits. We adopt a factor of two uncertainty for our SFR values (Bell, 2003). We have confirmed that hybrid TIR+UV SFRs for those galaxies that have measured UV fluxes yield similar results to TIR-only SFRs.

3.3.2 The Henriques et al. (2015) Semi-Analytic Model

Henriques et al. (2015) developed a semi-analytic model that uses the Millennium Simulations (Springel et al., 2005; Boylan-Kolchin et al., 2009) to provide the dark matter framework in which they embed their analytic prescriptions for the evolution of gas and stars (see Chapter 2 for a full description). Quiescence in the Henriques et al. (2015) model is primarily a result of heating from continuous radio-mode AGN feedback, which halts the cooling of the circumgalactic medium onto the galaxy's disk. This effectively cuts off the fuel needed to form stars. Analytically, the model is built so that the balance between heating and cooling depends strongly on M_{BH} and only somewhat on the hot gas mass, which correlates strongly with halo mass (M_{h}; see Figure 1 in Terrazas et al., 2016a).

3.3.3 The Illustris Hydrodynamic Simulation

The Illustris Project is a series of large-scale hydrodynamic simulations of galaxy formation (Vogelsberger et al., 2014a). These simulations use the moving-mesh technique AREPO (Springel, 2010) to follow individual particles in order to model the baryonic physics relevant to galaxy evolution. Similarly to the Henriques et al. (2015) model, galaxies in Illustris depend on a balance between heating and cooling in order to determine quiescence. Radio-mode AGN feedback transfers heat to the atmospheres around galaxies via the expansion of hot bubbles emanating from the black hole. The amount of thermal energy transferred depends on the growth of M_{BH} in the radio mode (Sijacki et al., 2015).

3.3.4 The EAGLE Hydrodynamic Simulation

The EAGLE Project (Schaye et al., 2015) is a suite of hydrodynamic simulations that use a modified version of the smoothed particle hydrodynamics code GADGET 3 (Springel, 2005) to model the physics of galaxy formation. They include one mode of AGN feedback most closely resembling the quasar mode, which the model depends upon to suppress star formation in high mass galaxies. Thermal energy is injected at a rate proportional to the gas accretion rate, which depends on M_{BH} along with the properties of the gas around it. In this model, AGN feedback works stochastically through short-lived events that inject heat into the interstellar medium of the galaxy.

3.3.5 The GalICS Semi-Analytic Model

We use the implementation of the GalICS semi-analytic model described in Cattaneo et al. (2006a). In this model, star formation is shut off above a critical halo mass, $M_{\mathrm{h,crit}} \sim 10^{12}\ \mathrm{M}_{\odot}$, which represents the sharp transition from free-falling cold-mode to shock-driven hot-mode gas accretion onto the galaxy. At larger halo masses, cold gas in the galaxy is heated to the virial temperature and added to the hot gas component. Once shock-heated gas is available, AGN are able to provide a source of feedback through inefficient accretion and maintain the high temperatures of the gas in order to prevent cooling and subsequent star formation.

In order to provide a common method for differentiating star-forming and quies-

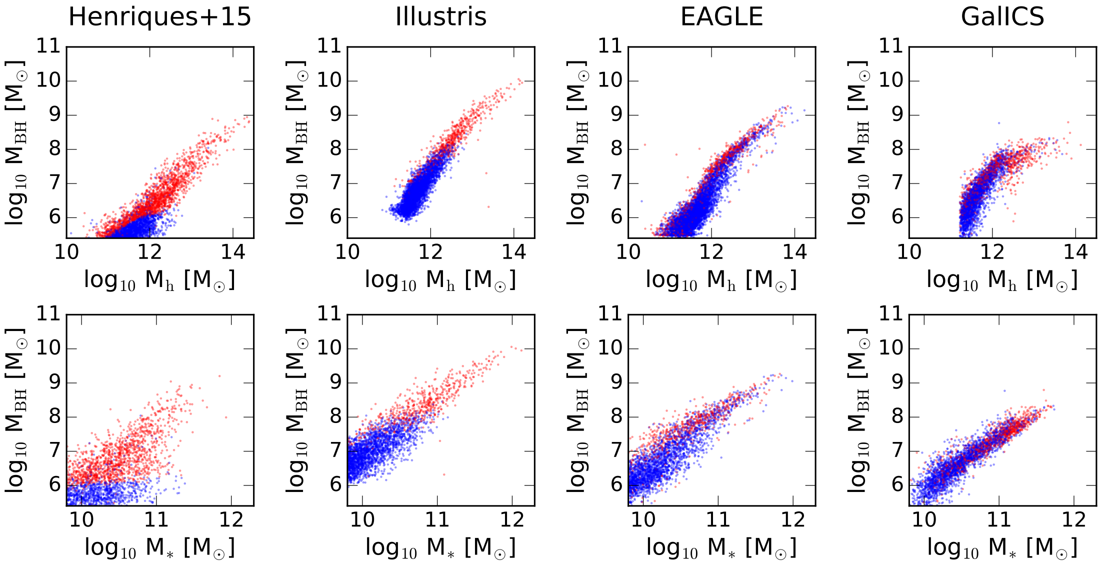

Figure 3.1: $M_{\rm BH}$ as a function of $M_{\rm h}$ (upper panels) and M_* (lower panels) for the Henriques et al. (2015), Illustris, EAGLE, and GalICS models. Blue and red points indicate star-forming and quiescent galaxies, respectively, chosen via the SFR selection described in §3.3.

cent galaxies at $z \sim 0$ for all models, we identify a best fit line to the star-forming main sequence for all four models and observations of a representative sample of local galaxies without $M_{\rm BH}$ measurements. We define quiescent galaxies as those that lie a factor of 4 or more below this line.

3.4 Results

Many observed galaxy properties correlate with each other and the mechanisms behind quiescence may be complex. Accordingly, we first use the models to generate intuition about how the physical drivers of quiescence may impact observational correlations before examining the observations.

3.4.1 A comparison between models

In Fig. 3.1, we show the physically-important but currently unobservable $M_{\rm BH}$–$M_{\rm h}$ plane in the upper panels, and the observable $M_{\rm BH}$–M_* plane in the lower panels for all models. We find a variety of distributions in $M_{\rm BH}$–M_*–$M_{\rm h}$ parameter space.

The *quantitative* differences in normalization result from the calibration of the $M_{\rm BH}$ growth efficiencies to different $M_{\rm BH}$-galaxy relations. The feedback efficiencies that regulate star formation are largely decoupled from the $M_{\rm BH}$ growth efficiencies in all models. This suggests that differences in the calibration of the $M_{\rm BH}$ growth efficiencies would not affect which galaxies are star-forming or quiescent. Therefore, the crucial features for our purposes are *qualitative* differences in the distribution of star-forming and quiescent galaxies between models, which can be used as a diagnostic of the physical drivers of quiescence in these models.

We find that the Henriques et al. (2015) and Illustris models show a qualitatively similar divide between star-forming and quiescent galaxies, a division that depends strongly on $M_{\rm BH}$ and much less strongly on $M_{\rm h}$ and M_*. In these models, a quiescent galaxy almost always has a larger black hole than a star-forming galaxy due to the connection between the $M_{\rm BH}$ and the heating rate from long-lived radio-mode AGN feedback. While the Henriques et al. (2015) model demonstrates this behavior by construction (see Chapter 2 and Terrazas et al., 2016a), this result emerges from Illustris naturally from their hydrodynamic recipes where there is no explicit link between the heating rate and galaxy properties such as $M_{\rm BH}$ or $M_{\rm h}$.

The EAGLE simulation shows similar behavior where quiescent galaxies are more likely to have massive black holes. Star-forming galaxies, however, span the entire range of $M_{\rm BH}$ and M_*, where galaxies with massive black holes can still be star-forming. This is confirmed in studies of the EAGLE simulation showing that the passive fraction at higher M_* is too low compared to observations (Furlong et al., 2015). We posit that the short-lived nature of the feedback that heats the interstellar medium in their model does not stop gas cooling in between these events, where star formation can continue in galaxies with a non-accreting yet massive black hole (see also Trayford et al., 2016).

Finally, the GalICS model shows overlapping distributions of star-forming and quiescent galaxies on the $M_{\rm BH}$–M_* plane with quiescent galaxies preferentially at higher M_*. The quenching mechanism is evident in the $M_{\rm BH}$–$M_{\rm h}$ plane where there is a dramatic deficit of star-forming galaxies above $M_{\rm h} \sim 10^{12.3}$ $\rm M_\odot$. The assumption of a critical $M_{\rm h}$ at which star formation stops results in $M_{\rm BH}$ having little to no importance for quiescence in this model.

3.4.2 Observational evidence of the link between black hole mass and quiescence

Given the diagnostic power of the lower panels of Fig. 3.1, we present a direct observational counterpart in Fig. 3.2. The inset plot shows the criterion (black dashed line) we choose in §3.3 for identifying star-forming (blue) and quiescent (red) galaxies when plotting the specific star formation rate (SFR/M_*, sSFR) against the M_* while also showing a subset of local galaxies without directly-measured black hole masses as gray points. The shaded region represents where the subset of local galaxies is no longer complete due to the detection limit of the infrared measurements.

Fig. 3.2 shows a pronounced divide between star-forming and quiescent galaxies where quiescent galaxies have more massive black holes than their star-forming counterparts. In addition, there is a M_* dependence to this divide, where lower M_* galaxies can be quiescent at lower $M_{\rm BH}$ than higher M_* galaxies.

Comparing our observational result with the model data in the lower panels of Fig. 3.1, we find that real galaxies more closely resemble models in which effective, more-or-less continuous AGN feedback quenches star formation in central galaxies – namely, the Henriques et al. (2015) model (§3.3.2) and Illustris (§3.3.3). As we

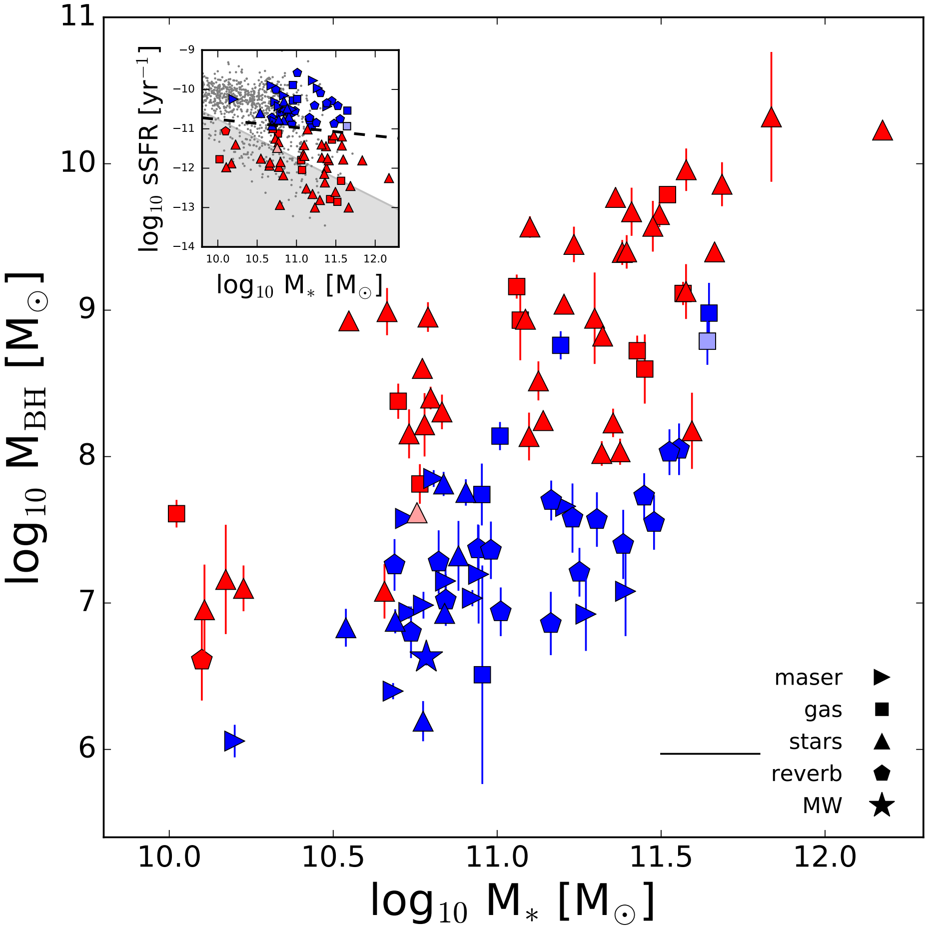

Figure 3.2: Directly-measured $M_{\rm BH}$ as a function of M_* for star-forming (blue) and quiescent (red) central galaxies in the nearby universe (z $<$ 0.034). The black line indicates the uncertainty on M_*. The inset plot shows the sSFR-M_* plane for a selection of local galaxies (gray points) and for all galaxies in our sample (colored points). The shaded region indicates where the selection of local galaxies is no longer complete. Lighter colored points represent mid-IR-derived SFRs that should be taken as upper limits.

have described in §3.4.1, these models result in a pronounced divide between star-forming and quiescent galaxies with little scatter – similar to Fig. 3.2. We note that the EAGLE simulation produces a more similar M_* dependence with regards to the divide, yet fails to replicate the separation between star-forming and quiescent galaxies on this plane.

3.4.3 Bulge Mass and Velocity Dispersion

The motivation for exploring the relationship between M_*, $M_{\rm BH}$, and quiescence was to test the importance of $M_{\rm BH}$ in driving quiescence. Previous works have linked quiescence with quantities that correlate with $M_{\rm BH}$, such as velocity dispersion (σ, e.g., Franx et al., 2008a) or bulge mass ($M_{\rm bul}$, e.g., Bluck et al., 2014a). As such, whether σ or $M_{\rm bul}$ correlates better with quiescence than $M_{\rm BH}$ may provide important physical insight.

This question is explored in Fig. 3.3, where we present the $M_{\rm BH}$–σ, $M_{\rm BH}$–$M_{\rm bul}$, M_*–σ, and M_*–$M_{\rm bul}$ relations for our sample, omitting those with no σ or $M_{\rm bul}$ measurements. σ was provided by van den Bosch (2016) and $M_{\rm bul}$ was obtained by adopting the bulge-to-total ratios in $K_{\rm s}$ band found in Kormendy & Ho (2013). Morphologies, if defined, are from Saglia et al. (2016) and are indicated using different symbols.

Figure 3.3c shows that quiescence correlates well with σ at a given M_*. This correlation is as strong as the correlation between $M_{\rm BH}$ and quiescence, possibly due to the tight correlation between σ and $M_{\rm BH}$ (Figure 3.3a). However, σ may also directly influence the ability of galaxies to form stars. Martig et al. (2009) found that shear modulates star formation efficiency by factors of a few in highly concentrated galaxies. Yet, in the context of cosmological models, this effect is insufficient to drive quiescence, instead requiring a much larger input of energy – generally from AGN feedback – to keep cold gas out of galaxies (see Chapter 1). Further study of cold gas

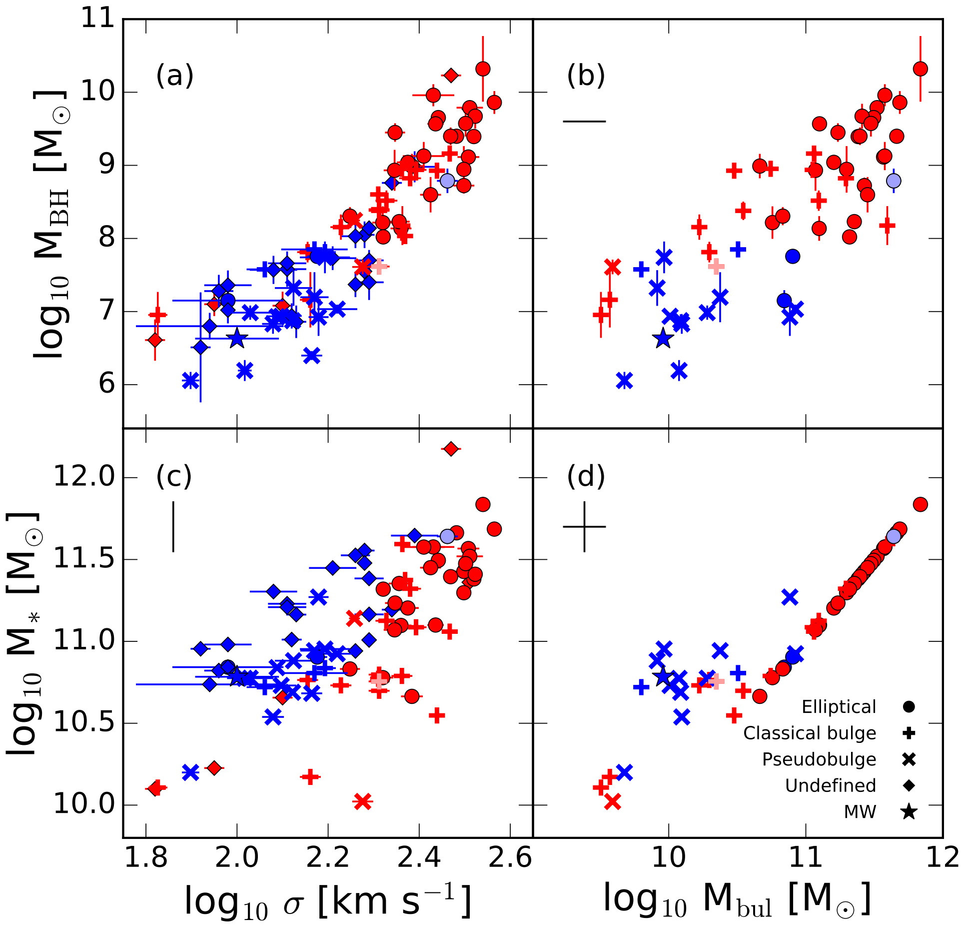

Figure 3.3: A collection of panels showing the (a) $M_{\rm BH}$-σ, (b) $M_{\rm BH}$-$M_{\rm bul}$, (c) M_*-σ, and (d) M_*-$M_{\rm bul}$ relations for star-forming (blue) and quiescent (red) galaxies, where we omit those with no σ or $M_{\rm bul}$ measurements. The black lines indicate the uncertainties on M_* and $M_{\rm bul}$. Morphologies, if defined, are from Saglia et al. (2016). Lighter colored points represent mid-IR-derived SFRs that should be taken as upper limits.

supply and SFRs as a function of M_{BH} and σ may help illuminate the relationship between these two factors and quiescence.

Figure 3.3b/d shows that M_{bul} correlates poorly with quiescence for our sample. Since M_{BH} correlates slightly better with M_{bul} than with M_*, one may expect that higher M_{BH} in quiescent galaxies are a result of larger bulge-to-total ratios. Figure 3.3b shows that this is not entirely the case – M_{BH} is higher in quiescent galaxies even at fixed M_{bul}.

Furthermore, we find that quiescence is common in elliptical galaxies and galaxies with classical bulges, whereas star-forming galaxies tend to have pseudobulges. This may suggest that the processes leading to the growth of classical bulges (e.g., mergers, misaligned gas infall) may result in more effective M_{BH} growth than those that create pseudobulges.

3.5 Discussion

The goal of this Letter is to probe the physical drivers of quiescence by looking for correlations between M_*, M_{BH}, and sSFR. Our main observational result is that central quiescent galaxies contain more massive black holes than their star-forming counterparts, with the boundary between these groups also having a dependence on M_*. When comparing our results with four galaxy formation models, we find the best agreement with models that simulate more effective and long-lived AGN feedback. Taken together, this analysis suggests that the central black hole has an essential role in shutting off star formation.

The clear division in the M_{BH}–M_* plane between star-forming and quiescent central galaxies is a powerful test of prescriptions for gas cooling, gas heating, and quiescence in models. Our results suggest that models that do not suppress star formation via quasi-continuous black hole-driven feedback will not produce a strong enough correlation between quiescence and M_{BH}.

This work connects well with previous studies by exploring much more explicitly the interplay between SFR and $M_{\rm BH}$. In Reines & Volonteri (2015) and Savorgnan et al. (2015), the morphology of galaxies was shown in the $M_{\rm BH}$–M_* plane. In both works, early and late type galaxies inhabit clearly distinct parts of the $M_{\rm BH}$–M_* plane. Our work is consistent with theirs, and frames the interpretation of this behavior much more explicitly in terms of a dominant role for AGN feedback in driving quiescence.

Other studies have used indirect proxies for $M_{\rm BH}$. For example, Bluck et al. (2014a) used indirect estimates of $M_{\rm BH}$ from σ and $M_{\rm bul}$ for central galaxies to find a transition between mostly active to mostly passive galaxies within ~1.5 orders of magnitude of $M_{\rm BH}$. This transition appears broader than ours, which may be influenced by uncertainties in their $M_{\rm BH}$ estimates, and may indicate, as our results seem to, that quiescence is a function of multiple parameters such as both $M_{\rm BH}$ and M_*.

Our sample is selected to have dynamically-derived $M_{\rm BH}$ estimates and includes both inactive galaxies (favoring larger $M_{\rm BH}$ to maximize detectability) and active galaxies (probing lower $M_{\rm BH}$ systems that are accreting gas and preferentially located in star-forming galaxies). Sample selection is currently very heterogeneous, making it impractical at this stage to impose observationally-motivated selections on our model samples (e.g., to make mock observations for Fig. 3.1). As observational methods improve and more representative measurements become available over a wider range of galaxy types, it will be important to check if this apparent division between star-forming and quiescent galaxies in the $M_{\rm BH}$–M_* plane remains.

3.6 Conclusions

Cosmological models of galaxy formation predict that the relationship between quiescence, $M_{\rm BH}$, and M_* is a crucial discriminator between models and a sensitive probe of the drivers of quiescence. We compare directly-measured $M_{\rm BH}$, M_*, and other properties of a sample of star-forming and quiescent galaxies, finding that observed quiescent galaxies have higher M_{BH} than star-forming galaxies with similar M_*. These trends are in good qualitative agreement with models in which star formation is suppressed due to quasi-continuous heating from AGN feedback. We assert that models that do not replicate this behavior are missing an essential element in their physical recipes. Our study suggests that the central black hole is critical to the process by which star formation is terminated within central galaxies, giving credence to the AGN quenching paradigm.

Acknowledgments

This chapter is a reproduction of an article of the same title published on October 7, 2016 in the Astrophysical Journal Letters in Volume 830, Issue 1. The co-authors of this article are Eric F. Bell, Bruno M. B. Henriques, Simon D. M. White, Andrea Cattaneo, and Joanna Woo. The article is copyright 2016, the American Astronomical Society, reproduced here under the non-exclusive right of republication granted by the AAS to the author(s) of the article.

B.A.T. is supported by the National Science Foundation Graduate Research Fellowship under Grant No. DGE1256260. We acknowledge helpful discussions with E. Gallo, J. Bregman, K. Gultekin, H. W. Rix, S. Faber, S. Ellison, A. Pontzen, and L. Sales. This work used the SIMBAD database at CDS, and the NASA/IPAC Extragalactic Database (NED), operated by the Jet Propulsion Laboratory, California Institute of Technology, under contract with NASA.

CHAPTER IV

Supermassive black holes as the regulators of star formation in central galaxies

4.1 Abstract

We present a relationship between the black hole mass, stellar mass, and star formation rate of a diverse group of 91 galaxies with dynamically-measured black hole masses. For our sample of galaxies with a variety of morphologies and other galactic properties, we find that the specific star formation rate is a smoothly decreasing function of the ratio between black hole mass and stellar mass, or what we call the specific black hole mass. In order to explain this relation, we propose a physical framework where the gradual suppression of a galaxy's star formation activity results from the adjustment to an increase in specific black hole mass and, accordingly, an increase in the amount of heating. From this framework, it follows that at least some galaxies with intermediate specific black hole masses are in a steady state of partial quiescence with intermediate specific star formation rates, implying that both transitioning and steady-state galaxies live within this region known as the "green valley." With respect to galaxy formation models, our results present an important diagnostic with which to test various prescriptions of black hole feedback and its effects on star formation activity.

4.2 Introduction

Large scale galaxy surveys have made it clear that there has been a pronounced growth in the number of galaxies that host little to no star formation (Bell et al., 2004; Brown et al., 2007; Muzzin et al., 2013; Ilbert et al., 2013; Tomczak et al., 2014; Mortlock et al., 2015), reflecting the overall declining cosmic star formation rate observed in the universe since $z = 2$ (Madau & Dickinson, 2014). In an effort to understand how the quiescent population grows, these observational studies have used color-magnitude diagrams to split galaxies into a blue cloud and red sequence. Traditionally, the gap or "green valley" between these two populations has been interpreted as evidence that galaxies undergo a rapid transition from star-forming to completely quiescent, forming a sparsely populated region in this parameter space (Baldry et al., 2004; Bell et al., 2004; Faber et al., 2007; Taylor et al., 2015). However, more recent studies have proposed various quenching timescales (Martin et al., 2007; Schawinski et al., 2014; Woo et al., 2015; Barro et al., 2015), where galaxies that quench slowly may account for a large fraction of the green valley population. As such, understanding the physical mechanism(s) behind how individual galaxies transform and traverse through the "green valley" in order to produce the growth of the quiescent population has been a major topic of research in extragalactic astrophysics.

Star formation requires gas cooling down to a cold molecular form before clumps and cores begin to form systems of stellar nurseries. Therefore, the physical mechanism producing quiescence must somehow either stop gas from cooling to this form or eject the gas completely for extended periods of time (see Chapter 1). In this work, we focus on the physics behind quiescence in central galaxies, or those at the centers of their dark matter halos, since satellite galaxies undergo unique processes that are specific to systems located well within the hot, gaseous atmospheres of other galaxies.

A multitude of possible mechanisms affecting central galaxies have been proposed: stellar and supernovae Ia feedback (White & Rees, 1978; Dekel & Silk, 1986; White

& Frenk, 1991; Hopkins et al., 2012), halo mass quenching (Dekel & Birnboim, 2006; Cattaneo et al., 2006a; Birnboim et al., 2007; Dekel et al., 2009; Gabor & Davé, 2015), morphological quenching (Kormendy & Kennicutt, 2004; Martig et al., 2009; Cisternas et al., 2011), stellar mass quenching (Peng et al., 2010), gravitational heating (Johansson et al., 2009), and varying forms of black hole feedback from active galactic nuclei (AGN, Kauffmann & Haehnelt, 2000; Di Matteo et al., 2005; Croton et al., 2006; Cattaneo et al., 2009; Fabian, 2012; Cicone et al., 2014).

Observationally, quiescent galaxies are more common with increasing stellar mass, and tend to host massive bulges, concentrated central stellar surface densities, concentrated light profiles, higher central velocity dispersions, and more massive dark matter halos (Kauffmann et al., 2003; Franx et al., 2008a; Bell et al., 2012; Lang et al., 2014; Bluck et al., 2014b; Woo et al., 2015; Mandelbaum et al., 2016b). Many of these properties are expected to correlate closely with the central supermassive black hole mass (Kormendy & Ho, 2013), lending support to the idea that black hole-driven feedback is important for producing quiescence in central galaxies.

Recently, a myriad of studies have compiled an ever-growing list of dynamically-measured black hole masses (e.g., Kormendy & Ho, 2013; Saglia et al., 2016; van den Bosch, 2016), allowing a more direct and statistical study of how black holes and galactic properties correlate with one another. Terrazas et al. (2016b), described in Chapter 3, used a combination of these compilations in order to show that quiescent galaxies have more massive black holes than star-forming galaxies at a given stellar mass. They also show that this behavior is naturally produced in models where star formation is regulated by long-lived radio-mode AGN feedback.

This work aims at expanding on this study by exploring how the star formation rate of a galaxy correlates with its black hole mass and stellar mass, thereby probing the way in which the black hole responsible for AGN feedback affects the amount of star formation occurring in the galaxy.

We begin by presenting the galaxy data we use in our analysis (§2) and go on to describe the resulting trends and correlations produced by the data (§3). We then discuss the physical framework we propose in order to interpret our results in the context of AGN feedback (§4.1). This motivates a discussion on whether galaxies which host intermediate amounts of star formation, or what we call 'partially quiescent' galaxies, are truly transitioning (§4.2). Model results are then shown in order to compare our physical interpretation with the results from detailed simulations of galaxy formation (§4.3). Finally, we end with concluding remarks (§5).

4.3 Data

We adopt the sample of nearby (z $\lesssim 0.034$ or d $\lesssim 150$ Mpc) galaxies with dynamical estimates of black hole masses ($M_{\rm BH}$) from Terrazas et al. (2016b), where the base sample comes from Saglia et al. (2016) and is supplemented by van den Bosch (2016, and references therein). Our sample selects only central galaxies, identified as the brightest or only members in their association within a $\sim$1 Mpc radius in order to focus on the physics of quiescence for galaxies at the centers of their potential wells.

We use extinction-corrected 2MASS 'total' $K_{\rm s}$ apparent magnitudes (Huchra et al., 2012) to infer galaxy stellar masses (M_*), adopting a single K-band stellar $M_*/L_{\rm K}$ ratio of 0.75 and assuming an uncertainty of 0.15 dex. In order to calculate star formation rates (SFRs), we use far-infrared (FIR) fluxes obtained by IRAS (Rice et al., 1988; Moshir & et al., 1990; Surace et al., 2004; Serjeant & Hatziminaoglou, 2009, see also corrections to Knapp et al., 1989 in NED by Knapp 1994) in conjunction with the methods to derive SFR described in Kennicutt & Evans (2012). Galaxies with no infrared detections or detections that result in SFR/$M_* < 10^{-13}$ yr^{-1} are shown as upper limits. We adopt a 0.3 dex uncertainty for our SFR values (Bell, 2003). Refer to Terrazas et al. (2016b) and Chapter 3 for more information on the methods for calculating galaxy properties.

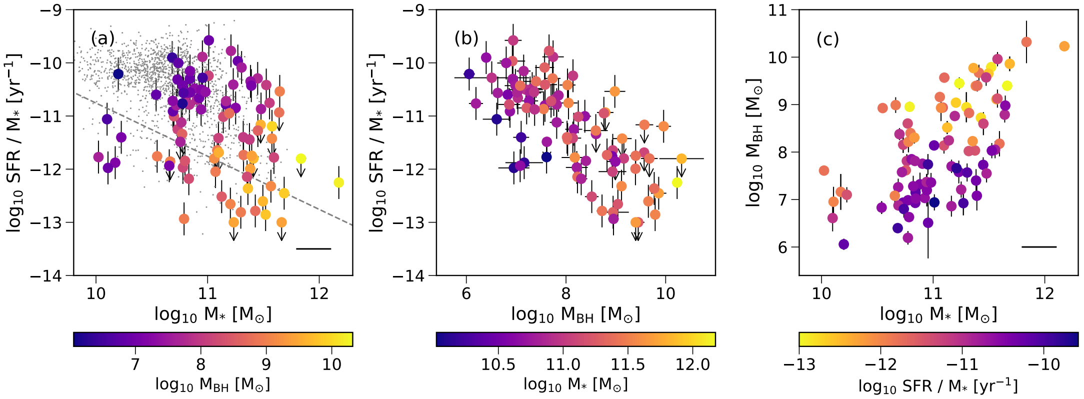

Figure 4.1: Projections of the 3-dimensional sSFR–$M_{\rm BH}$–M_* data cube: (a) sSFR as a function of M_*. The gray data points indicate a sample of local galaxies to show the star forming main sequence. The dashed line indicates the boundary below which the sample is no longer complete; (b) sSFR as a function of $M_{\rm BH}$; (c) $M_{\rm BH}$ as a function of M_*. Color gradients indicate the values for the axis not shown. The lines at the bottom right of (a) and (c) indicate the errors on M_*.

4.4 Results

Figure 4.1 shows the sSFR–M_*, sSFR–$M_{\rm BH}$, and $M_{\rm BH}$–M_* parameter space for our sample of 91 central galaxies. These plots show three projections of a 3-dimensional data cube where the color gradient in each panel represents the values of the axis not shown. We can see a clear correlation between sSFR, $M_{\rm BH}$, and M_* - namely, for a given M_*, quiescent galaxies have more massive $M_{\rm BH}$ than star-forming galaxies, as is shown and discussed in Terrazas et al. (2016b). However, galaxies at a given M_* can have diverse sSFRs which generally decrease with increasing $M_{\rm BH}$ as can be seen in the color gradient in the rightmost panel of Figure 4.1. This trend appears to be continuous in our data, motivating us to avoid classifying galaxies into two broad categories of 'star-forming' and 'quiescent.' Thus, we choose to explicitly explore whether the sSFR distribution produces a dichotomy or instead varies more continuously as a function of other galaxy parameters.

In order to investigate this, we focus on the central panel of Figure 4.1 and show

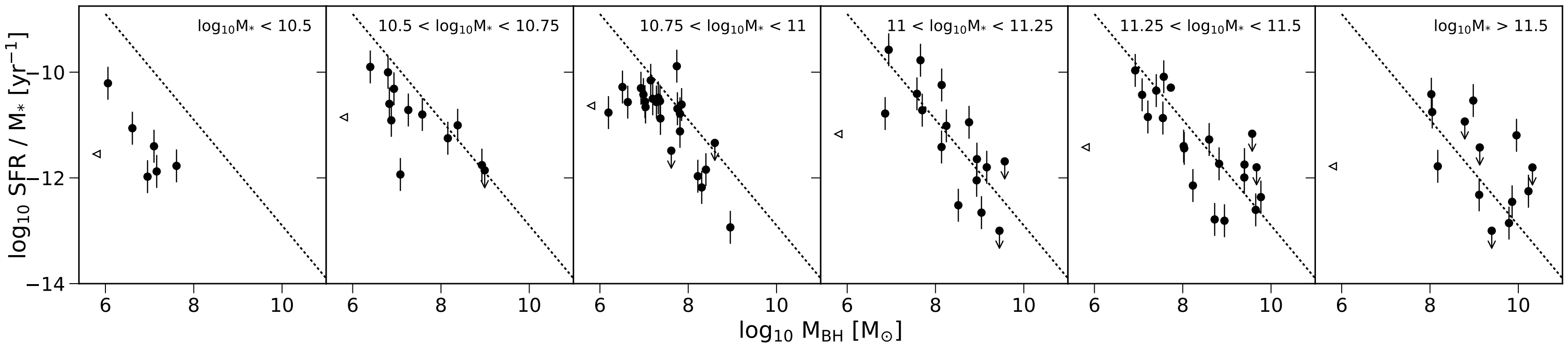

Figure 4.2: sSFR as a function of $M_{\rm BH}$ for different bins of M_*. The dotted lines are the same in each panel in order to compare the relations at high and low M_* bins. Open, left-facing triangles indicate the median sSFR at each M_* bin.

sSFR as a function of $M_{\rm BH}$ separated into bins of M_* in Figure 4.2. We find that the sSFR is a smoothly declining function of $M_{\rm BH}$ in each M_* bin. The dotted black line is the same in all panels in order to show the similar slope of the relation at all M_* bins. There is also an offset in the relation between different M_* bins where less massive galaxies tend to have lower sSFRs at a given $M_{\rm BH}$ than more massive galaxies. We also note that while there is a wide range of sSFRs at a given M_*, the median sSFR at each M_* bin (open, left-facing triangles) gradually decreases as M_* increases at $\log_{10} M_* > 10.75$, in accordance with the observation that more massive galaxies tend to be more quiescent. The galaxies detected at the two lowest M_* bins show lower median sSFRs. This is likely due to the fact that these galaxies are not representative of the general galaxy population at these M_* bins, since most low mass galaxies probably have central black holes with masses too low to be detected (Reines et al., 2013). Finally, we note that more massive galaxies tend to have more massive black holes although the scatter is substantial as is evident in the right panel of Figure 4.1.

The presence of a vertical offset for different M_* bins for the relations shown in Figure 4.2 hints at the fact that galaxies form a manifold in this three dimensional space. We choose to fit the simplest three-dimensional manifold – a plane – to the sSFR–$M_{\rm BH}$–M_* distribution for our sample of galaxies using a linear ordinary least squares analysis, excluding galaxies with sSFR upper limits from our fit. The result is described by the equation:

$$\begin{aligned}\log_{10}{\rm sSFR} = (0.80 \pm 0.18)\ &\log_{10}\frac{M_*}{M_{*,\rm avg}} \\ - (0.82 \pm 0.08)\ &\log_{10}\frac{M_{\rm BH}}{M_{\rm BH,avg}} \\ - (11.84 \pm 0.10)&,\end{aligned} \tag{4.1}$$

where we adopt bootstrap errors. We normalize M_* and $M_{\rm BH}$ by their average values for our sample, where $M_{*,\rm avg} = 1.62\times10^{11}\ {\rm M}_\odot$ and $M_{\rm BH,avg} = 8.71\times10^{8}\ {\rm M}_\odot$.

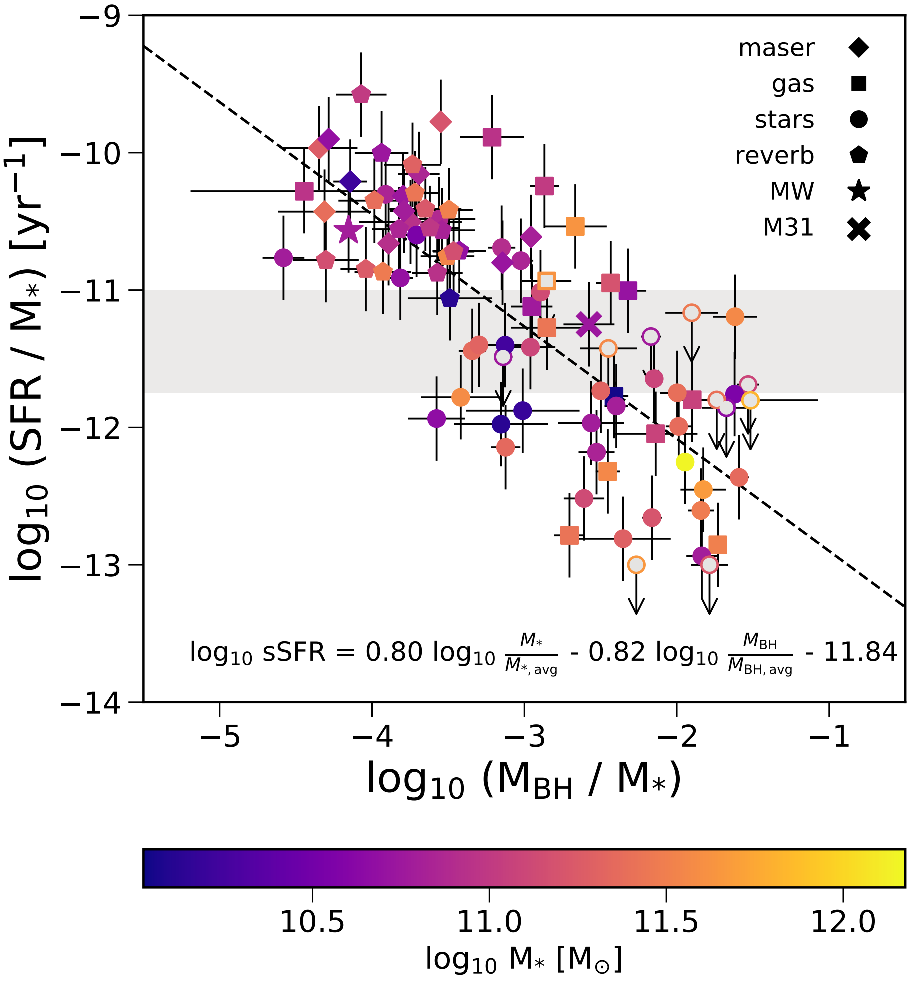

Figure 4.3: sSFR as a function of M_{BH}/M_* or sM_{BH} for our sample. The dashed line indicates the best fit plane described by the equation shown at the bottom of the panel. Upper limits are not included in the fit and are indicated by open, unfilled data points. The light gray shaded region highlights galaxies which are partially quiescent (See Section 4.5.2). The color gradient indicates M_*.

We note that the powers for M_* and $M_{\rm BH}$ are about equal. For this reason, Figure 4.3 shows a projection of this plane by plotting $\log_{10}$sSFR against the logarithm of the ratio between $M_{\rm BH}$ and M_*, or what we will call the galaxy's specific black hole mass ($sM_{\rm BH}$). Dividing by M_* effectively reduces the M_* dependence the sSFR has on the $M_{\rm BH}$. We find that the sSFR is a smoothly decreasing function of the $sM_{\rm BH}$ for the overall population where the scatter is $\sim$0.55 dex. Our result applies to a diversity of galaxy types, ranging from disky to spheroidal structures and spans a range of four orders of magnitude in sSFR, two orders of magnitude in stellar mass, and five orders of magnitude in black hole mass.

We color the data points by M_* to show two important features. First, we note that M_* and sSFR correlate poorly with one another compared to the correlation between $sM_{\rm BH}$ and sSFR. In other words, galaxies with similar M_* can be found anywhere along the relation, with any sSFR value, since they can have a wide variety of $sM_{\rm BH}$ values. Second, while this first point is true, more massive galaxies tend to preferentially have larger $sM_{\rm BH}$ and lower sSFRs while the opposite is true for less massive galaxies. This reflects the general trend that more massive galaxies tend to host less star formation while potentially hinting at the source of scatter in sSFR at a given M_*.

We note that a similar negative correlation is found in the central panel of Figure 4.1 where there is no dependence on M_*. We find that the scatter in sSFR at a given $M_{\rm BH}$ is 0.61 dex. Allowing the sSFR to be a function of both $M_{\rm BH}$ and M_* provides a better fit with 0.55 dex scatter – corresponding to a reduction by a fifth of the total variance in the central panel of Figure 4.1 – and is preferred at $>$99.99 percent level of all fits of bootstrapped samples having no M_* dependence. Even so, we stress that the exact powers of $M_{\rm BH}$ and M_* need to be confirmed with a larger and more complete sample than what current black hole data sets offer. We note that alternative versions of this fit, using different prescriptions for estimating SFR (e.g., including UV detections) and different selections for the central galaxy sample give similar results, with the fit parameters varying within their quoted errors.

4.5 Discussion

4.5.1 Physical Framework and Interpretation

Our main result is that the sSFR of a galaxy correlates smoothly with $sM_{\rm BH}$, suggesting that the star-forming properties of a galaxy are somehow aware of the properties of the central black hole. While the amount of scatter is significant at 0.55 dex, the negative correlation in our data is clearly present. In order to make physical sense of this, we argue that the sSFR can only know about the $M_{\rm BH}$ and M_* if one of two scenarios are occurring: (1) black hole feedback, assuming it is measurable via $M_{\rm BH}$, is regulating the amount of star formation in the galaxy to some degree, or (2) the increase in $M_{\rm BH}$ and decrease in sSFR are due to a strongly correlated but separate process where there is no direct causal connection between the two.

Recent galaxy formation models have relied on black hole-driven AGN feedback as the primary cause of quiescence (Croton et al., 2006; Sijacki et al., 2007; Guo et al., 2010; Vogelsberger et al., 2014a; Porter et al., 2014; Henriques et al., 2015; Schaye et al., 2015) since no other mechanism can produce a strong enough suppression of stellar mass build up in high mass galaxies (Bower et al., 2006). Results from Terrazas et al. (2016b), described in Chapter 3, show that out of the four models analyzed, only those models that use radio-mode AGN feedback to provide a continuous source of heat reproduce the observational result that quiescent and star-forming galaxies lie on distinct regions on the $M_{\rm BH}$-M_* plane where quiescent galaxies have more massive black holes than star-forming galaxies; this is unlike those models that use halo mass quenching or quasar-mode AGN feedback as the primary source of quiescence. As a result, we will set up a physical framework where we focus on scenarios which causally link the $M_{\rm BH}$ and the sSFR of a galaxy.

Successful simulations have modeled AGN feedback in the radio mode as bubbles expanding into the circumgalactic medium around a galaxy in order to heat the surrounding gas, thereby cutting off the fuel needed for star formation (e.g., Croton et al., 2006; Sijacki et al., 2007). While black hole feeding likely happens at irregular intervals depending on gas availability, bubbles formed by radio-mode AGN feedback are expanding into the medium long after accretion stops. In this physical scenario, the heating from the expansion of these bubbles is likely to be more or less continuous even though black hole feeding is not. Observationally, this idea is supported by the presence of long-lived X-ray cavities and 'ghost' cavities from past accretion events in the intracluster medium around cluster, group, and isolated galaxies (Bîrzan et al., 2004; David et al., 2009; Gitti et al., 2010; Shin et al., 2016).

Models also show that the $M_{\rm BH}$ correlates with the amount of heating from AGN feedback (Sijacki et al., 2015; Terrazas et al., 2016b). In accordance with this, our observational results in Section 5.6.2 show that larger values of $sM_{\rm BH}$ result in correspondingly lower values of sSFR to produce a negative correlation. A possible interpretation is that the sSFR adjusts to the $sM_{\rm BH}$ at least at $z = 0$ to produce a smoothly declining relation between these two parameters. This adjustment must happen on short enough time scales to allow such a relation between sSFR and $sM_{\rm BH}$. In other words, if either of these quantities could significantly change without allowing the other quantity to adjust, then a relation between these two parameters would not appear as clearly as it does in Figure 4.3.

In addition, we note that the shape of the relation is important: a smoothly declining relation may hint at the physics behind heating and cooling of gas around the galaxy. More specifically, this may mean that an intermediate $sM_{\rm BH}$ results in an intermediate amount of gas heating which decreases, but does not completely halt, the amount of gas cooling onto the disk to fuel star formation in the galaxy. We expand on this issue in Section 4.5.2 where we discuss the phenomenon of partial quiescence.

The vertical offset in the relations between sSFR and M_{BH} from low to high M_* bins in Figure 4.2 can be interpreted to mean that more massive galaxies need a more massive black hole to maintain the same degree of quiescence as less massive galaxies, since more massive galaxies have a deeper potential well and, in the absence of heating, would be forming more stars as a result of cooling and gravity. However, more massive galaxies also tend to have lower sSFRs than the less massive galaxies, in general agreement with other studies (Brinchmann et al., 2004; Salim et al., 2007). This implies that the M_{BH} of massive galaxies are significantly larger than those of less massive galaxies, resulting in the vast majority of the high M_* galaxy population to be predominantly quiescent. In addition, the fact that we normalize both the SFR and M_{BH} by M_* tells us that reducing the dependence on the depth of the potential well – represented by M_* in this work – gives us a similar relation across a diverse group of central galaxies with $M_* > 10^{10}$ $\mathrm{M}_{\odot}$.

We also note that the scatter between sSFR and M_{BH} increases in the highest M_* bin in Figure 4.2. This could be due to multiple factors. For one, M_* is likely an increasingly poor tracer of a galaxy's potential well at high M_* since the M_*–M_{h} relation becomes substantially flatter at these mass regimes (Moster et al., 2010; Behroozi et al., 2010, 2013). Instead, obtaining a halo mass may be more effective, albeit more difficult, and may eliminate the increased scatter. In addition, low sSFR values are increasingly difficult to measure and may have less meaning with regards to the actual amount of star formation in the galaxy. Another explanation may be that more massive galaxies are probing clusters rather than groups and isolated galaxies. Black hole feedback in these systems may differ in terms of how gas heating and cooling operates (Gaspari et al., 2011).

An important assumption we have made is that M_{BH} is measuring the amount of heating energy being injected into the gas around the galaxy while the sSFR is measuring the amount of gas cooling onto the galaxy. In the real Universe, these parameters may vary widely on a galaxy-to-galaxy basis based on the state of the gas, the star formation efficiency of the galaxy, the duty cycle and jet power of the black hole feedback and how that correlates with $M_{\rm BH}$, and potentially many other factors.

4.5.2 Partial Quiescence

Galaxies which have low yet significant amounts of star formation in our sample are shown in the light gray band in Figure 4.3. Previous studies have often referred to these galaxies as transitioning or "green valley" galaxies (Bell et al., 2004; Balogh et al., 2004; Martin et al., 2007; Brammer et al., 2009; Mendez et al., 2011; Wetzel et al., 2012; Gonçalves et al., 2012; Krause et al., 2013; Pan et al., 2014), assuming they are on their way to becoming completely quiescent. Given the dearth of galaxies in this region on a color-magnitude diagram, the traditional view is that galaxies quickly move from the blue cloud to the red sequence or, as has been interpreted, from star-forming to quiescent (e.g., Baldry et al., 2004).

A smoothly decreasing correlation between the sSFR and $sM_{\rm BH}$ shown in Figure 4.3 and described in Section 5.6.2 is perhaps unexpected given the commonly held belief that galaxies exist only briefly in this transition state. If the $M_{\rm BH}$ grows significantly, then in order to land on the relation in Figure 4.3 and agree with our observational result, the galaxy must also decrease its sSFR accordingly. Therefore, a star-forming galaxy that grows its black hole to an intermediate $sM_{\rm BH}$ must also decrease its sSFR to an intermediate value on timescales short enough to produce a relation between the two quantities.

We note that this framework *does not require central galaxies with intermediate sSFRs to be transitioning at all.* A central galaxy can stay in the "green valley" as long as it no longer grows its $sM_{\rm BH}$. In this scenario, the relation between sSFR and $sM_{\rm BH}$ represents the amount of star formation that results from the balance between heating and cooling represented by the ratio between a galaxy's $M_{\rm BH}$ and M_*. If this is the case, then this framework implies that all central, massive galaxies tend towards an equilibrium position defined by this relation which determines their sSFR from their $sM_{\rm BH}$, and that much of the scatter likely comes from the time it takes for the sSFR to adjust to the $sM_{\rm BH}$.

As a result, the fact that the sSFR, $M_{\rm BH}$, and M_* are smooth but scattered functions of each other leads us to argue that many of the partially quiescent galaxies in our sample may not be transitioning – instead they may maintain a quasi-stable state of quiescence that correlates with their $M_{\rm BH}$ and M_*.

One possible example of this in our sample is M31, labeled in Figure 4.3. M31 is not undergoing any significant event that suggests it is quenching and heading towards a completely quiescent state. Yet many studies have shown that M31 has a lower sSFR (Kang et al., 2009; Ford et al., 2013; Lewis et al., 2015) than expected based on where a galaxy with its stellar mass would be if it were on the star forming main sequence. In our framework, this simply comes from the fact that M31 has an over-massive black hole for its stellar mass (i.e. a higher $sM_{\rm BH}$) and as a result gives us a lower sSFR. Similarly, M81 also lands within the partially quiescent sample and does not exhibit any morphological signs of transitioning.

If there are a significant number of stable galaxies with intermediate sSFRs, then this implies a more populated "green valley" than previously observed. In support of this implication, Oemler et al. (2016) argue that the "green valley" is more populated than is otherwise believed due to the selection effects, systematic errors, and bias they find in one of the more popular collections of SFRs from SDSS (Brinchmann et al., 2004). They present a representative sample of local galaxies with updated and reliably-measured SFRs from ultraviolet and mid-IR fluxes and find a significantly larger, distinct population of galaxies with intermediate sSFRs. In addition, Eales et al. (2017) argue that the galaxy population exhibits a gradual difference in properties between star-forming and quiescent galaxies, a behavior that is erased in color-space due to colors varying minimally below a threshold value of sSFR. This would challenge the widely accepted view that galaxies live in two distinct populations, and instead argue for a more unitary approach. Finally, many studies have also argued for the existence of varying degrees of quiescence that could hint at a class of galaxies that spend an extended amount of time in the "green valley" (e.g., Lian et al., 2016; Pandya et al., 2016). Even so, our proposed framework of sSFR regulation by the black hole does not necessarily require a continuous distribution of galaxies along this relation since this distribution depends strongly on the details of black hole growth.

We note that our sample selection is biased and heterogeneous due to our requirement of a dynamical black hole mass measurement using a variety of detection methods. This impacts our analysis in two ways. First, while we do not detect a significantly underpopulated "green valley" for the data in our sample, the current black hole data available are insufficient to probe the prominence of the "green valley" in the general central galaxy population since the sample is not representative. Future work will be important for determining the prominence of the "green valley" and the strength of bimodality in sSFR parameter space for central galaxies at this mass regime using reliable SFR indicators (See Oemler et al. 2016 and Eales et al. 2017 for important progress). Second, while it is clear that sSFR is a smoothly decreasing function of $sM_{\rm BH}$ for the current black hole data for central galaxies, we caution that the exact form of the relation may be impacted by selection. For example, studies using the central stellar mass density within 1 kiloparsec ($\Sigma_{\rm 1kpc}$) as an indirect proxy for $M_{\rm BH}$ see a relatively sudden drop in sSFR as a function of $\Sigma_{\rm 1kpc}$ (Fang et al., 2013; Woo et al., 2015). We do not see evidence of this sudden drop in sSFR with our dataset, perhaps due to the inadequacy of such proxies for $M_{\rm BH}$ or due to our sample's size and inhomogeneities. It would be important to quantify the degree to which the dependence of sSFR is gradual and continuous with a larger and more complete sample, and to remain open to any higher order structure in the sSFR–$M_{\rm BH}$–M_* parameter space.

While we are proposing the possibility that much of the "green valley" population is in a quasi-stable state of partial quiescence, we also recognize that there likely exist various pathways a galaxy could take as it grows its black hole and stellar mass and varies its star formation rate. For example, rapid and more violent processes perhaps more common for giant ellipticals may skew the observed relationship between the sSFR, $M_{\rm BH}$, and M_* as may be shown in the increased scatter in the relation between $M_{\rm BH}$ and sSFR at high stellar masses. The existence of more than one quenching mode and speed has been discussed in other works (Martin et al., 2007; Barro et al., 2013; Schawinski et al., 2014; Woo et al., 2015; Lian et al., 2016). Whereas a quasi-stable state of partial quiescence would be consistent with slow quenching since the relevant timescales are comparable to or longer than a Hubble time, those experiencing faster quenching would likely account for some of the scatter between sSFR and $sM_{\rm BH}$. In addition, other processes that affect a galaxy's sSFR such as morphological quenching, stellar and supernovae Ia feedback, merging, or gravitational heating may affect a galaxy's position on the sSFR–$sM_{\rm BH}$ plane. Even so, the clear correlation between these three parameters shows that, if our physical framework is at least generally valid, black hole feedback is the most important physical mechanism in determining a galaxy's star formation properties and that a large part of the galaxy sample can be characterized as being in a quasi-steady state or approaching this state as the sSFR responds to the change in $sM_{\rm BH}$ that the galaxy has undergone.

4.5.3 Model Comparison

Terrazas et al. (2016b) (Chapter 3) shows a strong correlation between M_{BH} and quiescence at a given stellar mass. When comparing these results to state-of-the-art models, they found that the latest Munich semi-analytic model (Henriques et al., 2015) and the Illustris hydrodynamic simulation (Vogelsberger et al., 2014a) showed the best agreement with observations unlike the EAGLE hydrodynamic simulation (Schaye et al., 2015) and GalICS semi-analytic model (Cattaneo et al., 2006a). Here we focus on the Munich, Illustris, and EAGLE simulations since these explicitly use AGN feedback as the primary mechanism behind quiescence.

The Munich model includes a continuous heating rate affecting the temperature of the circumgalactic medium that depends on the hot halo gas mass and M_{BH}. Illustris introduces buoyant bubbles which expand into the atmosphere every time the black hole is fed cold gas. While the creation of these bubbles is stochastic, the effect they have on the temperature of the circumgalactic medium is gradual as the bubble slowly expands into the gas. Hence, both of these models use either continuous or quasi-continuous heating from radio-mode AGN feedback in order to shut off star formation in galaxies at the high end of the stellar mass function. In contrast, EAGLE uses quasar-mode feedback to intermittently inject energy into the interstellar medium only when there is gas available to the black hole.

We find that the quantitative relationship between sSFR, M_{BH}, and M_* vary from model to model. For example, at the stellar mass regimes of interest, the Munich model's determination of a central galaxy's sSFR has little to no dependence on the stellar mass of the central galaxy and instead depends strongly on a M_{BH} threshold, see Terrazas et al., 2016a and Chapter 2. Conversely, Illustris's sSFRs depend more strongly on M_* such that more massive galaxies need more massive black holes in order to have the same sSFR as a lower mass galaxy, see Terrazas et al., 2016b. In Section 5.6.2 we fit a plane to our observational data which demonstrated that *in the*

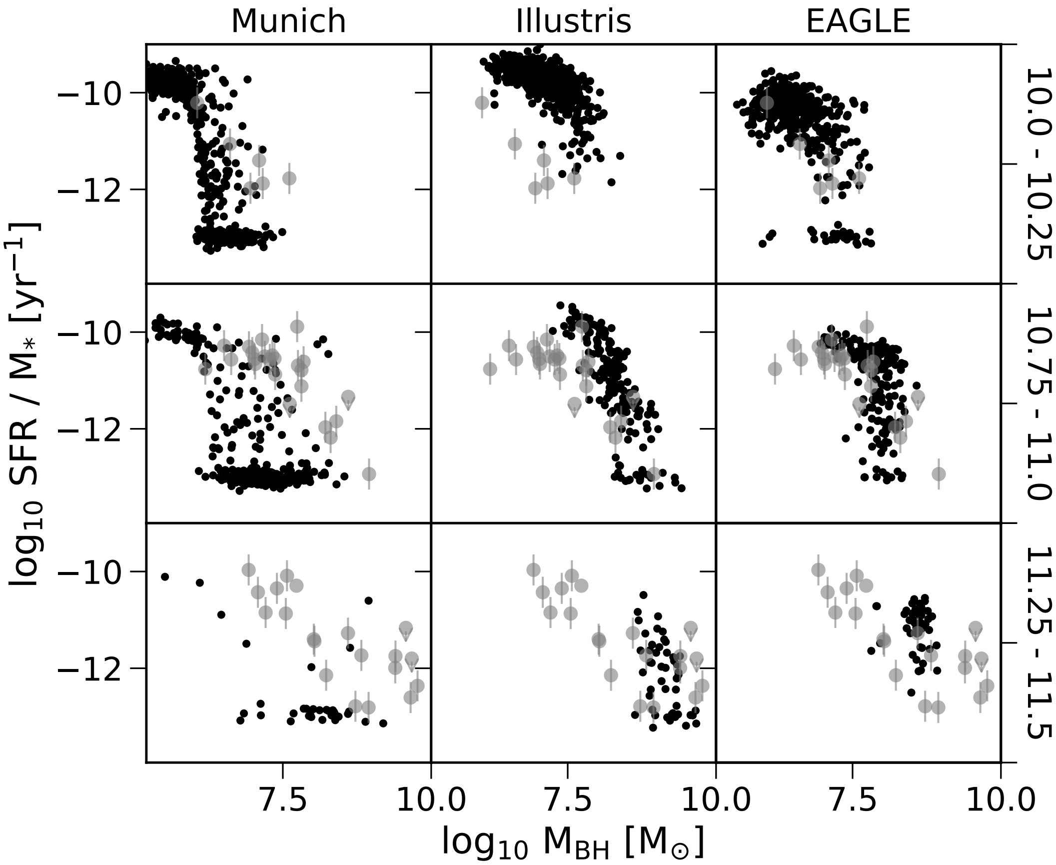

Figure 4.4: sSFR as a function of $M_{\rm BH}$ in three bins of M_* for the Munich, Illustris, and EAGLE galaxy formation models (black points). Overlaid is the observational data from Figure 4.2 in the corresponding M_* bins (gray translucent points). Each column indicates different models and each row indicates the M_* bin: $10.25 < \log_{10}$ $M_* < 10.5$ (top); $10.75 < \log_{10}$ $M_* < 11.0$ (middle); and $11.25 < \log_{10}$ $M_* < 11.5$ (bottom).

real Universe sSFR is a smoothly decreasing function of the ratio between $M_{\rm BH}$ and M_* (what we are calling the $sM_{\rm BH}$). However, in the Munich model, for example, a ratio of $M_{\rm BH}$ and $M_*^{0.1}$ would better reveal the physics behind quiescence since the Munich model's sSFRs barely depend on M_* and therefore requires M_* to have a smaller power. As a result, the $sM_{\rm BH}$ will not be useful for understanding the suppression of sSFR in the models since they do not agree with observations in this respect.

Rather than introducing different powers of M_*, we choose to compare the models to our observational results by presenting the sSFR–$M_{\rm BH}$ plane at different M_* bins for each of these models. This effectively focuses on the dependence between the sSFR and $M_{\rm BH}$ rather than the differences between M_* dependencies in the models. We show the distributions of these galaxies in Figure 4.4 where for each model we select only central galaxies within a 100 Mpc^3 volume at $z = 0$. The M_* bins are directly comparable to those in the first, third, and fifth panels of Figure 4.2 whose data points are overplotted in gray. Any galaxies with sSFR $< 10^{-13}$ yr^{-1} are assigned an arbitrarily low sSFR value defined by a normal distribution around this limit.

We find that the Munich model (left panels) exhibits a steep drop off in sSFR at a given $M_{\rm BH}$ for most central galaxies. A clear bimodality exists where galaxies either have high or low sSFRs with a few galaxies in between. In the highest M_* bin there are very few galaxies with most of them having a massive black hole and therefore having very low sSFR values. Terrazas et al. (2016a) (Chapter 3) show that most galaxies in this model are immediately quenched as soon as they reach a redshift-dependent critical $M_{\rm BH}$ (See their Section 3 for more details).

The Illustris simulation (center panels) shows a considerably different distribution on this plane. Rather than showing a steep drop in specific star formation rate as a function of $M_{\rm BH}$ at a given M_*, it shows a smoothly declining function for galaxies with massive enough black holes to begin suppressing star formation, much like what is seen in our observational results in Figure 4.2. It is clear, however, that black hole mass correlates more tightly with stellar mass in Illustris than in our observational sample since there there is a larger variety of black hole masses at each stellar mass bin in Figure 4.2 than for Illustris. In addition, galaxies with $M_{\rm BH} \lesssim 10^7$ $\rm M_\odot$ do not exhibit much dependence on $sM_{\rm BH}$ since these galaxies' sSFRs are likely not regulated by AGN feedback in this model.

The EAGLE simulation (right panels) exhibits an L-shaped distribution where galaxies are mostly star-forming until they reach a certain $M_{\rm BH}$ value depending on their M_*, where many but not all galaxies begin to have lower sSFRs. As discussed in Terrazas et al. (2016b), this behavior is not reflected in the observational results where star-forming and quiescent galaxies have distinct black hole mass distributions at a given M_*. The overlap in these distributions at high $M_{\rm BH}$ in this model is likely due to the fact that galaxies in EAGLE undergo intermittent heating episodes rather than a continuous injection of energy. EAGLE galaxies can continue forming stars once again in between feedback events even with a massive central black hole, producing an L-shaped distribution that is not reflected in our observational results. In other words, in EAGLE, a massive black hole is a necessary but not sufficient condition for quiescence in galaxies since star-forming galaxies can also host massive black holes.

Each of these models have been quite successful in reproducing many of the observational trends out to $z = 2$, particularly the Munich model. Even so, it is clear that different physical implementations of quiescence can affect the distributions in the sSFR–$M_{\rm BH}$–M_* parameter space, even when they use similar physical frameworks for AGN feedback. As such, none of the models match our observational results perfectly as is clear from the overlaid observational data (gray translucent points) in each panel. The models differ from each other and from the observations in this parameter space with respect to their variety of dependences on M_*, black hole mass distributions, stellar mass distributions, and strength of bimodality. This manifests itself as differences in the shape of the distributions, the slopes of the decline in sSFR, the normalization of the distributions in each M_* bin, and the scatter of sSFR as a function of $M_{\rm BH}$.

However, qualitatively, we find that the results from Illustris better resemble our observational results. We note that the smoothly-declining yet scattered relation between sSFR and $M_{\rm BH}$ in Illustris shows that even in an idealized simulation, an appreciable amount of scatter, such as what is seen in our observations, is expected within a framework where AGN feedback determines a galaxy's star formation properties.

Even so, it is well-established that the AGN feedback in Illustris is too violent and ejects too much gas out of its hot halo (Vogelsberger et al., 2014a). Further implementations of Illustris must be tested in order to understand whether this behavior persists with a less violent AGN feedback model (see Chapter 5). By extension, future models will need to consider how their prescriptions for AGN feedback correspond to the largely unexplored idea of a smoothly decreasing correlation between sSFR and $sM_{\rm BH}$ along with the idea of partial quiescence.

4.6 Conclusions

In order to more directly and statistically study AGN feedback in the context of galaxy relations, we choose to study the correlation between a galaxy's sSFR, $M_{\rm BH}$, and M_*. We have shown that for our diverse sample of 91 central galaxies with dynamically detected $M_{\rm BH}$, sSFR is a smoothly decreasing function of $M_{\rm BH}/M_*$, or what we call the specific black hole mass, $sM_{\rm BH}$. In an attempt to interpret this correlation, we propose a physical framework where the amount of gas heating from radio-mode AGN feedback is reflected by $M_{\rm BH}$ and reduces the supply of star-forming material within the galaxy. In this framework, a galaxy with a larger $sM_{\rm BH}$ value would have a correspondingly lower sSFR, in accordance with our observational result.

This framework provides an alternative to the idea that all "green valley" galaxies are transitioning from star-forming to quiescent phases. Instead, it predicts that these galaxies with intermediate values of $sM_{\rm BH}$ live in a stable state of partial quiescence between star-forming and quiescent galaxies.

No current models achieve the distribution of galaxies that we see in this three-dimensional parameter space, although Illustris comes close. Future work will need to take these observational constraints into account when implementing AGN feedback models in order to shut off star formation in central galaxies.

Acknowledgments

This chapter is a reproduction of an article of the same title published on August 3, 2017 in the Astrophysical Journal in Volume 844, Issue 2. The co-authors of this article are Eric F. Bell, Joanna Woo, and Bruno M. B. Henriques. The article is copyright 2017, the American Astronomical Society, reproduced here under the non-exclusive right of republication granted by the AAS to the author(s) of the article.

B.A.T. is supported by the National Science Foundation Graduate Research Fellowship under Grant No. DGE1256260. We acknowledge helpful discussions with S. White, E. Gallo, J. Bregman, K. Gultekin, H. W. Rix, S. Faber, S. Ellison, A. Pontzen, L. Sales, B. O'Shea, M. Donahue, and M. Voit. This work used the SIMBAD database at CDS, and the NASA/IPAC Extragalactic Database (NED), operated by the Jet Propulsion Laboratory, California Institute of Technology, under contract with NASA.

CHAPTER V

The relationship between black hole mass and galaxy properties: Examining the black hole feedback model in IllustrisTNG

5.1 Abstract

Supermassive black hole feedback is thought to be responsible for the lack of star formation, or quiescence, in a significant fraction of galaxies. We explore how observable correlations between the specific star formation rate (sSFR), stellar mass (M_{star}), and black hole mass (M_{BH}) are sensitive to the physics of black hole feedback in a galaxy formation model. We use the IllustrisTNG simulation suite, specifically the TNG100 simulation and a dozen model variations that alter the parameters of the black hole model. Focusing on central galaxies at z = 0 with $M_{star} > 10^{10}$ $M_{\odot}$, we find that the sSFR of galaxies in IllustrisTNG decreases once the energy from black hole kinetic winds at low accretion rates becomes larger than the gravitational binding energy of gas within the galaxy stellar radius. This occurs at a particular M_{BH} threshold above which galaxies are found to sharply transition from being mostly star-forming to mostly quiescent. As a result of this behavior, the fraction of quiescent galaxies as a function of M_{star} is sensitive to both the normalization of the M_{BH}-M_{star} relation and the M_{BH} threshold for quiescence found in TNG. Finally, we compare

TNG results to observations of 91 central galaxies with dynamical M_{BH} measurements with the caveat that this sample is not representative of the whole galaxy population. While IllustrisTNG reproduces the observed trend that quiescent galaxies host more massive black holes, the observations exhibit a broader scatter in M_{BH} at a given M_{star} and show a smoother decline in star formation rate with black hole mass.

5.2 Introduction

In the last 10 billion years, the amount of new star formation in the Universe has decreased substantially. Observational surveys of galaxy populations at different epochs have also shown a gradual increase in the number of galaxies whose light is dominated by older stellar populations signaling a lack of new stars in these systems (e.g., Bell et al., 2004; Baldry et al., 2004; Williams et al., 2009; Muzzin et al., 2013; Ilbert et al., 2013; Tomczak et al., 2014). Studies of quiescence, i.e. the state of reduced star formation activity, in galaxies have aimed at pinpointing a physical mechanism responsible for this behavior. In this work, as in the other chapters of this dissertation, we will focus on *central* galaxies situated at the centers of their dark matter halos since satellite galaxies undergo environmental processes that may affect their star formation activity due to their placement within a larger galaxy's halo.

One observational approach to understanding quiescence in central galaxies has focused on measuring correlations between galaxy properties and quiescence. For example, galaxies with high stellar masses (e.g., Kauffmann et al., 2003), bulge-dominated morphologies (e.g., Bell et al., 2012; Bluck et al., 2014b), high halo masses (e.g., Wang et al., 2018), high Sérsic indices (e.g., Cheung et al., 2012), high central stellar surface densities (e.g., Woo et al., 2015), and more massive black holes (e.g., Terrazas et al., 2016b, 2017; Martín-Navarro et al., 2018) have a higher likelihood of being quiescent. Many mechanisms attempting to explain these correlations have been proposed, such as supernovae/stellar winds (e.g., Tang & Wang, 2005; Conroy et al., 2015), gravitational heating (e.g., Johansson et al., 2009), morphological quenching (e.g., Martig et al., 2009), halo mass quenching (e.g., Dekel & Birnboim, 2006; Cattaneo et al., 2006a; Birnboim et al., 2007), and central black hole feedback (e.g., Kauffmann & Haehnelt, 2000; Di Matteo et al., 2005; Croton et al., 2006; Bower et al., 2006; Somerville et al., 2008; Fabian, 2012).

In a cosmological context, gas that falls into a dark matter halo is able to lose energy and cool via dissipative processes to form a disk of cold gas at the bottom of the halo's potential well (e.g. Silk, 1977; White & Rees, 1978; Fall & Efstathiou, 1980; Katz & Gunn, 1991). The gas that accumulates in the disk fragments, cools, and condenses into molecular clouds which eventually collapse into new stars.

One natural feedback channel that limits star formation is stellar feedback from star formation itself. Radiation from stars, stellar winds, and supernovae regulate the production of new stars by limiting the amount of cold dense gas (e.g., Silk, 2003; Springel & Hernquist, 2003; Hopkins et al., 2011). This form of feedback, however, is insufficient for producing quiescence in massive galaxies. Recent models show that the gas expelled from the galaxy by stellar feedback is reincorporated to provide fuel for continued star formation (e.g., Dubois et al., 2016; Pontzen et al., 2017; Su et al., 2018; Choi et al., 2018), a behavior that is more efficient for more massive systems (Oppenheimer et al., 2010; Bower et al., 2012; Christensen et al., 2016; Muratov et al., 2015). Thus, a picture emerges of galaxies undergoing a cycle of ejection and reincorporation that regulates cooling and star formation via stellar feedback similar to various 'bathtub' models that have been proposed (Bouché et al., 2010; Dutton et al., 2010; Davé et al., 2012; Peng & Maiolino, 2014; Birrer et al., 2014).

In this physically-motivated framework, quiescence can be defined as the consequence resulting from the disruption of this cycle. This disruption can take the form of 'ejective' and/or 'preventative' feedback (see Section 3.3 of Somerville & Davé 2015 for a full review). Ejective feedback pushes gas out of galaxies which may otherwise continue forming stars. Preventative feedback prevents galaxies from accumulating star-forming gas from the cooling of the circumgalactic medium. While both processes likely play a role in suppressing star formation, any proposed mechanism for long-term quiescence must be at least partly preventative in nature since any accretion of new gas would re-establish star formation in the galaxy.

A popular mechanism for producing quiescence in recent physics-based galaxy formation models is black hole feedback (Bower et al., 2006; Croton et al., 2006; Sijacki et al., 2007; Somerville et al., 2008; Guo et al., 2010; Booth & Schaye, 2011; Vogelsberger et al., 2014a; Henriques et al., 2015; Somerville & Davé, 2015; Schaye et al., 2015; Dubois et al., 2016; McCarthy et al., 2017; Bower et al., 2017; Weinberger et al., 2018). Theoretically, accretion onto a black hole has the potential to release an enormous amount of energy into the surrounding medium. Observationally, activity from central supermassive black holes has been seen in many forms.

When black holes undergo episodes of high accretion rate feedback, the radiation pressure created by the highly luminous accretion disk is thought to result in large scale outflows. Many X-ray luminous active galactic nuclei (AGN) are observed to host ionized gas outflows in support of this idea (Heckman et al., 1981; Crenshaw et al., 2010; Villar-Martín et al., 2011; Harrison et al., 2014; Cicone et al., 2014; Woo et al., 2016; Rupke et al., 2017). At lower accretion rates, black holes are thought to produce jets from their accretion disks which propel low-density buoyant bubbles into the atmospheres of galaxies. Indeed, large extended radio-emitting lobes which create cavities within the hot gas atmosphere visible in X-ray maps have been observed around massive galaxies in various environments from small groups to large clusters (e.g., Bîrzan et al., 2004; McNamara & Nulsen, 2007; Fabian, 2012; Shin et al., 2016; Werner et al., 2019). Some galaxies have been observed to exhibit signs of both a bright X-ray point source in conjunction with extended radio emission, further complicating the issue of the accretion physics that could produce these varied effects on the gas within and around galaxies (Komossa et al., 2006; Yuan et al., 2008; Berton et al., 2015; Coziol et al., 2017). More recently, some galaxies with low luminosity AGN have been observed to produce bisymmetric winds of ionized gas which are thought to affect star formation in the galaxy (Cheung et al., 2016; Penny et al., 2018). Finally, our own Milky Way galaxy also hosts evidence of a possible relic from black hole feedback in the form of Fermi bubbles (Su et al., 2010; Guo & Mathews, 2012).

The black hole accretion physics occurring at parsec-scales and producing these observed forms of black hole activity is not well understood. As a result, there is substantial freedom in the subgrid physics used between different cosmological simulations to model the effects black holes may have on the surrounding gas. This can result in important differences in the star formation histories, gas content, and stellar mass distributions of simulated galaxy populations which can then be compared to observational data (e.g., Terrazas et al., 2016b, 2017; Bluck et al., 2016, 2019). As such, understanding the details of how small-scale subgrid physics affects large scale galaxy population statistics in models can improve our understanding of the feedback mechanisms that may produce quiescence in the real Universe.

With these considerations in mind, the central challenge this work seeks to address is understanding how observed galaxy correlations between specific star formation rate (sSFR), stellar mass ($\mathrm{M_{star}}$), and black hole mass ($\mathrm{M_{BH}}$) at $z = 0$ can be interpreted in light of the results from a physical model of black hole feedback. In this work, we use the IllustrisTNG simulation suite (TNG; Springel et al., 2018; Marinacci et al., 2018; Naiman et al., 2018; Pillepich et al., 2018; Nelson et al., 2018a) in order to explore this question, focusing on central galaxies with $\mathrm{M_{star}} > 10^{10}\ \mathrm{M_\odot}$. TNG uses black hole feedback in order to suppress the SFRs and $\mathrm{M_{star}}$ content of galaxies with $\mathrm{M_{star}} \gtrsim 10^{10}\ \mathrm{M_\odot}$ (Weinberger et al., 2017, 2018). Thus, as we will show, the sSFR, $\mathrm{M_{star}}$, and $\mathrm{M_{BH}}$ of galaxies are causally related to one another through the model's mechanism for quiescence.

One important feature of TNG for our purposes is the availability of dozens of TNG model variations, first introduced in Pillepich et al. (2018). We use these model variations to study the impact of different parameter choices, as is similarly done in Weinberger et al. (2017). By using the model variations explicitly related to black hole feedback, we can explore how changes to the model can affect TNG's galaxy population statistics. We aim to link these differences in observable correlations to the effects of black hole feedback on the physical properties of the gas within the galaxy and in the surrounding circumgalactic medium. Thus, our work will show how these observed correlations may be physically interpreted in the real Universe.

We organize our results as follows: Section 5.3 describes the TNG simulation suite, the model variations, the black hole physics model, and our definitions of galaxy properties in the model. Section 5.4 describes the necessary conditions for quiescence in TNG using three of the model variations. Section 5.5 describes the effects of black hole feedback on gas and outlines a phenomenological framework for the physics of quiescence in TNG. Section 5.6 compares the model results to observational correlations, illuminating how the sSFR, $\mathrm{M_{star}}$, and $\mathrm{M_{BH}}$ can encode information on the physics behind quiescence within the context of black hole feedback. Section 5.7 uses model variations to illuminate how observables may be affected by changes in the way black hole feedback operates. In Section 5.8 we reflect on our results and present future outlooks. Section 5.9 summarizes our findings and contains our concluding remarks.

Table 5.1: The list of model variations we use for this work. Columns: (1) model number, (2) model name, (3) parameter changed, (4) fiducial model value, (5) changed value, (6) short description of the alteration. See Section 5.3.1 for more information on each of the model parameters in column (3).

Model No. (1)	Name (2)	Parameter changed (3)	Fiducial value (4)	Changed value (5)	Description (6)
0000	TNG35	n/a	n/a	n/a	Same physics as the larger TNG volumes
2201	NoBHs	n/a	n/a	n/a	Black holes turned off
3000	NoBHwinds	χ_0	0.002	0	Thermal mode at all $\dot{\mathrm{M}}_{\mathrm{BH}}$
3101	LowKinEff	$\varepsilon_{\mathrm{f,kin,max}}$	0.2	0.05	Lower gas coupling efficiency for BH kinetic feedback
3102	HighKinEff	$\varepsilon_{\mathrm{f,kin,max}}$	0.2	0.8	Higher gas coupling efficiency for BH kinetic feedback
3103	HighThermEff	$\varepsilon_{\mathrm{f,high}}$	0.1	0.4	Higher gas coupling efficiency for BH thermal feedback
3104	LowThermEff	$\varepsilon_{\mathrm{f,high}}$	0.1	0.05	Lower gas coupling efficiency for BH thermal feedback
3301	HighChi0	χ_0	0.002	0.008	Higher Eddington ratio threshold normalization
3302	LowChi0	χ_0	0.002	0.0005	Lower Eddington ratio threshold normalization
3403	HighMpiv	M_{piv}	1e8 $\mathrm{M}_\odot$	4e8 $\mathrm{M}_\odot$	Higher pivot mass in Eddington ratio threshold
3404	LowMpiv	M_{piv}	1e8 $\mathrm{M}_\odot$	2.5e7 $\mathrm{M}_\odot$	Lower pivot mass in Eddington ratio threshold
3801	LessBursty	f_{re}	20	5	Lower minimum energy for BH kinetic winds
3802	MoreBursty	f_{re}	20	80	Higher minimum energy for BH kinetic winds

5.3 The Illustris TNG Simulation Suite

The IllustrisTNG project is a large-scale cosmological and gravo–magneto–hydro–dynamical simulation suite of galaxy formation in the context of a ΛCDM Universe (Springel et al., 2018; Marinacci et al., 2018; Naiman et al., 2018; Pillepich et al., 2018; Nelson et al., 2018a). TNG is the descendant of the original Illustris project (Vogelsberger et al., 2014a,b; Genel et al., 2014; Sijacki et al., 2015), modifying and adding numerous features with the goal to improve the agreement between the simulation and observational results by providing a comprehensive physical model of galaxy formation from the early Universe to the present day. The simulation uses the Arepo code to solve the equations of ideal magnetohydrodynamics and self-gravity on a moving, unstructured mesh (Springel, 2010; Pakmor et al., 2011, 2016). For more information on the numerical aspects of the TNG model, we refer the reader to Pillepich et al. (2018) and Weinberger et al. (2017).

The simulation suite contains three simulation volumes TNG50, TNG100, and TNG300 sized at 51.7^3, 110.7^3, and 302.6^3 comoving Mpc^3 volumes, respectively. In this work, we will be focusing on results from TNG100 as it has roughly the same resolution (within a factor of 2) as the model variations which we will use extensively in this chapter and which are detailed in Section 5.3.2. This will allow a comparison without the complications of resolution effects present in TNG300 (see Appendix 5.11). TNG100 has 2×1820^3 initial resolution elements with a baryonic mass resolution of 1.4×10^6 $\mathrm{M}_\odot$ and gravitational softening length of 0.74 kpc at $z = 0$. The cosmological parameters of the model are based on Planck Collaboration et al. (2016) with a matter density $\Omega_{M,0} = 0.3089$, baryon density $\Omega_{b,0} = 0.0486$, dark energy density $\Omega_{\Lambda,0} = 0.6911$, Hubble constant $\mathrm{H}_0 = 67.74$ km/s/Mpc, power spectrum normalization factor $\sigma_8 = 0.8159$, and spectral index $n_s = 0.9667$.

TNG models the physics of primordial and metal-line gas cooling, magnetic fields, star formation, stellar evolution and feedback, chemical enrichment, and black hole growth and feedback. There are several key differences between the original Illustris model and TNG which are described in Pillepich et al. (2018). For our purposes, the most relevant modification is how black hole feedback operates at low accretion rates. Instead of the thermal bubble model implemented by the original Illustris model and described in Sijacki et al. (2007, 2015), TNG adopts a kinetic wind model that inputs kinetic energy originating at the black hole into nearby gas particles (Weinberger et al., 2017). The primary motivation for changing the physical prescription for black hole feedback was to prevent the ejection of large amounts of gas from the halos of intermediate to high mass galaxies ($\mathrm{M_{star}} > 10^{10}$ $\mathrm{M_{\odot}}$). The amount of halo gas around many of these galaxies in Illustris is much lower than observations suggest (see, for example, Figure 10 in Genel et al., 2014), yet the interstellar medium gas fractions within galaxies were too high, thus leading to the implementation of a modified form of feedback.

5.3.1 The formation, growth, and feedback of black holes in TNG

Here we provide a brief description of the relevant features of the black hole model in TNG. For full details, see Weinberger et al. (2017).

Black holes are placed at the center of a halo's potential well with a seed mass of $\mathrm{M_{seed}} = 1.18 \times 10^{6}$ $\mathrm{M_{\odot}}$ once a halo grows past a threshold mass of $\mathrm{M_h} = 7.38 \times 10^{10}$ $\mathrm{M_{\odot}}$. Once seeded, black holes grow either through accretion at the Eddington-limited Bondi accretion rate or by merging with other black holes during a galaxy merger. Additionally, black holes are made to stay at the potential minimum of their host subhalos at each global integration time step in order to avoid numerical effects that may displace them.

TNG employs a $\mathrm{M_{BH}}$-dependent Eddington ratio threshold for determining whether a black hole provides either pure thermal or pure kinetic mode feedback energy to the galaxy. Kinetic mode feedback in TNG is turned on when a galaxy's black hole accretion rate drops below an Eddington ratio of

$$\chi = \min\left[\chi_0\left(\frac{M_{\rm BH}}{M_{\rm piv}}\right)^{\beta}, \chi_{\rm max}\right], \tag{5.1}$$

where $M_{\rm BH}$ is the black hole mass and the parameters for the fiducial model are $\chi_0 = 0.002$, $M_{\rm piv} = 10^8\ {\rm M}_\odot$, $\beta = 2$, and $\chi_{\rm max} = 0.1$ (refer to Equation 5 and Figure 6 of Weinberger et al. (2017)).

Apart from $\chi_{\rm max}$, which is chosen to be the canonical, observationally-suggested value of 0.1 for the Eddington ratio of black holes in quasars (Yu & Tremaine, 2002), none of the other parameter values were adopted based on empirical evidence or other theoretical models of black hole physics and accretion. The parameters have been chosen to ensure that the TNG model returns the observed stellar mass content of massive haloes and the observed location of the knee in the stellar mass function at the current epoch.

Thermal mode feedback energy is parameterized as $\dot{E}_{\rm thermal} = \varepsilon_{\rm f,high}\varepsilon_{\rm r}\dot{M}_{\rm BH}c^2$, where $\varepsilon_{\rm f,high}$ is the fraction of thermal energy that couples to the surrounding gas (set to 0.1 for the fiducial model) and $\varepsilon_{\rm r}$ is the black hole radiative efficiency (set to 0.2 for the fiducial model). Kinetic mode feedback energy is parameterized as $\dot{E}_{\rm kinetic} = \varepsilon_{\rm f,kinetic}\dot{M}_{\rm BH}c^2$, where $\varepsilon_{\rm f,kinetic}$ is the fraction of kinetic energy that couples to the surrounding gas (set to a maximum value of $\varepsilon_{\rm f,kin,max} = 0.2$ for the fiducial model, see Equation 9 of Weinberger et al. 2017 for a full description). Once the black hole accumulates enough energy in this mode to reach a minimum energy threshold, $E_{\rm inj,min}$, the gas immediately surrounding the black hole receives a momentum kick with energy equal to $E_{\rm inj,min}$ in a random direction away from the black hole. This minimum energy threshold contains a dimensionless free parameter, $f_{\rm re}$ (set to 20 in the fiducial model), that controls the frequency and power of these momentum kicks.

5.3.2 Model Variations

Along with the fiducial TNG100 simulation, there are dozens of smaller simulations sized at 36.9^3 comoving Mpc^3 volumes that vary individual parameters of the model (Pillepich et al., 2018). These simulations have 2×512^3 initial resolution elements with roughly the same baryonic mass resolution (2.4×10^6 $\mathrm{M}_\odot$) and gravitational softening length (0.74 kpc at $z = 0$) as TNG100. Each of these simulations have identical cosmological initial conditions resulting in similar dark matter structures and galaxy placement throughout the volume. This allows a galaxy-by-galaxy comparison of the model variations, providing us with a powerful tool to explore the effects of each component of the model relevant for quiescence.

In Table 5.1 we describe the model variations that we use in this work. The first row describes a model with the same physics as TNG100 but with the same initial conditions, resolution, and volume as all other model variations. We will refer to this run as the FiducialModel simulation. Each of the other model variations alters the black hole feedback model described in Section 5.3.1. These variations will affect how galaxies populate the M_{BH}-$\mathrm{M}_{\mathrm{star}}$-sSFR parameter space, as we will show in later sections. The details of each altered parameter in the third column are given in Section 5.3.1, with a brief description of the change in the sixth column. We will refer to each simulation according to their names in the second column of Table 5.1.

5.3.3 Definitions of physical properties in TNG

We calculate the $\mathrm{M}_{\mathrm{star}}$ and SFR within the galaxy radius, defined as twice the stellar half mass radius. SFRs are calculated by averaging the star formation activity in the last 200 Myr in order to reasonably compare our results to observational SFR indicators. Our results remain qualitatively the same whether we use instantaneous SFRs or those averaged over 50, 100, or 200 Myr.

Star-forming and quiescent galaxies are defined as having sSFRs above or below

10^{-11} yr^{-1}, respectively, providing a consistent separation between galaxies on and off the star-forming main sequence for both observations and simulations at z = 0.

TNG100 and the model variations are sensitive to 200 Myr-averaged SFRs above $\sim 10^{-2.5}$ M$_\odot$ yr^{-1}, below which star formation is unresolved (see Figure 2 in Donnari et al., 2019). This value is related to the mass resolution limit of a single stellar particle in TNG100 and the model variations. Since we focus on galaxies with M$_{\rm star} > 10^{10}$ M$_\odot$, any values for sSFR $< 10^{-12.5}$ yr^{-1} will be taken as an upper limit. This ensures that all sSFRs above this limit are resolved. Upper limits will be shown as a value chosen from a gaussian distribution centered at sSFR $= 10^{-12.5}$ yr^{-1} in order to visualize what would be observed as non-detections.

Black hole parameters are taken for the most massive black hole at the center of the galaxy. Halo properties such as gas cooling rates ($\mathcal{C}_{\rm halo}$), gas masses (M$_{\rm gas,halo}$), and dark matter halo masses (M$_{\rm DM,halo}$) are the sum values for each cell within the radius at which the density within is 200 times the critical density of the Universe, $R_{\rm 200c}$. Halo gas cooling times (t$_{\rm cool}$) are the average of gas particles within $R_{\rm 200c}$.

Additionally, our analysis will use a measure of the gravitational binding energy of gas within the galaxy, which we define as

$$E_{\rm bind,gal}(< r_{\rm gal}) = \frac{1}{2} \sum_{\rm g(<r_{gal})} m_{\rm g}\phi_{\rm g}, \tag{5.2}$$

where $r_{\rm gal}$ is twice the stellar half mass radius, g indexes gas cells in the simulation, $m_{\rm g}$ is the mass of the gas cell, and $\phi_{\rm g}$ is the gravitational potential felt at the gas cell's position within the galaxy. This value represents the energy needed to unbind those gas cells from the galaxy's position to infinity, taking into account not only the mass within the galaxy but also the mass within the halo. We choose to calculate the binding energy of gas within this radius in order to match the radius within which the SFR and M$_{\rm star}$ are calculated.

5.4 The necessary conditions for quiescence

We begin by exploring the necessary conditions under which quiescence can occur for central galaxies with $\mathrm{M_{star}} > 10^{10}$ $\mathrm{M_\odot}$ in the context of the TNG model. In Figure 5.1, we show histograms of the number of galaxies as a function of sSFR for three model variations at $z = 0$. Due to their smaller box size, there are very few galaxies with $\mathrm{M_{halo}} > 10^{13}$ $\mathrm{M_\odot}$. We also plot galaxies from TNG100 (renormalized to match the box size of the FiducialModel run) in gray to show the results from a larger sample size with more massive halos.

In light green, we show the TNG model variation with no black holes, where the only feedback channel is stellar feedback. This simulation results in a distribution of galaxies centered at sSFR $\sim 10^{-10}$ $\mathrm{yr^{-1}}$, denoting the existence of the star forming main sequence.

In dark green, we show the model variation with black holes included where thermal mode black hole feedback operates for all accretion rates (the NoBHwinds model in Table 5.1). In TNG, a black hole accreting in the thermal mode injects pure thermal energy into the surrounding gas particles. Weinberger et al. (2018) show that the total amount of thermal energy released in this mode can be large yet has little effect on cooling and the galaxy's SFR. Thermally injected energy, as implemented for black hole thermal mode feedback in TNG, is more likely to be immediately radiated away rather than have any lasting impact on the thermodynamic properties of the gas, especially for dense gas where the cooling times are short (Navarro & White, 1993; Katz et al., 1996). This is due, at least in part, to a numerical effect as a result of the limited resolution of the simulation, leading to the 'over-cooling' problem (e.g., Springel & Hernquist, 2002). The pileup of galaxies at sSFR $\sim 10^{-10}$ $\mathrm{yr^{-1}}$ illustrates the inability of thermal energy injection to prevent gas cooling and star formation in TNG galaxies.

The black histogram shows galaxies in the FiducialModel simulation, where kinetic

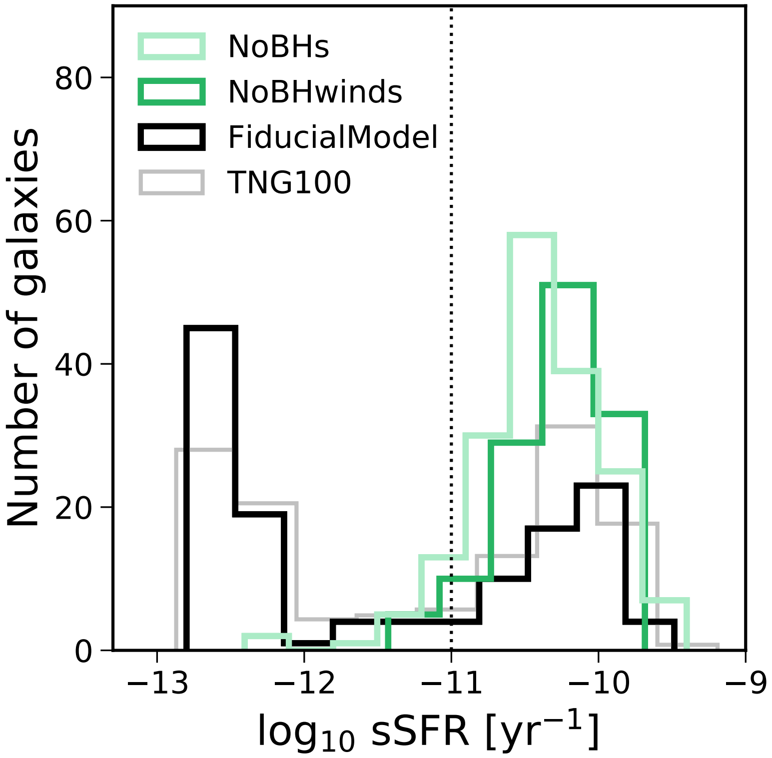

Figure 5.1: Histograms of sSFR for central galaxies with $M_{\rm star} > 10^{10}$ $M_\odot$ at $z = 0$ for the model variations with no black holes (light green), thermal mode at all accretion rates (dark green), and both thermal and kinetic modes included as in the fiducial model (black). The number of galaxies shown in each of these histograms is roughly the same. Due to the smaller box size, there are very few galaxies with $M_{\rm halo} > 10^{13}$ $M_\odot$. TNG100 scaled to the volume of the smaller box simulations is shown in gray. The star forming main sequence is present in all simulations but a quiescent population only appears in the models with kinetic mode black hole feedback.

mode black hole feedback is turned on at low accretion rates. This black histogram along with the TNG100 results in gray show a significant population of quiescent galaxies at low sSFRs, most of which have upper limit values placed at sSFR $\sim 10^{-12.5}$ yr^{-1}. These results show that the existence of a quiescent population in TNG depends on the model's implementation of low accretion rate kinetic mode feedback from the central black hole. Similar conclusions have been made in previous studies of TNG both in terms of color (Weinberger et al., 2017; Nelson et al., 2018a) and sSFR (Weinberger et al., 2018).

5.5 The physics of quiescence from black hole-driven kinetic winds

In this section we describe how black hole-driven kinetic winds employed by TNG affect the gas within and around galaxies in order to produce quiescence.

5.5.1 Comparing TNG with semi-analytic approaches to quiescence

Semi-analytic models of galaxy formation often use prescriptions of gas cooling and heating rates in order to determine the net rate of cold gas accreted onto a galaxy (e.g., De Lucia & Blaizot, 2007b; Somerville et al., 2008; Guo et al., 2010; Henriques et al., 2015). In these models, once the heating rate from black hole feedback equals or exceeds the halo gas cooling rate, cold gas accretion onto the galaxy halts and star formation subsequently shuts off. This describes a method to model *preventative* black hole feedback, where fuel for star formation is prevented from reaching the galaxy.

In order to test whether a similar physical scenario occurs for TNG galaxies, we show the sSFR as a function of the ratio between the instantaneous energy released from black hole-driven kinetic feedback, $\dot{E}_{\text{kinetic}}$ (see Section 5.3.1), and the instan-

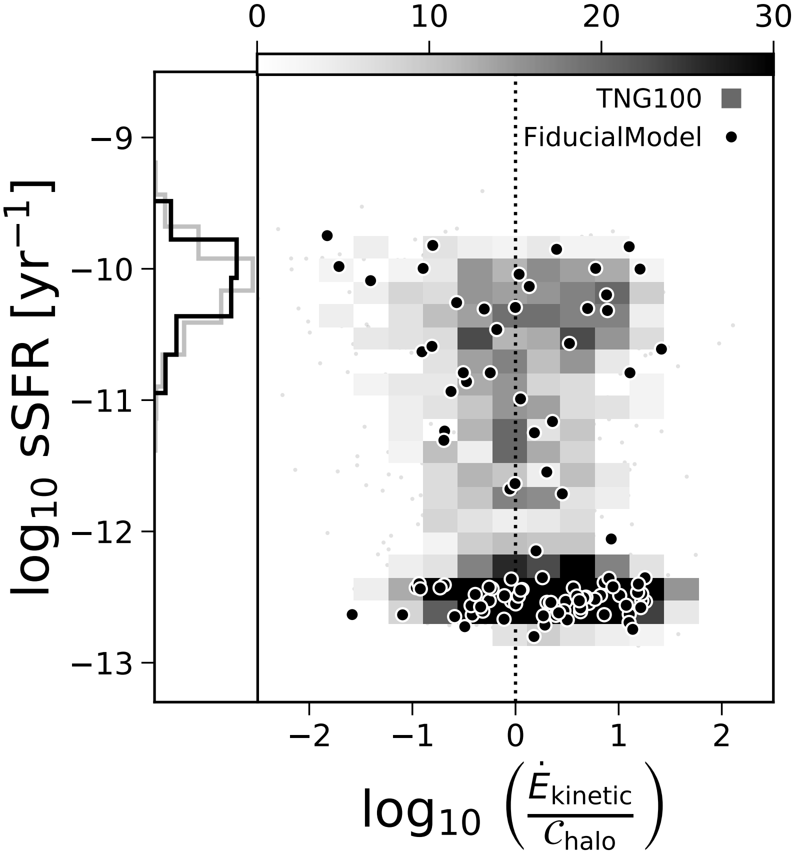

Figure 5.2: sSFR as a function of the ratio between the instantaneous black hole wind energy injection rate, $\dot{E}_{\mathrm{kinetic}}$, and the instantaneous halo gas cooling rate, $\mathcal{C}_{\mathrm{halo}}$. The vertical dotted line shows where these two energy rates equal. The grayscale heatmap shows the distribution of galaxies in TNG100 and the black points show galaxies in the FiducialModel simulation at z = 0. The histogram shows the distribution of sSFR for galaxies with no black hole wind energy injection, $\dot{E}_{\mathrm{kinetic}} = 0$, for the TNG100 (gray, scaled to the volume of the FiducialModel run) and FiducialModel (black) simulations. While kinetic winds are required for quiescence, comparing the kinetic energy injection rate to the halo gas cooling rate is a poor indicator of a galaxy's star formation properties.

taneous cooling rate of the gas halo, $\mathcal{C}_{\rm halo}$[1] at $z = 0$. The distribution of TNG100 galaxies is shown as a grayscale heatmap and FiducialModel galaxies are shown as black points. The vertical dotted line indicates where the two rates are equal. Since many galaxies are not in the kinetic mode (with $\dot{E}_{\rm kinetic} = 0$) and therefore cannot be represented on this plot, we show the distribution of their sSFRs as a histogram to the left of the main plot for both the TNG100 (gray, scaled to the volume of the FiducialModel run) and FiducialModel (black) simulations.

We find that all galaxies that are not currently experiencing kinetic mode black hole feedback (with $\dot{E}_{\rm kinetic} = 0$) are actively forming stars (left panel histogram in Figure 5.2). The main panel of this figure shows that galaxies must be experiencing kinetic mode black hole feedback in order to be quiescent, in agreement with our results from Section 5.4.

However, a significant number of galaxies releasing black hole-driven kinetic winds are star-forming. In fact, whether these galaxies are star-forming or quiescent does not correlate tightly with whether the black hole wind energy greatly exceeds or falls below the cooling rate of the gas halo. As such, the TNG simulation cannot be easily described using the logic employed by semi-analytic models. We note that the comparison between these ‘heating’ and ‘cooling’ rates in TNG differ in detail to those analytically determined in semi-analytic approaches. This is due to the fact that these rates in TNG are sensitive to internal gas hydrodynamics whereas in semi-analytic models these rates are calculated using global galaxy and halo properties. Even so, this analysis indicates differences between how black hole feedback energy is transferred to the surrounding gas to produce quiescence in TNG and how it is transferred in purely preventative semi-analytic black hole feedback models.

---

[1] Due to the lack of numerical resolution, star forming cells are described by an effective equation of state model once a density threshold is reached (Springel & Hernquist, 2003). As such, cooling rates for these cells are excluded in the calculation of the halo cooling rate. Star forming cells account for a negligible amount of mass in the gas halo.

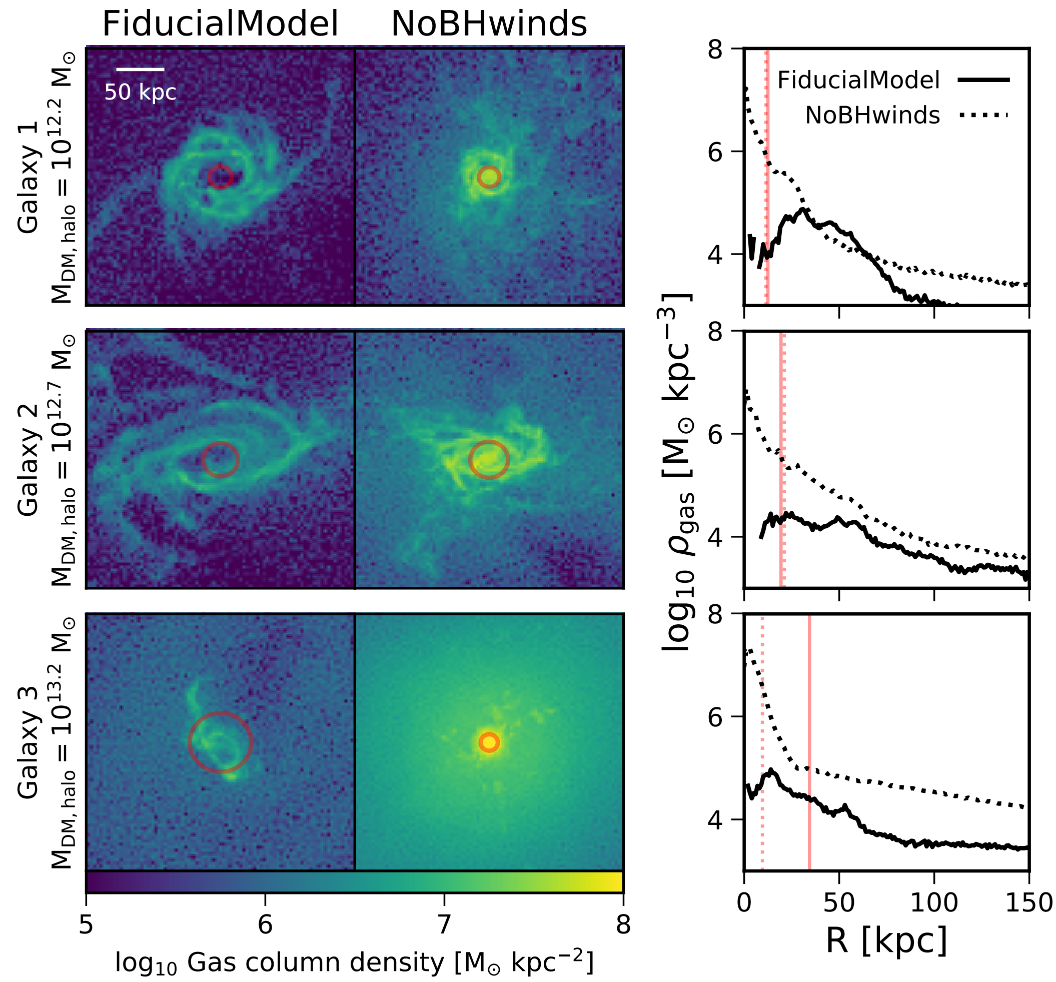

Figure 5.3: *Left panels*: The leftmost galaxy images show the projected (across 300 kpc) gas column density distributions of three quiescent galaxies in the FiducialModel simulation at z = 0 ordered by increasing mass from top to bottom. The images to the right show galaxies identified to be the centrals of the same halos as those on the left but in the NoBHwinds simulation. Each image is 300×300 kpc in size in order to directly compare the sizes and distributions of gas in each simulation. The red circles indicate the galaxy radius, defined as twice the stellar half mass radius. *Right panels:* The radial gas density distributions of the galaxies in the FiducialModel (solid lines) and NoBHwinds (dotted lines) simulations. The vertical red lines indicate the galaxy radius. The density of gas in the central regions of galaxies experiencing kinetic winds is depleted by orders of magnitude.

5.5.2 Gas distributions in TNG galaxies

A useful approach for understanding the effects of black hole feedback on the gas within and around galaxies in TNG is to visualize and quantify the distribution of this gas. We use the model variations described in Section 5.3.2 in order to do this. Figure 5.3 shows the gas column densities of three quiescent galaxies of increasing mass at $z = 0$ in the FiducialModel simulation (left images) and their direct counterparts in the NoBHwinds simulation (right images). Their radial density profiles are shown in the rightmost panels. We match these galaxies between the two model variations by the position of its dark matter halo and by ensuring that at least half of the dark matter particles have the same IDs. Each panel for both simulations is at the same spatial scale of 300×300 kpc. The circle in the center of each figure depicts twice the stellar half mass radius of the galaxy from its center in order to show where a galaxy's visible matter would lie in the image.

We find that there is very little dense gas in the central regions of the galaxies undergoing kinetic feedback. The disks of these galaxies are extended and disturbed, showing that black hole-driven kinetic winds produce outflows that push gas out of galaxies, in agreement with recent TNG50 results described in Nelson et al. (2019). In addition, the densities of the gas extending past the disk and into the circumgalactic medium is also depleted. We find that the same galaxies in the NoBHwinds universe have retained large amounts of dense gas within the galaxy's radius and that the radial density profile is centrally peaked (dotted lines in the right hand panels).

5.5.3 Overcoming gravitational binding energies

The results from Figure 5.3 strongly suggest that black hole-driven kinetic winds drive gas out of the galaxy, producing a form of ejective feedback. Therefore, we choose to test whether the gravitational binding energy of the gas within the galaxy (defined in Section 5.3.3) can be a useful parameter for characterizing quiescence in

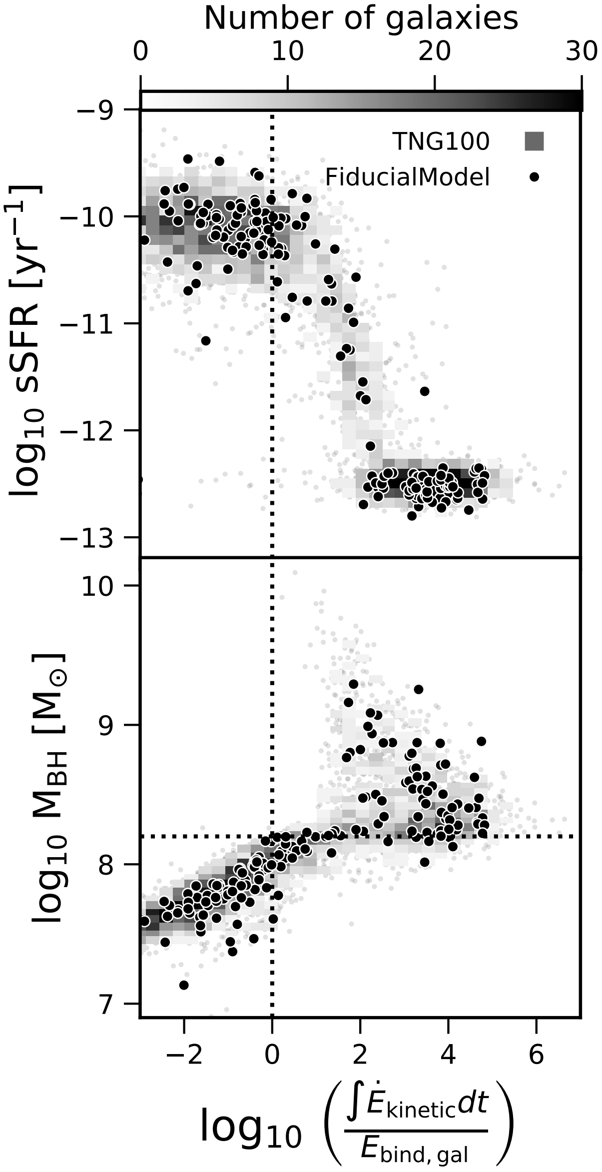

Figure 5.4: sSFR (top) and M_{BH} (bottom) as a function of the ratio between the cumulative kinetic energy released from black hole feedback, $\int \dot{E}_{\rm kinetic}dt$, and the binding energy of the gas within twice the stellar half mass radius, $E_{\rm bind,gal}$. The vertical dotted line shows where these two energies equal. The grayscale heatmap shows the distribution of galaxies in TNG100 and the black points show galaxies in the FiducialModel simulation at z = 0. The sSFR decreases once the cumulative energy from black hole-driven winds exceeds the binding energy of gas in the galaxy. This drop in sSFR occurs when M_{BH} exceeds $10^{8.2}$ $M_\odot$ shown as a horizontal dotted line in the bottom panel.

the TNG model.

We compare this value to the time-integrated amount of black hole-driven wind energy that has been released into the gas particles near the black hole at each time-step, $\int \dot{E}_{\rm kinetic} dt$[2]. Nelson et al. (2018a) and Weinberger et al. (2018) have demonstrated that quiescent galaxies have released more of this cumulative black hole wind energy relative to star-forming galaxies.

The top panel of Figure 5.4 shows sSFR as a function of the ratio between the cumulative black hole wind energy, $\int \dot{E}_{\rm kinetic} dt$, and the gravitational binding energy of gas within the galaxy, $E_{\rm bind,gal}$, in the TNG100 (gray heatmap) and FiducialModel (black points) simulations at $z = 0$. We find that star-forming galaxies lie to the left of the vertical dotted line, showing that they exhibit cumulative black hole wind energies that fall below the binding energy of the gas. Galaxies with intermediate sSFRs between sSFR $\sim 10^{-11} - 10^{-12}$ yr^{-1} exhibit cumulative black hole wind energies that exceed the binding energy of the gas (to the right of the vertical dotted line) by up to a factor of 100. Above an energy ratio of 100, galaxies host very low sSFRs shown as upper limits at $\sim 10^{-12.5}$ yr^{-1}.

It is important to note that the binding energy of the gas decreases as gas leaves the system since the total mass of the system decreases and there is less gas to push out. The high ratios of cumulative black hole wind energy to gravitational binding energy exceeding a factor of 1000 tend to have very low gas masses and therefore low binding energies. While this is true, we verify that sSFR correlates only slightly with the binding energy of gas within the galaxy, and that the cumulative black hole wind energy drives most of the correlation seen in the top panel of Figure 5.4. The fact that sSFR begins to drop when these two energies equal indicates that gas is being gravitationally unbound from the central galaxy and pushed into the circumgalactic

---

[2] This value is tracked for each black hole in the simulation and given as an output at each snapshot.

medium by black hole-driven kinetic winds.[3]

The bottom panel of Figure 5.4 shows that galaxies with cumulative black hole wind energies lower than the binding energy of the gas have $\mathrm{M_{BH}} \lesssim 10^{8.2}\ \mathrm{M_\odot}$, whereas those with higher ratios have $\mathrm{M_{BH}} \gtrsim 10^{8.2}\ \mathrm{M_\odot}$. This indicates that black hole winds are effective at removing gas and producing quiescence for a majority of galaxies once the black hole exceeds the threshold mass at $\sim 10^{8.2}\ \mathrm{M_\odot}$ (shown as a horizontal dotted line).

We also note that the most massive black holes ($\mathrm{M_{BH}} \gtrsim 10^{9}\ \mathrm{M_\odot}$) tend to have lower ratios of black hole wind energy to binding energy, whereas less massive black holes (with $\mathrm{M_{BH}}$ still $\gtrsim 10^{8.2}\ \mathrm{M_\odot}$) can have much higher ratios. This is likely due to the fact that more massive black holes live in more massive galaxies and halos where the gravitational potential is much deeper. As such, many of the galaxies with intermediate sSFRs (between $\sim 10^{-11} - 10^{-12}\ \mathrm{yr^{-1}}$) are hosted by some of the most massive halos, whereas those with very low sSFRs (shown as upper limits at $\sim 10^{-12.5}$) are those in lower mass halos (with $\mathrm{M_{BH}}$ still $\gtrsim 10^{8.2}\ \mathrm{M_\odot}$). We expand on this result in the following section.

5.5.4 The effects of black hole-driven kinetic feedback on the interstellar and circumgalactic media

The bottom panel of Figure 5.4 indicates that there exists a $\mathrm{M_{BH}}$ threshold for quiescence (also see Figure 5 in Weinberger et al. 2018). In this section, we explicitly explore the gas properties of galaxies in TNG as a function of $\mathrm{M_{BH}}$. Figure 5.5 shows the average gas density within the galaxy (top panel), the average cooling time of the

---

[3] We confirm that using various physically-motivated definitions for the binding energy of the galaxy results in similar qualitative results. Another possible experiment is to check if the black hole wind energy would evacuate the gas that would otherwise be present without these winds. Since we can match galaxies across model variations, we confirm that the qualitative trends seen in Figure 5.4 are reproduced if we use the black hole wind energy from the FiducialModel simulation and the gas binding energies from the NoBHwinds simulation.

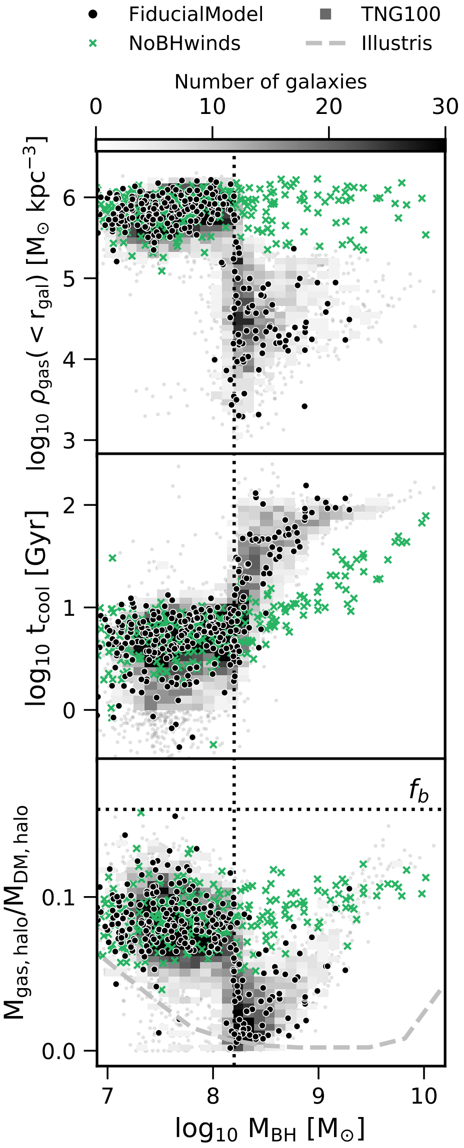

Figure 5.5: The average gas density within the galaxy radius (top panel), the average cooling time of the halo gas (middle panel), and the ratio of halo gas mass to dark matter halo mass (bottom panel) as a function of $M_{\rm BH}$ for galaxies in the TNG100 (grayscale heatmap), FiducialModel (black), and NoBHwinds (green) simulations at $z = 0$. Including black hole-driven winds in TNG abruptly lowers the density of gas within the galaxy, increases the cooling time of the halo gas, and reduces the amount of halo gas for galaxies with $M_{\rm BH} \gtrsim 10^{8.2}$ $M_\odot$. The most massive black holes live in the most massive halos, where affecting gas kinetically is more difficult due to the halo's deep potential well. As a result, the galaxies whose SFRs are most affected by kinetic mode feedback are the least massive galaxies that have $M_{\rm BH} \gtrsim 10^{8.2}$ $M_\odot$.

entire gas halo[4] (middle panel), and the ratio of total halo gas mass to dark matter halo mass (bottom panel) as a function of M_{BH} for galaxies in the NoBHwinds (green crosses) and FiducialModel (black points) simulations at $z = 0$. The distribution of galaxies in TNG100 is shown as a grayscale heatmap.

Without kinetic winds (green crosses), the average gas density within twice the stellar half mass radius is similar across galaxies with different M_{BH} (top panel). We verify that this is because galaxy gas masses correlate closely with galaxy radii when they are star-forming. The average cooling time of these galaxies' gas halos is a fairly flat function of M_{BH} at low masses and gradually rises for more massive black holes that live in more massive halos where cooling becomes less efficient (middle panel). Additionally, the total halo gas masses of these galaxies correlate with dark matter halo mass, producing a scattered, flat relation as a function of black hole mass (bottom panel).

Introducing kinetic winds significantly alters these gas properties for galaxies above the M_{BH} threshold for quiescence at $\sim 10^{8.2}$ $M_{\odot}$, as is seen in all three panels of Figure 5.5 (black points). Once feedback from kinetic winds becomes effective, there is a sharp decrease in the average gas density within galaxies, a sharp increase in the average cooling time of halo gas, and a sharp decrease in the fractions of halo gas mass to dark matter halo mass compared to the NoBHwinds model.

In the bottom panel we also show the median values from the original Illustris model with a dashed gray line. This demonstrates that while TNG retains more gas in massive halos on average, it still removes large quantities of gas from within the halo's radius once black hole winds are produced at the M_{BH} threshold for quiescence. The lowest halo gas fractions (with $M_{gas,halo}/M_{DM,halo} \sim 0$) are seen in galaxies with M_{BH} near the threshold mass at $\sim 10^{8.2}$ $M_{\odot}$. The gas fraction increases with M_{BH} thereafter. This is likely because M_{BH} correlates closely with M_{star} (as we will show

---

[4] We calculate this value excluding star-forming cells. Refer to the footnote in Section 5.5.1.

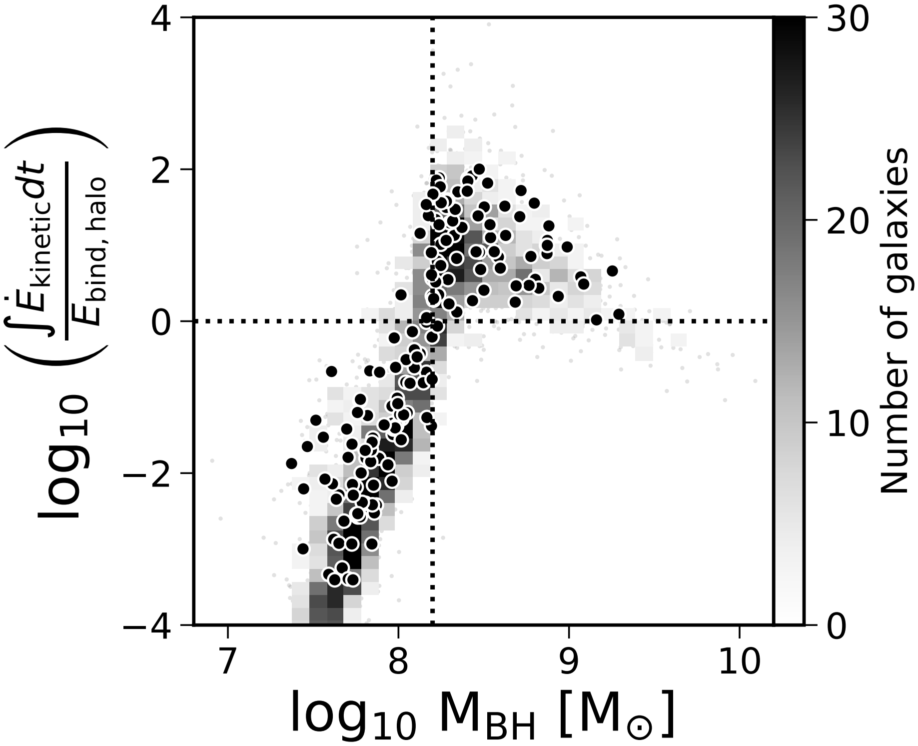

Figure 5.6: The ratio between the cumulative energy from black hole winds, $\int \dot{E}_{\rm kinetic}dt$, and the binding energy of gas within the *halo* radius, $E_{\rm bind,halo}$ as a function of M$_{\rm BH}$ for the TNG100 (grayscale heatmap) and FiducialModel (black points) simulations at z = 0. The horizontal dotted line indicates where the black hole wind energy equals the halo gas binding energy and the vertical dotted line indicates the M$_{\rm BH}$ threshold for quiescence (see Section 5.5.3). The black hole wind energy exceeds the halo gas binding energy by the largest amount just above the M$_{\rm BH}$ threshold for quiescence.

in Figure 5.7), and therefore $\mathrm{M}_{\mathrm{halo}}$, for TNG galaxies. The feedback from black holes in more massive galaxies must overcome a larger potential well in order to expel gas from the galaxy's halo.

To illustrate this, Figure 5.6 shows the ratio between the cumulative energy from black hole winds and the gravitational binding energy of the *halo gas* as a function of M_{BH}. The binding energy of the halo gas is calculated by replacing r_{gal} with r_{halo} in Eqn. 5.2 (see Section 5.3.3). The horizontal dotted line shows where the black hole kinetic wind energy equals the halo gas binding energy. Galaxies hosting black holes just over the M_{BH} threshold for quiescence (vertical dotted line) have the highest ratios of black hole wind energy to halo gas binding energy. This coincides with the lowest gas mass fractions in the lower panel of Figure 5.5. This indicates that a significant fraction of gas is evacuated from many of the halos once black hole wind energies exceed not only the binding energy of the gas in the galaxy (Figure 5.4) but also of the gas in the halo.

Progressively higher mass black holes live in more massive halos with deeper gravitational potentials. In Figure 5.6 as well as in the lower panel of Figure 5.4, the ratio between the energy from black hole winds and the binding energy of gas in both the galaxy and the halo decreases for more massive black holes. The decrease in this ratio with black hole mass coincides with an increase in the halo gas fraction in the lower panel of Figure 5.5. This behavior indicates that black hole winds are less effective at removing gas at higher mass regimes.

5.6 Comparisons to Observations

In this section we evaluate the extent to which the kinetic wind model in TNG can produce results which agree with currently available observational correlations related to quiescence. Here we use the observational diagnostics and data from Terrazas et al. (2016b, 2017) in order to examine and compare the relationship between $\mathrm{M}_{\mathrm{star}}$, M_{BH}, and sSFR in TNG. We aim to link the phenomenological description of quiescence we put forth for this model in Section 5.4 and 5.5 to these observable properties of simulated galaxies since these properties are causally tied to one another in this model as a result of the black hole feedback prescriptions.

5.6.1 Observational sample

The 91 galaxies in Terrazas et al. (2016b, 2017, also described in Chapter 3 and referred to hereafter as T17) represent a diverse collection of local galaxies (distances within ∼150 Mpc) with various morphologies, SFRs, colors, and environments (isolated, group, or cluster) with $\mathrm{M_{star}} > 10^{10}\ \mathrm{M_{\odot}}$. The sample represents central galaxies – defined as the most massive galaxy within ∼1 Mpc – that have a dynamical $\mathrm{M_{BH}}$ measurement using stellar dynamics (45 galaxies), gas dynamics (15), masers (12), or reverberation mapping (18). Black hole mass measurements were taken from Saglia et al. (2016) and van den Bosch (2016).

T17 measures the stellar masses using 2MASS K_{s}-band luminosities (Huchra et al., 2012) with a single $\mathrm{M_{star}}/L_{\mathrm{K_s}}$ ratio of 0.75 since mass-to-light ratios for $L_{\mathrm{K_s}}$ do not vary much (Bell & de Jong, 2001). Their scatter in mass-to-light ratios are ∼0.15 dex, thus they assume the same value for their uncertainty. SFRs are measured following Kennicutt & Evans (2012) where T17 use IRAS far-infrared flux measurements to estimate a total infrared luminosity. This SFR estimate is sensitive to star formation during the past ∼100 Myr. SFRs are assumed to have an uncertainty of 0.15 dex following Bell (2003). Any SFRs with no far-infrared detection, fluxes below the detection limits of IRAS, or detections below $\mathrm{sSFR} < 10^{-12.5}\ \mathrm{yr^{-1}}$ are taken as upper limits. We define star-forming and quiescent galaxies to be those with sSFRs above or below $10^{-11}\ \mathrm{yr^{-1}}$, respectively, just as we do with TNG galaxies.

We note that these data are not representative of the entire galaxy population at $z = 0$ due to the requirement that their $\mathrm{M_{BH}}$ be large enough and their host galaxies close enough to detect their gravitational sphere of influence. The various detection methods used for this sample make it difficult to fully understand the biases associated with the sample. For example, black hole masses detected with reverberation mapping or masers are more likely to be in star-forming galaxies where there is enough gas to produce the emission required to use these measurement techniques. Black holes measured with stellar dynamics, however, are likely in systems that are close enough to resolve the gravitational sphere of influence and that have low enough gas masses in their nuclear regions to allow starlight to dominate. These factors make it difficult to compare these observations directly with the simulation results, since the selection function and bias for the observational sample with regards to its sSFR, $\mathrm{M_{star}}$, and $\mathrm{M_{BH}}$ distributions are not well understood.

One may decide to use a sample with proxies instead, with the advantage that a complete, representative sample may be obtained. However, proxies for $\mathrm{M_{BH}}$ such as velocity dispersion, bulge mass, or Sérsic index exhibit intrinsic scatter that likely indicates differences in the physics that set these properties (e.g., Gültekin et al., 2009; Beifiori et al., 2012; Shankar et al., 2016; Terrazas et al., 2016b; Martín-Navarro et al., 2016, 2018). Using proxies for $\mathrm{M_{BH}}$ would also introduce unknown uncertainties that likely depend on $\mathrm{M_{star}}$. While the number density of galaxies at a given sSFR, $\mathrm{M_{star}}$, and $\mathrm{M_{BH}}$ are uncertain for this sample, our primary concern for this study is accuracy. Using dynamical black hole masses also ensures that the measurements for $\mathrm{M_{BH}}$ and $\mathrm{M_{star}}$ are independent from one another. Finally, while the sample may not be representative quantitatively, it contains a large diversity of galaxy properties ranging 4 orders of magnitude in sSFR, 2 orders of magnitude in $\mathrm{M_{star}}$, and 4 orders of magnitude in $\mathrm{M_{BH}}$. This results from the variety of $\mathrm{M_{BH}}$ measurement techniques that sample distinct parts of the whole galaxy population. As such, we opt to use high-quality $\mathrm{M_{BH}}$ estimates instead of proxies in order to reliably understand how galaxy properties correlate with central $\mathrm{M_{BH}}$.

5.6.2 Results

Figure 5.7 shows the M_{BH}-M_{star} (top left), sSFR-M_{BH} (top center), and sSFR-M_{star} (top right) parameter spaces for the TNG100 simulation at $z = 0$ (star-forming: blue heatmap, quiescent: red heatmap), and the observational data from T17 (star-forming: gray circles, quiescent: black circles). On the lower right corner of each panel we indicate the 0.15 dex uncertainties on the sSFR and M_{star} of the observational sample. We convolve the simulation quantities for sSFR and M_{star} with these uncertainties in order to more fairly compare the observations with the simulation results. Similarly, we convolve the simulation quantities for M_{BH} with uncertainties from the observed M_{BH} sample. The bottom panels show sSFR as a function of M_{BH} in bins of stellar mass, whose value is denoted above each plot.

The top leftmost panel of Figure 5.7 shows that TNG produces a tight M_{BH}-M_{star} relation, even with added observational uncertainties that increase the scatter. While TNG is in good agreement with the qualitative result that quiescent galaxies host more massive black holes, quantitatively the distributions of star-forming and quiescent galaxies differ between TNG and the observations.

The observational data show significant scatter in M_{BH} as a function of *total* M_{star}. The relation shown in the top leftmost panel of Figure 5.7 differs from canonical M_{BH}-galaxy scaling relation studies in that a *total* M_{star} is preferred in this work over a *bulge-only* M_{star}. Additionally, the T17 sample incorporates a large diversity of galaxies ranging from bulge-dominated, quiescent systems to disk-dominated, star-forming galaxies.

The scatter in the observed M_{BH}-M_{star} relation correlates well with the sSFR of these galaxies, where quiescent galaxies host more massive black holes than star-forming galaxies. TNG does not easily produce galaxies with the M_{BH} and M_{star} demographics of star-forming galaxies in the T17 sample. For example, the Milky Way (included in the T17 sample) with $M_{star} \approx 10^{10.7}$ $M_\odot$ and $M_{BH} \approx 10^{6.7}$ $M_\odot$ is not

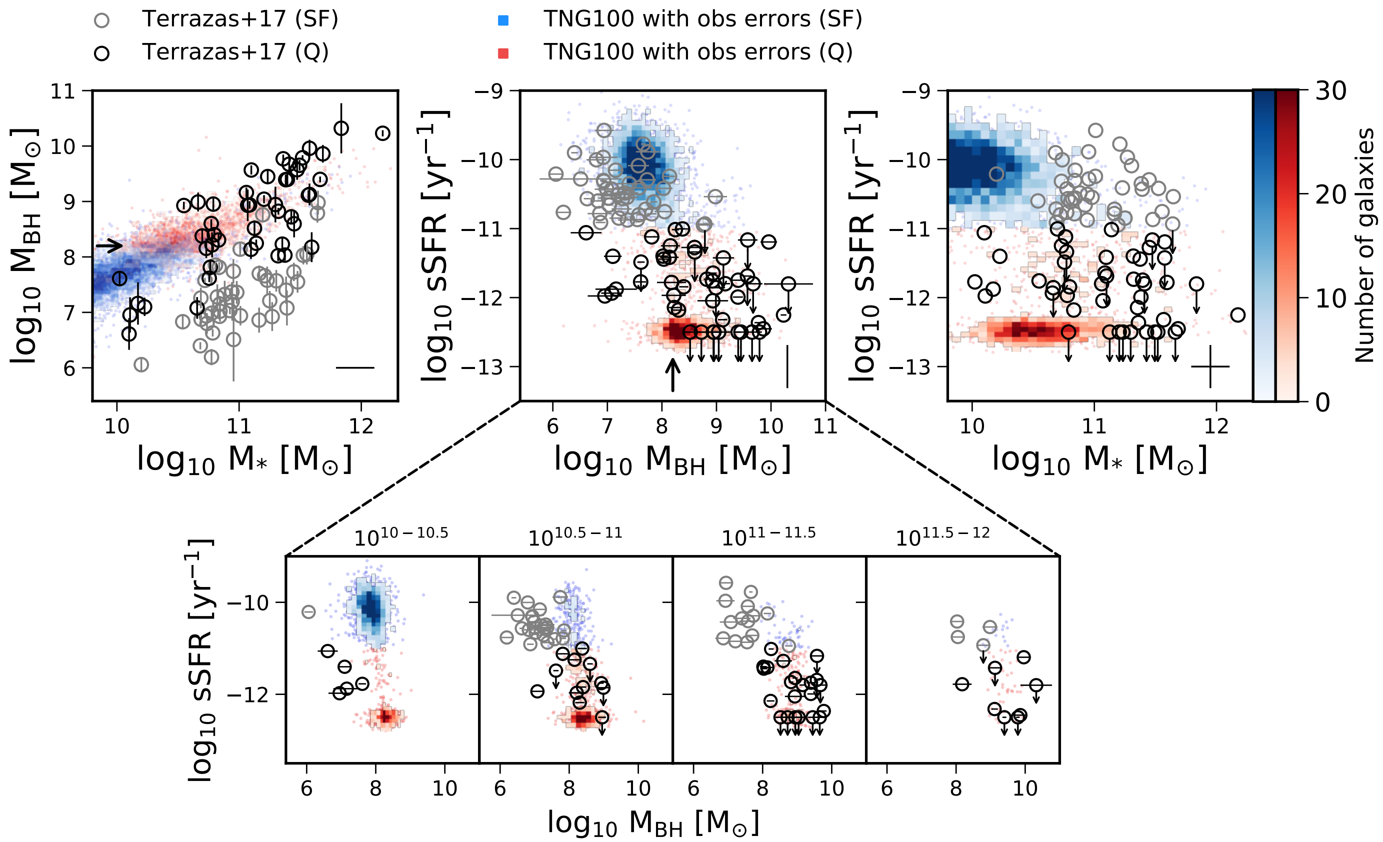

Figure 5.7: *Top panels:* The $\mathrm{M_{BH}}$-$\mathrm{M_{star}}$ (left), sSFR-$\mathrm{M_{BH}}$ (center), and sSFR-$\mathrm{M_{star}}$ (right) parameter spaces for TNG100 galaxies in blue and red heatmaps and the observational sample in gray and black circles, for star-forming and quiescent galaxies, respectively, at $z = 0$. An uncertainty of 0.15 dex is added to sSFR and $\mathrm{M_{star}}$ values for TNG100 galaxies. Observational uncertainties for $\mathrm{M_{BH}}$ in TNG100 are taken into account by convolving them with the errors from the T17 data. *Bottom panels:* sSFR as a function of $\mathrm{M_{BH}}$ in bins of $\mathrm{M_{star}}$ for TNG100 galaxies and the T17 observational sample.

represented in TNG100. Instead, TNG predicts that the distribution of star-forming galaxies lies far to the left of where they lie in the observational sample.

In addition, the boundary between star-forming and quiescent galaxies on the top leftmost plot showing the $\mathrm{M_{BH}}$-$\mathrm{M_{star}}$ relation for TNG is flat, representing a $\mathrm{M_{BH}}$ threshold for quiescence at $\sim 10^{8.2}$ $\mathrm{M_\odot}$, as was discussed in Section 5.5. The slope of the boundary in the observational data is positive with a value of ~ 1. T17 note that this slope represents lines of constant $\mathrm{M_{BH}/M_{star}}$ and that the sSFR decreases perpendicular to these lines moving towards more massive black holes. As such, while quiescence does correlate with $\mathrm{M_{BH}}$ in the observational sample, a threshold for quiescence does not exist at a particular $\mathrm{M_{BH}}$ value as it does in TNG.

We show this more explicitly in the top middle panel of Figure 5.7 where sSFR is shown as a function of $\mathrm{M_{BH}}$. There is a sharp transition between star-forming and quiescent galaxies at the $\mathrm{M_{BH}}$ threshold for quiescence at $\sim 10^{8.2}$ $\mathrm{M_\odot}$ for TNG galaxies. Galaxies having very low sSFRs shown as upper limits at sSFR $\simeq 10^{-12.5}$ $\mathrm{yr^{-1}}$, make up 73% of the total quiescent galaxy population in TNG. This produces a strong bimodality in sSFR for the simulated galaxies (in agreement with TNG results shown in Donnari et al. 2019) as a result of the black hole feedback model at low accretion rates.

The observational data show a scattered, more gradual decrease in sSFR as a function of $\mathrm{M_{BH}}$ compared to TNG. Namely, there is no indication in the observational data that there is a sharp $\mathrm{M_{BH}}$ threshold where galaxies mostly exhibit very low sSFRs ($\simeq 10^{-12.5}$ $\mathrm{yr^{-1}}$). T17 measure significant, intermediate sSFR values ($\sim 10^{-11} - 10^{-12}$ $\mathrm{yr^{-1}}$) for many galaxies with massive black holes $\gtrsim 10^{8.2}$ $\mathrm{M_\odot}$. Empirically, the sSFR of the observational sample is a tighter and more smoothly declining function of $\mathrm{M_{BH}/M_{star}}$ rather than $\mathrm{M_{BH}}$ alone, resulting in the scattered relationship between sSFR and $\mathrm{M_{BH}}$.

We note that low star formation rates in early-type galaxies are notoriously difficult to measure (e.g. Crocker et al., 2011). The sSFRs from T17 are measured using far-infrared IRAS luminosities in order to avoid contamination from possible AGN. They also used ultraviolet luminosities from GALEX to check the robustness of their values, finding consistent results using different techniques. Additionally, recent work indicates the existence of a population of galaxies with low but significant levels of star formation (Oemler et al., 2016), especially when measured in the infrared (Eales et al., 2017). The morphologies and colors of galaxies at intermediate sSFRs in the T17 sample are also visually more disk-like and bluer compared to the more spheroidal and redder galaxies at lower sSFRs, providing further evidence for the robustness of the measured difference between galaxies at intermediate ($\simeq 10^{-11} - 10^{-12}$ yr^{-1}) compared to low ($\simeq 10^{-12.5}$ yr^{-1}) sSFRs in the T17 sample.

In order to more clearly show the relationship between sSFR and $\mathrm{M_{BH}/M_{star}}$ in the observational sample, we plot sSFR as a function of $\mathrm{M_{BH}}$ in four bins of $\mathrm{M_{star}}$ in the bottom panels of Figure 5.7. These plots show a gradual decrease in sSFR as a function of $\mathrm{M_{BH}}$ in each $\mathrm{M_{star}}$ bin for the observational sample (see Terrazas et al. 2017 for a full quantitative discussion on this empirical relationship). TNG adequately reproduces the $\mathrm{M_{BH}}$ distribution of the quiescent population in all but the lowest $\mathrm{M_{star}}$ bin since the normalization of TNGs's $\mathrm{M_{BH}}$-$\mathrm{M_{bulge}}$ relation has been calibrated to the relation from Kormendy & Ho (2013) which omits pseudobulges that are preferentially hosted in star-forming galaxies. TNG and the observational data differ significantly for the star-forming population, where TNG predicts much higher $\mathrm{M_{BH}}$ values compared to the observational data at each $\mathrm{M_{star}}$ bin. Additionally, TNG shows a much narrower distribution of $\mathrm{M_{BH}}$ values at each $\mathrm{M_{star}}$ bin than in the observations due to the tightness of their $\mathrm{M_{BH}}$-$\mathrm{M_{star}}$ relation.

The top right plot shows the sSFR as a function of $\mathrm{M_{star}}$. The strong bimodality in TNG galaxies as a result of black hole winds is evident, particularly between $\mathrm{M_{star}} = 10^{10-11}$ $\mathrm{M_\odot}$. Additionally, the most massive galaxies in TNG exhibit low yet significant amounts of sSFRs moreso than galaxies at lower masses. We discussed this in Section 5.5.4, where black hole wind energy was less effective against a more massive potential well where the gas can be more readily retained due to the higher binding energies in these galaxies.

The sSFR-$\mathrm{M_{star}}$ parameter space also highlights the biases in the T17 sample. There is no star forming main sequence, as is seen in more representative samples of galaxies in this parameter space (e.g., Chang et al., 2015). However, this panel also shows how the sample spans a large range of $\mathrm{M_{star}}$ and sSFR.

5.7 Implications of the black hole feedback model on observational diagnostics

In this section, we explore how the distribution of galaxies on the sSFR-$\mathrm{M_{star}}$-$\mathrm{M_{BH}}$ parameter space is sensitive to changes in the physics of quiescence using the TNG model variations.

5.7.1 The coevolution of $\mathrm{M_{BH}}$ and $\mathrm{M_{star}}$

The strong correlation between $\mathrm{M_{BH}}$ and $\mathrm{M_{star}}$ paired with a $\mathrm{M_{BH}}$ threshold for quiescence produces a fairly narrow range of $\mathrm{M_{star}}$ where both quiescent and star-forming galaxies can coexist with comparable numbers in TNG. The quiescent fraction rises from 0.3 to 0.7 between $\mathrm{M_{star}} = 10^{10.25-10.55}$ $\mathrm{M_\odot}$ (in general agreement with Donnari et al. 2019), giving a 0.3 dex range. As a consequence of these features, the distribution of star formation as a function of a galaxy's $\mathrm{M_{star}}$ is particularly sensitive to the normalization of the $\mathrm{M_{BH}}$-$\mathrm{M_{star}}$ relation.

We show this in Figure 5.8 where we plot the $\mathrm{M_{BH}}$-$\mathrm{M_{star}}$ relations at $z = 0$ for the LowThermEff (light blue and red) and HighThermEff (dark blue and red) model variations, which show two simulations where thermal mode feedback is less and more efficient, respectively. The blue and red colors indicate whether galaxies are star-forming or quiescent, i.e. above or below sSFR $= 10^{-11}$ yr^{-1}. The top and right panels show the quiescent fraction as a function of $M_{\rm star}$ and $M_{\rm BH}$ for the LowThermEff (gray) and HighThermEff (black) simulations.

In TNG, the thermal mode primarily regulates the growth of the black hole (see Fig. 7 in Weinberger et al. 2018 and the discussion therein for a detailed description of $M_{\rm BH}$ growth in TNG during different accretion phases). A high efficiency of thermal mode feedback more readily suppresses a black hole's growth since it transfers thermal energy to the gas immediately surrounding it, reducing the amount of cold gas that can accrete. As a result, while the $M_{\rm BH}$ threshold for quiescence does not change as a result of different thermal mode efficiencies (see right hand panel of Figure 5.8), the distribution of star formation amongst galaxies at different $M_{\rm star}$ (i.e., the quiescent fraction as a function of $M_{\rm star}$) does change. The top panel of Figure 5.8 shows that the quiescent fraction significantly increases at different $M_{\rm star}$ values as a result of the change in the normalization of the $M_{\rm BH}$-$M_{\rm star}$ relation. This indicates changes to the extent of the star forming main sequence on a sSFR-$M_{\rm star}$ plot.

We find, however, that the observational sample from T17 exhibits a larger intrinsic scatter in the $M_{\rm BH}$-$M_{\rm star}$ relation that is not produced by TNG, as discussed in Section 5.6.2. We confirm that lowering the seed $M_{\rm BH}$ only increases the scatter for low $M_{\rm star} \lesssim 10^{10.2}$ $M_\odot$, above which the scatter remains small. This discrepancy likely comes from the particular circumstances by which black holes coevolve and grow with their host galaxies in TNG (Li et al. in prep). The broad scatter in the observational sample's $M_{\rm BH}$-$M_{\rm star}$ relation suggests that black holes can exhibit different mass assembly histories in different galaxies. If $M_{\rm BH}$ is truly an indicator of quiescence, then the intrinsic scatter in how galaxies can host black holes of different masses will largely affect the observed relationship between sSFR and $M_{\rm star}$.

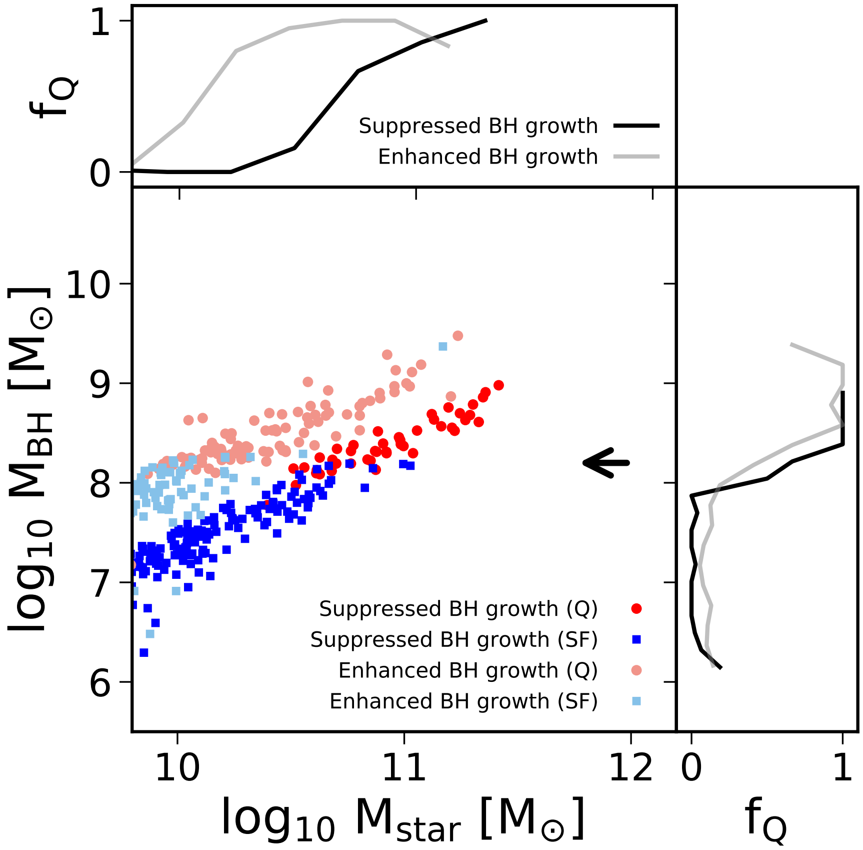

Figure 5.8: The M_{BH}-M_{star} relation at $z = 0$ for the LowThermEff (light blue and red points) and HighThermEff (dark red and blue points) model variations. The top and right panels show the quiescent fraction as a function of M_{star} and M_{BH}, respectively, for the LowThermEff (gray) and HighThermEff (black) simulations. The main difference between the two models is the normalization of the M_{BH}-M_{star} relation since thermal mode feedback primarily regulates M_{BH} growth. Both simulations have the same M_{BH} threshold for quiescence (black arrow) yet the change in normalization alters the quiescent fraction as a function of M_{star}.

5.7.2 The M_{BH} threshold for quiescence

The top middle panel of Figure 5.7 shows that for TNG galaxies with $M_{star} > 10^{10}$ $M_\odot$ there exists a M_{BH} threshold for quiescence at $\sim 10^{8.2}$ $M_\odot$ where below this mass most (>90%) of these galaxies are star-forming and above this mass most (>90%) are quiescent. The majority of these quiescent central galaxies (73%) have very low sSFRs shown as upper limits at $\sim 10^{-12.5}$ yr^{-1}, demonstrating that black hole kinetic winds are extremely effective at preventing star formation in most galaxies undergoing this form of black hole feedback in TNG. In this section, we show that the M_{BH} threshold at $\sim 10^{8.2}$ $M_\odot$ is sensitive to the parameter choices that constitute the TNG fiducial model.

The four model variations that illustrate this point are the HighMpiv, LowMpiv, HighChi0, LowChi0 models (see Table 5.1). In Section 5.3.1, we describe how TNG uses a M_{BH}-dependent Eddington ratio threshold (Eqn. 5.1) for determining whether a black hole is releasing thermal or kinetic mode feedback energy. Each of the four model variations we analyze in this section changes the Eddington-ratio threshold, χ, that determines the feedback mode by a certain factor, η:

$$\chi = \min\left[\eta\chi_{\rm fid}, \chi_{\rm max}\right], \tag{5.3}$$

where $\chi_{\rm fid}$ is the fiducial M_{BH}-dependent Eddington ratio threshold (see Eqn. 5.1), $\chi_{\rm max} = 0.1$ as described in Section 5.3.1, and $\eta = \frac{1}{16}, \frac{1}{4}, 4, 16$ for the HighMpiv, LowChi0, HighChi0, and LowMpiv model variations, respectively. These variations effectively change the normalization of the threshold.

In Figure 5.9 we show the Eddington ratio as a function of M_{BH} for these four model variations (median distributions shown as solid blue lines), explicitly showing the changes to the Eddington ratio threshold between thermal and kinetic mode feedback (shown as dotted blue lines). The variation in the Eddington ratio threshold

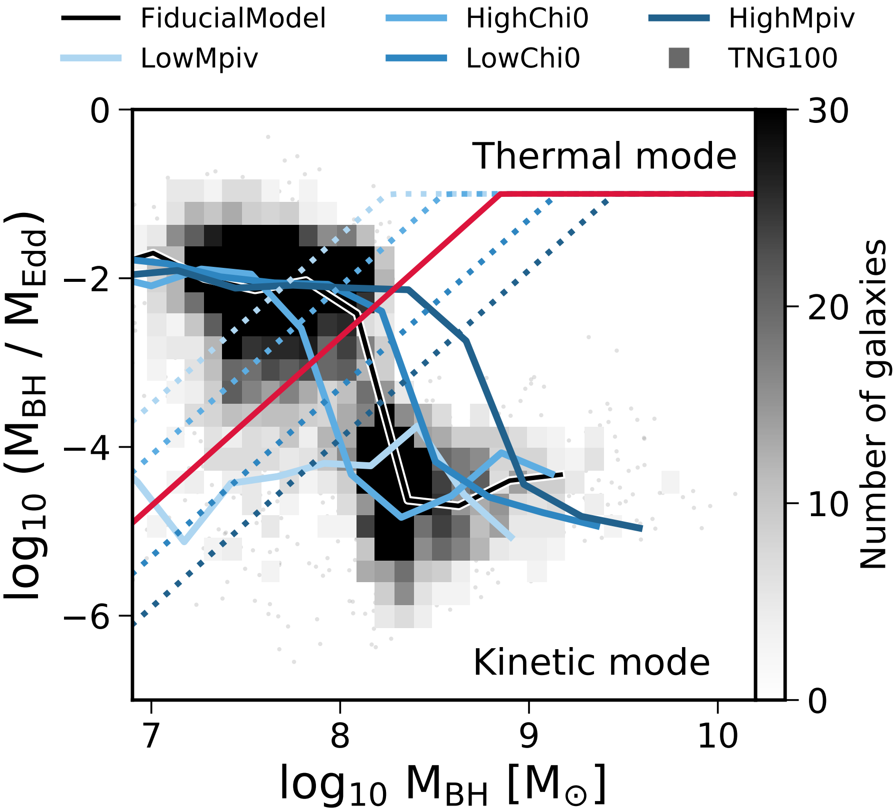

Figure 5.9: The Eddington ratio as a function of M_{BH} for the TNG100 population of galaxies (grayscale heatmap) along with the Eddington ratio threshold that determines whether a black hole is producing kinetic or thermal feedback energy (red solid line) at $z = 0$. The median distributions of the LowMpiv, HighChi0, LowChi0, and HighMpiv model variations at $z = 0$ are also plotted (blue lines). These are models that alter the threshold described in Eqn. 5.1 (shown as blue dotted lines).

changes how galaxies populate this parameter space.

The changes to the normalization of the Eddington ratio threshold change the $\mathrm{M_{BH}}$ at which black hole kinetic wind energy can begin to accumulate. Since kinetic winds from black holes are necessary to produce quiescence in TNG (see Section 5.4), changes in the normalization of χ result in changes to the $\mathrm{M_{BH}}$ threshold for quiescence since χ is $\mathrm{M_{BH}}$-dependent.

This behavior is shown in Figure 5.10, where the $\mathrm{M_{BH}}$-$\mathrm{M_{star}}$ relation is shown for each model variation at $z = 0$. From left to right, the $\mathrm{M_{BH}}$ threshold at which galaxies become mostly quiescent moves down as the normalization of χ increases. The quiescent fraction as a function of $\mathrm{M_{star}}$ and $\mathrm{M_{BH}}$ are shown on the top and right panels of each plot, respectively. As the $\mathrm{M_{BH}}$ threshold for quiescence decreases, the $\mathrm{M_{star}}$ at which galaxies begin exhibiting quiescence also decreases, until $\chi = 16\chi_{\mathrm{fid}}$ (rightmost panel) where most of the population above $\mathrm{M_{star}} = 10^{10}\ \mathrm{M_{\odot}}$ is quiescent and above this threshold.

We also note that the number of galaxies at high $\mathrm{M_{BH}}$ and $\mathrm{M_{star}}$ decreases as χ increases from left to right in Figure 5.10. This is because increasing the χ value makes it easier for black holes to satisfy the conditions necessary for kinetic mode feedback to be activated. Namely, black holes do not need to be as massive or accrete as inefficiently as would be necessary with a lower χ value. This effectively increases the amount of time that galaxies spend in the kinetic mode since lower mass systems can become quiescent earlier. We show in Section 5.4 that kinetic winds are necessary to produce quiescence and therefore largely stop the growth of galaxies via in situ star formation. Kinetic winds also largely halt the growth of the black hole as can be seen in Figure 5.9, where the Eddington ratio decreases significantly once galaxies enter the kinetic mode (also see Weinberger et al., 2018; Habouzit et al., 2019). Therefore, massive black holes and massive galaxies become rarer in the model variations with larger χ values due to the inefficient growth of $\mathrm{M_{BH}}$ and $\mathrm{M_{star}}$ for these galaxies.

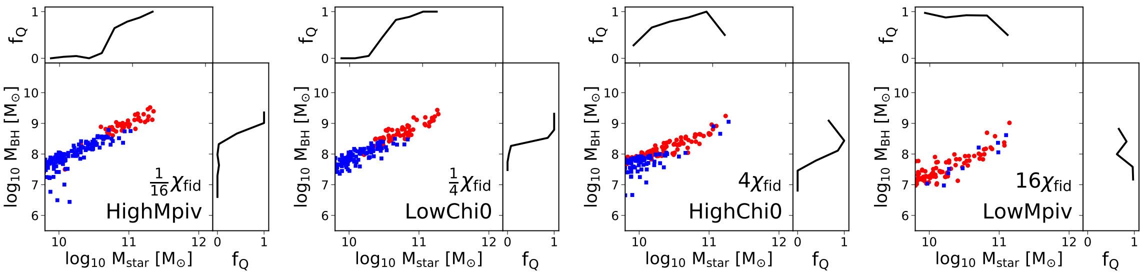

Figure 5.10: The M_{BH}-M_{star} relation for HighMpiv, LowChi0, HighChi0, and LowMpiv model variations at z = 0. The quiescent fraction as a function of M_{star} and M_{BH} is shown on top and to the right of each plot, respectively. As the Eddington ratio threshold between thermal and kinetic mode black hole feedback (χ) increases in units of the fiducial model's value from left to right, the black hole mass at which galaxies are able to become quiescent decreases.

We note that the M_{BH} threshold for quiescence at $\sim 10^{8.2}$ $M_\odot$ emerges from the ensemble of parameter choices that produce a realistic z = 0 galaxy population. TNG model parameters were calibrated in order approximately return the shape and amplitudes of certain observables mostly related to the stellar mass content of z = 0 galaxies (see Pillepich et al., 2018). While the model variations shown in Figure 5.10 produce unrealistic galaxy populations that would violate the observational constrains described in Pillepich et al. (2018), they demonstrate the sensitivity of galaxy star forming properties as a function of a changing M_{BH} threshold.

While different TNG model variations exhibit different behaviors in the sSFR-M_{BH}-M_{star} parameter space, we note that the binding energy correlation described in Section 5.5.3 continues to hold. Namely, for all model variations, the accumulated energy from black hole-driven kinetic winds must exceed the binding energy of gas within the galaxy in order for quiescence to be produced in each model (See Appendix 5.10). Differences in the model variations occur when the galaxy properties required to meet this condition are changed. This occurs, for example, by allowing lower mass black holes to accumulate kinetic feedback energy (as in this section), or by changing the way black holes occupy galaxies of different M_{star} (as in Section 5.7.1).

5.8 Discussion

This work aims to illuminate how the effects of black hole feedback on gas within and around galaxies can alter the observable properties of sSFR, $\mathrm{M_{BH}}$, and $\mathrm{M_{star}}$ in the context of a physical model of galaxy formation. We have used the IllustrisTNG simulation suite and its model variations to characterize and assess the black hole model and the resulting physics of quiescence for central galaxies with $\mathrm{M_{star}} > 10^{10}$ $\mathrm{M_\odot}$. In this section, we discuss how our results may aid in understanding the link between black hole feedback and quiescence in the real Universe, and how other approaches to modeling this feedback both in current and future simulations may benefit from the type of analysis we do in this work.

5.8.1 Assessing models using the sSFR-$\mathrm{M_{BH}}$-$\mathrm{M_{star}}$ parameter space

We turn our attention first to the sharp transition from a mostly star-forming to a mostly quiescent galaxy population above a particular $\mathrm{M_{BH}}$ threshold at $\sim 10^{8.2}$ $\mathrm{M_\odot}$ in TNG. We compare this to a sample of 91 galaxies with dynamical $\mathrm{M_{BH}}$ measurements from T17. We note that this sample is not representative of the entire galaxy population due to the biases associated with various dynamical $\mathrm{M_{BH}}$ measurement techniques.

The current data available, however, do not indicate the existence of a particular $\mathrm{M_{BH}}$ threshold for quiescence as is seen in TNG (See the middle panel of Figure 5.7). Instead, these data show that the sSFR is a smoothly decreasing function of the $\mathrm{M_{BH}}/\mathrm{M_{star}}$ ratio of these galaxies (for a full discussion see Terrazas et al., 2017). This empirical relationship provides a constraint for models that use black hole feedback in order to produce quiescence. Future work using more representative samples of dynamical $\mathrm{M_{BH}}$ measurements with an understanding of their selection biases will be important for more precisely quantifying the observed correlations between sSFR, $\mathrm{M_{star}}$, and $\mathrm{M_{BH}}$ found in T17.

Another point of discussion centers on the fact that TNG produces a $\mathrm{M_{BH}}$-$\mathrm{M_{star}}$ relation with significantly less intrinsic scatter compared to the observational data from T17 (See the left panel of Figure 5.7). Earlier studies of black hole demographics were heavily biased towards the most massive black holes and mostly took into account those within quiescent, early-type galaxies and a few bulge components of late-type galaxies (Magorrian et al., 1998; Ferrarese & Merritt, 2000; Gebhardt et al., 2000). The tight correlation between black holes and the galaxy properties of their early-type components led to the use of samples like these (e.g., Figure 2 of McConnell & Ma, 2013, showing the $\mathrm{M_{BH}}$-$\mathrm{M_{bulge}}$ relation for early-type galaxies) to assess a model's black hole demographics for the entirety of the galaxy population, early-types or otherwise. The small scatter seen in TNG's $\mathrm{M_{BH}}$-$\mathrm{M_{star}}$ relation is a common feature in other galaxy formation models for similar reasons (e.g., Section 3.3 of Volonteri et al., 2016).

While recent studies of black hole demographics using $\mathrm{M_{BH}}$ measurements are still biased due to the specifics of each detection method, they incorporate a more diverse set of galaxies and show a significantly more pronounced intrinsic scatter in the relationship between $\mathrm{M_{BH}}$ and $\mathrm{M_{star}}$ (Reines & Volonteri, 2015; Savorgnan et al., 2015; Terrazas et al., 2016b, 2017; Davis et al., 2018; Sahu et al., 2019). Namely, they show that late-type, star-forming galaxies lie below the canonical $\mathrm{M_{BH}}$-$\mathrm{M_{star}}$ relations for early-type, quiescent galaxies, increasing the scatter in the relation for the whole population (see also Li et al. in prep). Models need to take both the large scatter and its correlation with star formation properties into account when assessing whether their black hole demographics adequately represent the whole galaxy population.

The coevolution of $\mathrm{M_{star}}$ and $\mathrm{M_{BH}}$ is difficult to constrain, especially since the processes governing the growth of these two properties function at spatial and temporal scales that differ by several orders of magnitude. Observations show that $\mathrm{M_{BH}}$ accretion rates differ for galaxies of different masses and star formation properties

(Aird et al., 2012, 2017, 2018). Additionally, studies have shown that different black hole seeding mechanisms can affect the evolution of both the black hole and its host galaxy (Wang et al., 2019). These factors are likely important for determining the intrinsic scatter between M_{star} and M_{BH}.

Uncertainties on how to model accretion onto a black hole and how this relates to large-scale gas accretion onto its host galaxy also exacerbates the issue of linking M_{star} and M_{BH} in simulations. Many studies argue that Bondi-Hoyle accretion (Hoyle & Lyttleton, 1939; Bondi & Hoyle, 1944) is an oversimplification, assuming the gas immediately surrounding the black hole has zero angular momentum. This assumption fails to take into account the fact that non-spherical accretion is an important factor for growing black holes (e.g., Hopkins & Quataert, 2011). While Bondi-Hoyle accretion is an attractive model due to its simplicity, it may prove to be an important limitation when attempting to reproduce large scale galaxy properties. Other models for black hole growth, such as the gravitational torque model (Hopkins & Quataert, 2011; Anglés-Alcázar et al., 2015, 2017a,b), will provide different avenues for exploring possible black hole-galaxy coevolutionary scenarios once they are fully incorporated into a large scale cosmological model of galaxy formation that includes black hole feedback.

Black hole feedback itself can also affect the growth of black holes in galaxies. In Section 5.7.1, we show that the thermal mode feedback implemented at high accretion rates in TNG regulates M_{BH} growth, effectively playing a role in setting the normalization of the M_{BH}-M_{star} relation. Figure 5.9 shows that the Eddington ratio drops to low values once the distribution of galaxies on this plot crosses the threshold where kinetic mode feedback takes effect (Weinberger et al., 2018). Habouzit et al. (2019) explore the black hole population and the the properties of AGN in TNG, showing that their kinetic wind feedback implementation may be too effective at suppressing M_{BH} growth compared to observational constraints.

Stellar feedback can also slow M_{BH} growth by reducing the amount of cold gas present near the black hole, particularly in shallow potential wells during the early growth of the black hole (Habouzit et al., 2017; McAlpine et al., 2017). At the galaxy mass scales relevant to this work with $M_{star} > 10^{10}$ $M_{\odot}$, stellar feedback is also expected to play an important role in setting the mass scale above which quiescent galaxies begin to dominate the galaxy population. Bower et al. (2017) and Henriques et al. (2019a) both demonstrate this by showing that black hole activity can be triggered once stellar feedback becomes ineffective at preventing cooling from the gaseous halo to the galaxy in progressively more massive systems.

The prescriptions for black hole accretion, the implementation of stellar and black hole feedback, and the complex interactions between feedback's effect on the availability of gas for M_{BH} and M_{star} growth all contribute to the characteristics of simulated M_{BH}-M_{star} relations. In this work, we show that if M_{BH} is causally related to quiescence, then the shape, normalization, and scatter of the M_{BH}-M_{star} relation will determine the M_{star} distributions of star-forming and quiescent galaxies. This is a fundamental observational diagnostic for models. As such, it is essential that the the observed scatter in the M_{BH}-M_{star} relation and its correlation with its host galaxy's sSFR are reproduced for any model where M_{BH} correlates with quiescence. This will largely determine the stellar mass distribution of the star forming main sequence and the galaxies that lie off of it, as we describe in Section 5.7.

5.8.2 Characterizing the impact of black hole kinetic winds in TNG

In Section 5.5.3, we show that quiescent galaxies have black hole wind energies that exceed the binding energy of the gas in the galaxy. This supports a framework where black hole kinetic winds gravitationally unbind gas from the galaxy above a M_{BH} threshold $\sim 10^{8.2}$ $M_{\odot}$.

Following our analysis in Section 5.5.3 and visually indicated by Figure 5.3, black hole winds push dense gas out of galaxies in TNG, effectively producing quiescence. However, high density, cooler gas is more difficult to gravitationally unbind or heat with feedback energy than gas which is more diffuse. Other studies confirm that energy from these winds in TNG galaxies affects not only the cold gas but also the more diffuse gas phases that preferentially reside at high scale heights above the galaxy and within the circumgalactic medium (Nelson et al., 2018b; Henriques et al., 2019b, Zinger et al. in prep).

This likely explains the behavior seen in the bottom panel of Figure 5.5, where many galaxies just above the M_{BH} threshold for quiescence exhibit an abrupt decrease in halo gas mass. More massive black holes that live in more massive halos are able to retain a larger fraction of their gas since it is increasingly difficult to push gas out of a deeper potential well. Davies et al. (2019) and Oppenheimer et al. (2019) independently found similar behavior in the EAGLE simulation, where the gas fraction decreases when the ratio of black hole feedback energy and halo binding energy is high.

Figures 4 and 8 in Pillepich et al. (2018) and Figure 11 in Weinberger et al. (2017) show rough agreement with the halo gas masses around galaxies with dark matter halo masses $> 10^{13}$ $M_{\odot}$, showing an improvement compared to the original Illustris model where halo gas masses were severely underestimated. However, while there is evidence to suggest that halo gas masses must be suppressed by feedback in order to agree with cluster mass estimates (e.g., Choi et al., 2015, 2017; Barnes et al., 2017), the evacuation of more than $\sim 80\%$ of halo gas for a large population of intermediate mass galaxies undergoing black hole feedback should be corroborated before the agreement between TNG and observations is taken at face value. Upcoming work will compare the the observational signatures of the gaseous atmospheres in TNG haloes with observational data (Pop et al. in prep, Truong et al. in prep).

Within the framework of ejective and preventative feedback, TNG's kinetic wind model at first glance seems to produce quiescence through sustained ejective feedback. This is further supported by our analysis in Section 5.5.1 where we find that quiescence in TNG cannot be easily described using the logic of balancing heating and cooling rates employed by purely preventative semi-analytic models. However, Figure 5.5 shows that the cooling time in galaxies exhibiting black hole winds is significantly greater than in the model variation where no black hole winds are present. Weinberger et al. (2017) demonstrate that these winds are able to thermalize at large distances from the black hole, indicating that the kinetic mode black hole feedback mechanism employed in TNG is partly preventative, resulting in the increase of the gas halo's average cooling time. Additionally, the ejective nature of TNG's black hole kinetic winds likely aids the process that leads to quiescence since it reduces the mass of the reservoir from which star-forming gas is accreted onto the galaxy.

5.8.3 Black hole feedback prescriptions in models

Another key issue for large-volume simulations is the need to implement subgrid physics that models the small-scale phenomena important for galaxy evolution. One crucial approximation is how energy from feedback is transferred to the surrounding gas. Feedback from both stars and black holes has been modeled using a variety of different subgrid physics. The details of these subgrid physics will inevitably affect observable galaxy properties and the transfer of feedback energy to the gas within and around galaxies.

In the case of TNG, we have described a two-mode black hole feedback model separating the forms of energy injection at high- and low-accretion rates, corresponding to radiatively efficient and inefficient accretion. High- and low- accretion phases have been modeled in TNG as an injection of pure thermal energy or pure kinetic energy, respectively. The low-accretion phase injection of kinetic winds in TNG was motivated by recent observational evidence of strong outflows in galaxies hosting low accretion rate black holes (Cheung et al., 2016; Wylezalek et al., 2017; Penny et al., 2018). Theoretically, this implementation was also motivated by the wind launching mechanism from inefficient accretion onto black holes put forth by studies such as Blandford & Begelman (1999).

In this work, we show that thermal mode black hole feedback in TNG regulates $\mathrm{M_{BH}}$ growth (Section 5.7.1) whereas kinetic mode feedback suppresses $\mathrm{M_{BH}}$ and, most notably for this work, $\mathrm{M_{star}}$ growth (Sections 5.4 and 5.5). The abrupt change in galaxy and halo gas properties at the particular $\mathrm{M_{BH}}$ threshold we describe in this work (e.g., Figure 5.5) indicates an abrupt change in physical processes affecting galaxies that are undergoing kinetic mode as opposed to thermal mode feedback. Similar two-mode black hole feedback models have been implemented in a number of other large-volume simulations (e.g. Croton et al., 2006; Somerville et al., 2008; Vogelsberger et al., 2014a; Henriques et al., 2015; Dubois et al., 2016).

However, this dichotomy between feedback modes is likely an oversimplification of the physics that occurs in the real Universe. As discussed in Section 5.2, there is an abundance of observational evidence for supermassive black hole activity in galaxies. However, the interpretation of this evidence for constructing a generalizable black hole feedback model for all forms of accretion is not straightforward. For example, radio jets and lobes, generally attributed to low accretion rate feedback, have also been seen in galaxies that are producing large-scale outflows from supposedly high rates of accretion (e.g., Komossa et al., 2006; Yuan et al., 2008; Berton et al., 2018).

While TNG produces winds through low rates of accretion, some higher resolution zoom-in simulations that explicitly include kinetic feedback from high rates of accretion have shown that this process can also effectively eject cold gas from galaxies, depress the central density of the circumgalactic medium, and reduce star formation in galaxies over long timescales (e.g., Choi et al., 2012, 2015, 2017, 2018). This is supported by observational evidence of outflows in AGN and quasars (e.g., Heckman et al., 1981; Villar-Martín et al., 2011; Cicone et al., 2014). These types of zoom-in studies take advantage of their smaller volumes in order to incorporate multiple avenues of feedback energy transfer from black holes (e.g., kinetic, thermal, and/or radiative) simultaneously that may more comprehensively model the complex interactions between black holes and the ambient medium (e.g., Bourne & Sijacki, 2017; Mukherjee et al., 2018; Brennan et al., 2018).

As such, a consensus on how black hole feedback should be implemented in cosmological simulations within the limitations of finite resolution has not yet been reached. These complications need to be considered when assessing models that simplify black hole feedback physics into low- and high-accretion rate modes. This dichotomy is likely missing important physical recipes that may shape the way galaxies grow in simulations.

5.9 Conclusions

We explore the effects of black hole feedback on the properties of central galaxies with $\mathrm{M_{star}} > 10^{10}$ $\mathrm{M_\odot}$ in the context of the IllustrisTNG simulation suite. In particular, we use TNG100 and a dozen model variations to assess how observable correlations between the sSFR, $\mathrm{M_{star}}$, and $\mathrm{M_{BH}}$ of these galaxies are sensitive to changes in the physics model. We also connect these correlations to the effects of black hole feedback on the gas distribution within and around galaxies. Finally, we compare results from TNG with observational data of galaxies with dynamical $\mathrm{M_{BH}}$ measurements. We highlight our main results below:

- TNG requires low accretion rate black hole feedback in the form of kinetic winds in order to produce a quiescent galaxy population (Section 5.4, Figure 5.1, and also shown in Weinberger et al. 2017).

- A decline in the sSFR of simulated galaxies is seen when the accumulated black hole wind energies exceed the gravitational binding energies of the gas within galaxies, $\int \dot{E}_{\mathrm{kinetic}} dt > E_{\mathrm{bind,gal}}$ (top panel of Figure 5.2). This behavior is seen for all model variations we examine in this work (See Appendix 5.10). This provides strong evidence that black hole-driven kinetic winds push cold gas out of the galaxy to produce quiescence in TNG (Section 5.5.3, Figure 5.3).

- Simulated galaxies with black hole wind energies that fall below the binding energy of gas within the galaxy have black hole masses below a $\mathrm{M_{BH}}$ threshold of $\sim 10^{8.2}$ $\mathrm{M_\odot}$. Those that have wind energies exceeding the binding energies host black holes above this $\mathrm{M_{BH}}$ threshold (bottom panel of Figure 5.2). This produces a sharp decrease in the amounts of interstellar and circumgalactic gas at this $\mathrm{M_{BH}}$ threshold (Section 5.5.4, Figure 5.5).

- Below the $\mathrm{M_{BH}}$ threshold at $\sim 10^{8.2}$ $\mathrm{M_\odot}$, most (>90%) simulated central galaxies with $\mathrm{M_{star}} > 10^{10}$ $\mathrm{M_\odot}$ are star-forming and above this mass most (>90%) are quiescent. 73% of the quiescent population have very low sSFRs (with upper limits at $10^{-12.5}$ $\mathrm{yr^{-1}}$), indicating that black hole winds are extremely effective at suppressing star formation once low-accretion rate feedback takes effect in TNG (see also Weinberger et al. 2018).

- We compare TNG to observational data of 91 central galaxies with dynamical $\mathrm{M_{BH}}$ measurements from Terrazas et al. (2016b, 2017), with the caveat that these data are not representative of the entire galaxy population. We find that TNG qualitatively reproduces the result that quiescent galaxies host more massive black holes than star-forming galaxies. However, the $\mathrm{M_{BH}}$-$\mathrm{M_{star}}$ relation for TNG produces a much smaller scatter compared to what is seen in the observational data (Section 5.6.2, top left panel of Figure 5.7). Additionally, these observational data, while incomplete, show a smoother decline in sSFR as a function of $\mathrm{M_{BH}}$, showing no indication of an abrupt suppression of sSFR at a particular M_{BH} threshold (Section 5.6.2, top middle and bottom panels of Figure 5.7).

- The distribution of star-forming and quiescent galaxies across M_{star} parameter space in TNG is sensitive to both the normalization of the M_{BH}-M_{star} relation and the M_{BH} at which black holes produce kinetic winds. We show that the normalization of the M_{BH}-M_{star} relation depends on the efficiency of thermal mode feedback on regulating the growth of M_{BH}.

These results demonstrate that the relationship between M_{BH}, M_{star}, and sSFR is a powerful tool for exploring the physics of quiescence within the context of black hole feedback. We show that if the M_{BH} and sSFR of galaxies are causally linked, as is the case in TNG, then the way M_{BH} pairs with galaxies of different M_{star} will determine the star formation properties of the entire central galaxy population. We find important differences between the results from TNG and the observational data for galaxies with dynamical M_{BH} measurements from (Terrazas et al., 2016b, 2017). These differences illuminate the importance of taking into account the scattered relationship between M_{BH} and M_{star} and its dependence on sSFR found in current samples of galaxies with dynamical M_{BH} measurements.

5.10 Appendix A: The Physics of Quiescence in the Model Variations

Here we append further evidence in support of our phenomenological framework presented in Section 5.5.3. This framework describes a physically-motivated picture of quiescence in TNG, where a majority of galaxies shut off their star formation once black hole-driven winds accumulate enough energy to push gas out of their host galaxy. This framework comes from the fact that the sSFR of a galaxy declines once

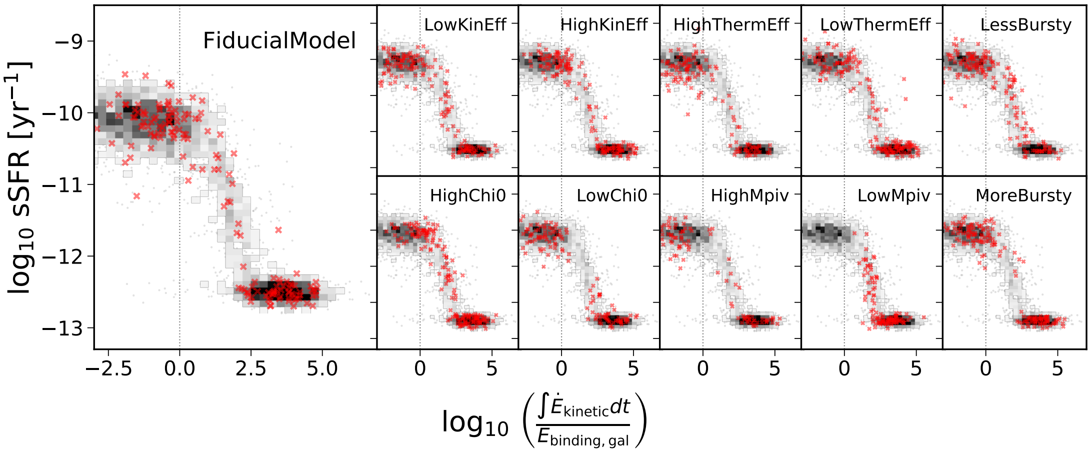

Figure 5.11: The sSFR as a function of the ratio between the cumulative energy from black hole-driven kinetic winds and the binding energy of gas in the galaxy for all model variations listed in Table 5.1 (red crosses). The gray heatmaps are the same in each panel and show the distribution of galaxies in TNG100.

the cumulative energy from black hole-driven winds becomes larger than the binding energy of gas in the galaxy.

The model variations listed in Table 5.1 alter the parameters of the black hole physics model in TNG, producing significantly different galaxy populations. This is described in Section 5.7 and shown in Figures 5.9, 5.8, and 5.10. Even so, the evidence for our phenomenological framework holds true for every model variation we assess in this work. In Figure 5.11, we show the sSFR as a function of the ratio between accumulated black hole wind energy and the binding energy of gas in the galaxy (the same parameter space as the top panel of Figure 5.4). Each panel shows the distribution of TNG100 galaxies as a grayscale heatmap, while the individual galaxies in each model variation are shown as red crosses. The fiducial TNG model is shown in the large panel on the left, whereas the 10 model variations that include black hole-driven kinetic winds are to the right.

Despite the differences in galaxy population statistics in each model variation, we find that galaxies in all of the simulations reproduce the same relation on these plots as the fiducial model runs. The only differences are where galaxies lie along the distribution compared to one another. For example, in Section 5.7.2 and Figure 5.10 we show that most of the galaxies in the HighMpiv model variation are star-forming since the criteria for producing kinetic winds is only satisfied by the most massive black holes and therefore the most massive galaxies. For the LowMpiv model variation, the criteria for producing kinetic winds is satisfied by all galaxies with $\mathrm{M}_{\mathrm{star}} > 10^{10}$ $\mathrm{M}_{\odot}$ in this simulation. In Figure 5.11, the distribution of galaxies in these two model variations reflect this since in the LowMpiv model all black holes produce enough accumulated energy to overcome the binding energy of the gas within the galaxy. Namely, all galaxies in this simulation lie to the right of the vertical dotted line where these two energies equal. The HighMpiv model shows galaxies that have not yet produced enough black hole wind energy to do this and as such also populate the star-forming region of this plot to the left of the vertical dotted line.

The NoBHs and NoBHwinds simulations do not have a value for $\int \dot{E}_{\mathrm{kinetic}} dt$. However, we have shown in Figure 5.1 that they do not produce a population of quiescent galaxies, further supporting our phenomenological framework.

5.11 Appendix B: Resolution effects in TNG 300 compared with TNG100

In this work, we exclusively use results from TNG100 in order to directly compare with the model variations that have roughly the same resolution. Here we describe resolution effects present in TNG300 that further motivate the exclusive use of TNG100 for the purposes of our study.

TNG300 is one of the flagship simulations of the IllustrisTNG project with a 302.6^3 comoving Mpc^3 volume. TNG300 has 2×2500^3 initial resolution elements with a baryonic mass resolution of 1.1×10^7 $\mathrm{M}_{\odot}$ and gravitational softening length of

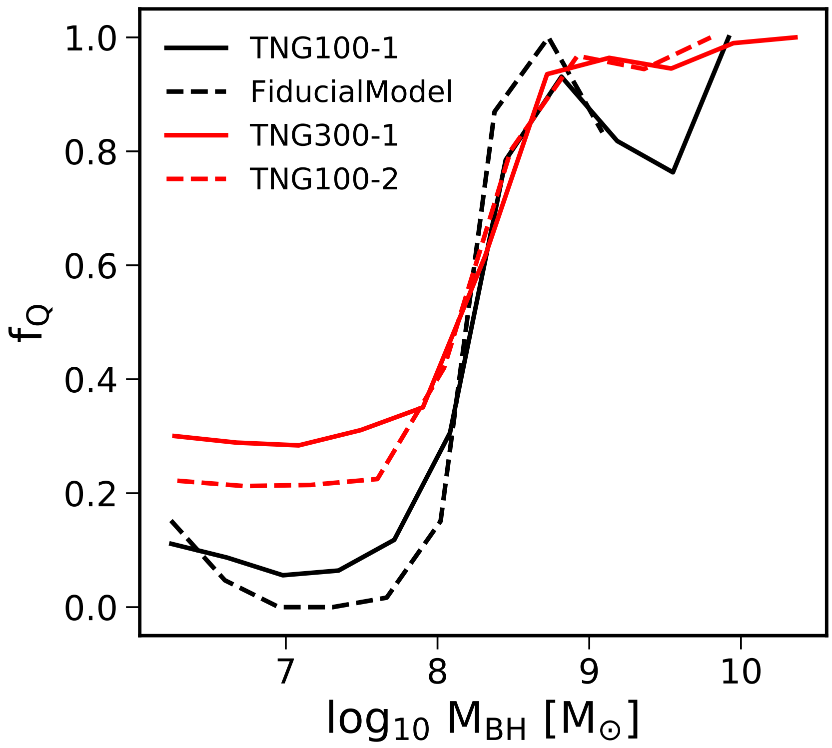

Figure 5.12: The fraction of quiescent galaxies as a function of M_{BH} in TNG100-1 (black, solid line), FiducialModel (black, dashed line), TNG300-1 (red, solid line), and TNG100-2 (red, dashed line). The black lines represent simulations run at higher resolution than those represented by the red lines. The dashed lines represent smaller volume simulations than those represented by the solid lines. Lower resolution TNG runs produce up to 20% more quiescent galaxies at $M_{BH} \lesssim 10^{8.2}$ and $\gtrsim 10^9$ $M_\odot$.

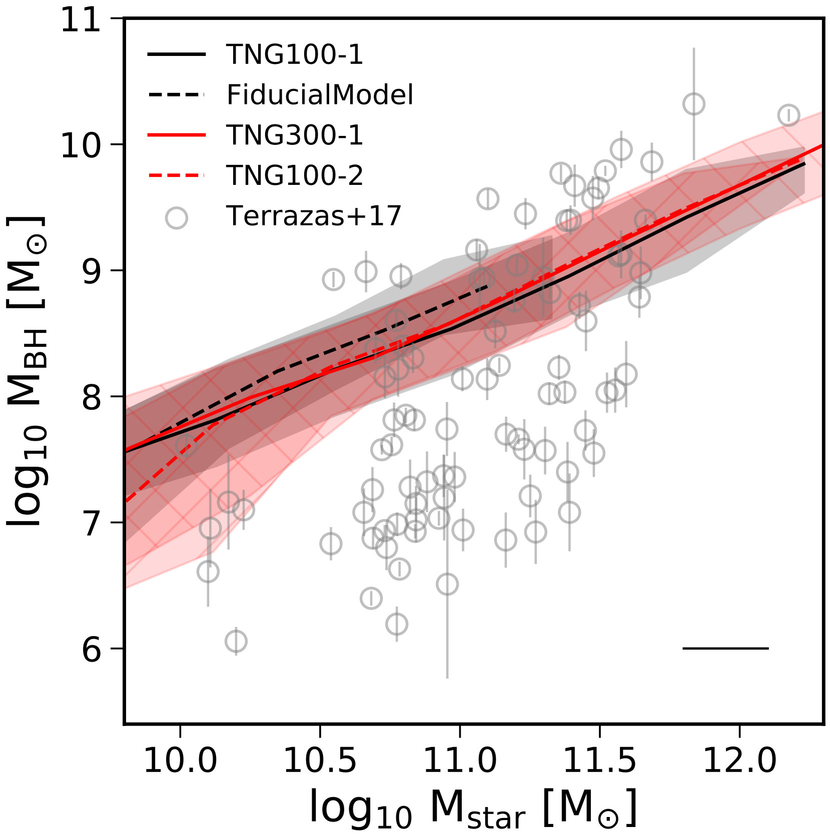

Figure 5.13: The median M_{BH}-M_{star} relation for TNG100-1 (black, solid line), FiducialModel (black, dashed line), TNG300-1 (red, solid line), and TNG100-2 (red, dashed line). The 10 and 90 percentiles below and above the median are shown as translucent regions matching the color of their median lines. Similar to Figure 5.12, black and gray colors represent simulations run at higher resolution than those represented by red and the dashed lines represent smaller volume simulations than those represented by the solid lines. Lower resolution TNG runs produce a slightly more scattered relation at $M_{star} \lesssim 10^{10.4}$ $M_\odot$. Above this mass, the scatter is consistent between simulations. The observational sample of galaxies with dynamical M_{BH} measurements are shown as gray circles and its M_{star} error bar is shown in the lower right corner.

1.48 kpc at $z = 0$. This represents approximately an order of magnitude decrease in mass resolution and an increase in the gravitational softening length by a factor of 2 compared to TNG100.

In order to differentiate between the effects of a smaller/larger box size in comparison to higher/lower resolution, we will use four TNG runs - two with the same resolution as the fiducial TNG100 but different box volumes (TNG100-1 sized at 110.7^3 Mpc^3 and FiducialModel sized at 36.9^3 Mpc^3) and two with the same resolution as TNG300 but different box volumes (TNG300-1 sized at 302.6^3 Mpc^3 and TNG100-2 sized at 110.7^3 Mpc^3). In both Figures 5.12 and 5.13 the black and red lines indicate the simulations with higher and lower resolution, respectively. Larger and smaller box sizes are indicated with solid and dashed lines, respectively.

In Section 5.5, we describe how quiescence occurs above a particular $\mathrm{M_{BH}}$ threshold for TNG galaxies. Figure 5.12 shows the fraction of quiescent galaxies as a function of $\mathrm{M_{BH}}$ for these four simulations. Regardless of box size, those simulations with lower resolution produce up to 20% more quiescent galaxies at $\mathrm{M_{BH}} \lesssim 10^{8.2}$ and $\gtrsim 10^{9}$ $\mathrm{M_\odot}$. This indicates that the feedback present in the lower resolution runs is more effective at suppressing star formation and producing quiescence despite the fact that they have the same subgrid prescriptions.

Our analysis in Section 5.6.2 indicates that the scatter in the $\mathrm{M_{BH}}$-$\mathrm{M_{star}}$ relation is much smaller than the scatter seen in the observations. To determine whether the scatter would increase for a larger box simulation, we show the median $\mathrm{M_{BH}}$-$\mathrm{M_{star}}$ relations and their 10 and 90 percentile distributions around their medians for the four simulations we discuss in this section. We convolve these $\mathrm{M_{star}}$ and $\mathrm{M_{BH}}$ values with observational errors just as we do in Section 5.6.

Regardless of box size, those simulations with lower resolution produce a slightly larger scatter than the higher resolution simulations at $\mathrm{M_{star}} \lesssim 10^{10.4}$ $\mathrm{M_\odot}$, indicating that this increase in scatter is a resolution effect. Above this mass, the scatter is similarly small for all simulations. We also show the observational data for 91 galaxies with dynamical M_{BH} measurements to show that in all these models, the scatter does not easily reproduce the broad distribution of galaxies in the Terrazas et al. (2017) sample.

Acknowledgments

This chapter is a reproduction of an article of the same title that is in preparation for publication. The co-authors of this article are currently Eric F. Bell, Annalisa Pillepich, Dylan Nelson, Rachel S. Somerville, Shy Genel, Mélanie Habouzit, Rainer Weinberger, Yuan Li, and Lars Hernquist.

B.A.T. is supported by the National Science Foundation Graduate Research Fellowship under Grant No. DGE1256260. The Flatiron Institute is supported by the Simons Foundation. The flagship simulations of the IllustrisTNG project used in this work (TNG100) have been run on the HazelHen Cray XC40-system at the High Performance Computing Center Stuttgart as part of project GCS-ILLU of the Gauss centres for Supercomputing (GCS). Ancillary and test runs of the project were also run on the Stampede supercomputer at TACC/XSEDE (allocation AST140063), at the Hydra and Draco supercomputers at the Max Planck Computing and Data Facility, and on the MIT/Harvard computing facilities supported by FAS and MIT MKI. In particular, the model variation runs adopted in this study (Table 1) have been run on the Draco supercomputer.We thank David Barnes, Rahul Kannan, Kareem El-Badry, Mariska Kriek, Kayhan Gültekin, August Evrard, Elena Gallo, Brian O'Shea, and Chung-Pei Ma for helpful discussions.

CHAPTER VI

Epilogue

6.1 Summary

Galaxy surveys at different redshifts reveal the steady increase in the number density of galaxies with little to no new star formation (e.g., Bell et al., 2004; Tomczak et al., 2014). While many possible causes have been explored, a consensus on the physical mechanism driving 'quiescence' has not yet been reached. Observational evidence from across the electromagnetic spectrum supports the current leading theory that black hole feedback suppresses the amount of cold gas that serves as fuel for star formation (Heckman & Best, 2014). Additionally, several lines of evidence from theoretical models of galaxy formation support the idea that black hole feedback is essential for producing a quiescent population similar to what is seen in observations (Benson et al., 2003; Bower et al., 2006; McCarthy et al., 2010).

While there exists ample evidence in support of black hole feedback as the physical mechanism for quiescence, the exact form of this feedback and how it operates remains uncertain. Despite being physically motivated and broadly reproducing the desired effects on the galaxy population, subgrid models of black hole growth and energetic feedback remain largely unconstrained. Additionally, the observational evidence that black holes produce quiescence at intermediate masses similar to that of the Milky Way is scarce and indirect.

This work approaches the issue of what causes quiescence and how black holes may be involved by using the power of black hole-galaxy scaling relations. The L-Galaxies simulation (Henriques et al., 2015) revealed a striking correlation between the black hole mass and star formation rate of simulated galaxies (Chapter 2). This led to the central question of this dissertation: *How can observable correlations between black holes and the properties of their host galaxies reveal the underlying mechanism behind quiescence?*

To answer this, a sample of local galaxies with reliable, dynamical black hole masses was compiled. The $z = 0$ black hole-stellar mass relation for this sample has significant scatter which can be explained with a third parameter: galaxies with more massive black holes exhibit less star formation activity (Chapter 3). In fact, for this diverse sample ranging from massive ellipticals to isolated spirals, the specific star formation rate of all galaxies is a smoothly decreasing function of the black hole-stellar mass ratio (Chapter 4). These results quantify for the first time the empirical relationship between black holes and star formation.

Galaxy formation models attempting to include black hole physics produce a variety of results in this parameter space (Chapter 3). Only models that continuously transfer energy from black hole feedback to the gas halo can qualitatively reproduce the result that quiescent galaxies host more massive black holes (e.g., L-Galaxies, Illustris). Models that use short, bursty black hole feedback (e.g., EAGLE) or a halo mass threshold to produce quiescence (e.g., GalICS) produce overlapping distributions, in conflict with observations. These results present a decisive observational test for black hole feedback models and support the idea that low accretion rate black hole feedback causes quiescence by supplying energy that suppresses gas accretion onto the galaxy.

This work also explores the physics behind quiescence and its effects on black hole-galaxy scaling relations in the IllustrisTNG galaxy formation model (Pillepich et al., 2018). In addition to the flagship simulations, there are also dozens of smaller-box versions that alter individual parameters of the TNG model. We find that the sSFR of galaxies in IllustrisTNG decreases once the energy from black hole-driven kinetic winds at low accretion rates becomes larger than the gravitational binding energy of gas within galaxies. This occurs at a particular black hole mass, above which galaxies abruptly transition from being mostly star-forming to mostly quiescent. Due to this feature of the model, we find that the star formation properties of the simulated galaxy population are sensitive to both the normalization of the black hole-stellar mass relation and the mass at which black holes drive kinetic winds. When comparing simulation results to the observations from Chapters 3 and 4, we find that IllustrisTNG qualitatively reproduces the observed trend that quiescent galaxies host more massive black holes. However, the observations exhibit a broader scatter in black hole mass at a given stellar mass and show no indication of an abrupt black hole mass threshold at which galaxies are completely quiescent.

6.2 Future outlook

Decades of studies support the idea that black holes shape their host galaxy's stellar mass growth. The work described in this dissertation shows how the physics of quiescence may be encoded in the observable correlations between galaxy properties. Specifically, the correlations between stellar mass, black hole mass, and star formation rate have been shown to be a powerful tool for exploring the mechanisms behind quiescence. Recent galaxy formation models that attempt to simulate black hole physics produce considerably different results, indicating major gaps in the current understanding of how black holes and galaxies relate to one another.

In order to improve upon the theoretical understanding of black hole feedback and its wide-reaching effects on galaxy formation and evolution, black hole physics must be more readily constrained by observations. I plan to dedicate future work primarily on constraining our understanding of two physical processes: (1) the coevolution of black hole and galaxy mass and (2) the transfer of energy from black hole feedback into the gas around galaxies.

6.2.1 Black hole-stellar mass coevolution

Despite ample evidence indicating the importance of black holes for galaxy formation, the coevolution of black hole and stellar mass growth remains largely unconstrained. One reason for this is that the current census of galaxies with black hole mass measurements is incomplete and biased towards detecting the most massive, most highly accreting, or closest black holes. As such, models that attempt to simulate black hole growth produce considerably different results (Chapters 3 and 4). Furthermore, as the number of black hole mass measurements have increased, studies have revealed a large scatter in the relationship between black hole and stellar mass (Reines & Volonteri, 2015; Terrazas et al., 2016b). This behavior is not reproduced in any of the latest models, indicating a major gap in the understanding of how black holes grow with their host galaxies.

As such, I plan to model a framework for how black holes grow within galaxies based on currently available observational data. I plan on incorporating black hole growth histories into a galaxy formation model by using observational constraints of black hole masses and accretion rates. The goal is to characterize how black holes occupy and grow with their host galaxies by tracing the full range of possible black hole growth histories and their uncertainties in a cosmological context.

The physics governing black hole growth is complex and simulations use various methods to model it. These methods produce considerably different trajectories for individual galaxies on the black hole-stellar mass relation. Therefore, instead of attempting to model the physics of this growth, I will focus on observed correlations between black hole and galaxy properties to constrain these growth histories. To connect black holes and galaxies in this way, I will use an empirical model that also relies on observed correlations. The UniverseMachine (Behroozi et al. 2018) is a publicly-available model that uses well-established, observational constraints to grow galaxies on top of a dark matter simulation. The statistical nature of this method builds galaxy growth histories to reproduce a range of observational data without the need to assume any physics.

In order to build black hole growth histories within the framework of the UniverseMachine, I will use two observables: black hole accretion rates and black hole masses. Aird et al. (2012, 2017, 2018) build bias-corrected probability distributions of accretion rates as a function of stellar mass, star formation rate, and redshift. They use a sample of galaxies from the CANDELS and UltraVISTA surveys, cross-matching these sources with Chandra X-ray data. They use a Bayesian approach to correct for incompleteness due to sensitivity limits (out to $z \sim 4$ for $M_{\rm star} > 10^{10}$ $M_{\odot}$). With these distributions, I will assign galaxies in the UniverseMachine a black hole accretion rate based on its stellar mass, star formation rate, and redshift.

Along with black hole accretion rates, a black hole mass must be specified as the boundary condition. In Chapter 4 of this dissertation, I find a correlation between the star formation rate, stellar mass, and black hole mass. This relation provides an empirical black hole mass distribution at $z = 0$ for galaxies given their stellar masses and star formation rates. This method avoids the uncertainties of attempting to directly model the physics of black hole growth, and instead builds them through statistical and empirical methods. To test this method, I will use two models, discussed throughout this dissertation work: L-Galaxies and IllustrisTNG. I will create 'mock' data from these simulations and implement the method above. If successful, the predicted growth histories will broadly match the 'real' simulated growth histories.

Using these empirically-derived black hole growth histories, I will address several issues regarding black hole-galaxy coevolution. For example, the work described in

Aird et al. (2012, 2017, 2018) reveal that black hole accretion rates change as a function of galaxy properties, indicating that black hole and stellar masses likely do not coevolve in step. With the model proposed, I will be able to measure the intrinsic scatter in this relation across redshift as a result of differences in star formation and black hole accretion rates. Additionally, observational data support the idea that quiescence correlates with both the dark matter halo (Wang et al., 2018) and the central black hole (Chapter 3). The results from this future work will allow me to characterize the empirical connection between black holes and the halos in which they live. With this bias-corrected framework for black hole growth, I will also be able to assess how bias may affect current and future observational work aimed at measuring black hole-galaxy scaling relations at many redshifts. Finally, more massive galaxies are expected to become quiescent at earlier times. Observational evidence suggests that quiescent galaxies host more massive black holes, at least at $z = 0$. I will be able to systematically track whether these correlations persist at high redshift and determine how quiescence manifests in galaxies during the peak of black hole and stellar mass growth. These will provide important predictions for future observations.

The goal of this future work is to constrain how black holes and galaxies grow together using currently available observational data. Decades of work support the idea that black holes shape their host galaxy's stellar mass growth. Yet, despite years of effort to characterize the role of black holes in galaxies, their coevolution in a cosmological context remains largely unknown. This future work will place constraints on how black holes occupy and grow with their host galaxies from an empirical standpoint, thereby paving the way for the improvement of black hole models in future simulations.

6.2.2 The interaction between gas halos and energetic feedback

The circumgalactic medium is a key factor in the regulation of star formation within the galaxy since it is the reservoir by which star formation is fueled. Therefore, in order to reasonably model black hole feedback in galaxy formation simulations, it is essential to understand how the circumgalactic medium is affected by feedback processes occurring within the galaxy. An explicit study of the link between the black hole and the gaseous halo is critical in order to improve the theoretical understanding of star formation and quiescence.

The work presented here has shown how quiescence manifests differently in galaxies depending on how gas halos are affected. For example, Illustris evacuates a majority of gas from the halo of the galaxy once low accretion rate black hole feedback becomes effective. IllustrisTNG also does this but only for lower mass galaxies that don't have enough gravitational binding energy to keep gas from escaping. EAGLE, however, keeps too much of its gas halo (Barnes et al., 2017) and its ejective black hole feedback model at high accretion rates cannot keep gas from cooling back onto the galaxy once accretion rates become low again (Chapter 3). Each of these models produces varied effects on the stellar mass, black hole mass, specific star formation rate parameter space as a result of these differences.

Theoretically, feedback from either stars or black holes can provide energy to regulate the amount of cooling that can occur onto the galaxy (e.g., Hopkins et al., 2011; Hayward & Hopkins, 2017). Quantifying how energy from feedback is transferred to the gaseous halo will be important for characterizing this regulation. Additionally, understanding how these effects influence the future of its star formation and stellar mass growth will allow a connection between its more easily observable galaxy properties and the circumgalactic medium.

I plan on modeling galaxy atmospheres constrained by the results from multiwavelength observational studies of the circumgalactic medium around galaxies. A considerable challenge will be bridging the gap between cluster environments and group environments, the latter of which is dominated by non-gravitational processes. A characterization of the differences between halos hosting different kinds of galaxies will require probing the multiphase gas around individual galaxies through results from absorption line (e.g., Tumlinson et al., 2011; Werk et al., 2014) and X-ray studies (e.g., Vikhlinin et al., 2006).

The latest galaxy formation models represent the implementation of current state-of-the-art theory for galactic quiescence. However, this dissertation has shown that all of these models disagree in terms of their black hole growth and feedback prescriptions as well as their galaxies' halo gas properties. The future work on galaxy atmospheres described in this section coupled with the empirically-derived study of black hole-stellar mass coevolution in the previous section will provide critical constraints for galaxy formation models that use black hole feedback in order to suppress star formation in galaxies.

BIBLIOGRAPHY

Aarseth, S. J. 1963, *MNRAS*, 126, 223

Aird, J., Coil, A. L., & Georgakakis, A. 2017, *MNRAS*, 465, 3390

—. 2018, *MNRAS*, 474, 1225

Aird, J., Coil, A. L., Moustakas, J., et al. 2012, *ApJ*, 746, 90

Anglés-Alcázar, D., Davé, R., Faucher-Giguère, C.-A., Özel, F., & Hopkins, P. F. 2017a, *MNRAS*, 464, 2840

Anglés-Alcázar, D., Faucher-Giguère, C.-A., Quataert, E., et al. 2017b, *MNRAS*, 472, L109

Anglés-Alcázar, D., Özel, F., Davé, R., et al. 2015, *ApJ*, 800, 127

Angulo, R. E., & Hilbert, S. 2015, *MNRAS*, 448, 364

Angulo, R. E., & White, S. D. M. 2010, *MNRAS*, 405, 143

Arakelyan, M. A., & Kalloglyan, A. T. 1970, *Soviet Ast.*, 13, 953

Bahcall, J. N., & Spitzer, Lyman, J. 1969, *ApJ*, 156, L63

Baldassare, V. F., Reines, A. E., Gallo, E., & Greene, J. E. 2015, *ApJ*, 809, L14

Baldry, I. K., Balogh, M. L., Bower, R. G., et al. 2006, *MNRAS*, 373, 469

Baldry, I. K., Glazebrook, K., Brinkmann, J., et al. 2004, *ApJ*, 600, 681

Baldwin, J. E. 1954, *Nature*, 174, 320

—. 1955, *MNRAS*, 115, 690

Balmaverde, B., Marconi, A., Brusa, M., et al. 2016, *A&A*, 585, A148

Balogh, M. L., Baldry, I. K., Nichol, R., et al. 2004, *ApJ*, 615, L101

Balogh, M. L., Morris, S. L., Yee, H. K. C., Carlberg, R. G., & Ellingson, E. 1997, *ApJ*, 488, L75

Balogh, M. L., Pearce, F. R., Bower, R. G., & Kay, S. T. 2001, *MNRAS*, 326, 1228

Barnes, D. J., Kay, S. T., Bahé, Y. M., et al. 2017, *MNRAS*, 471, 1088

Barnes, J. E. 1988, *ApJ*, 331, 699

Barnes, J. E., & Hernquist, L. 1992, *ARA&A*, 30, 705

Barro, G., Faber, S. M., Pérez-González, P. G., et al. 2013, *ApJ*, 765, 104

—. 2014, *ApJ*, 791, 52

Barro, G., Faber, S. M., Koo, D. C., et al. 2015, ArXiv e-prints, arXiv:1509.00469

Baugh, C. M., Cole, S., Frenk, C. S., & Lacey, C. G. 1998, *ApJ*, 498, 504

Begelman, M. C. 2001, in Astronomical Society of the Pacific Conference Series, Vol. 240, Gas and Galaxy Evolution, ed. J. E. Hibbard, M. Rupen, & J. H. van Gorkom, 363

Begelman, M. C., Blandford, R. D., & Rees, M. J. 1984, Reviews of Modern Physics, 56, 255

Begelman, M. C., McKee, C. F., & Shields, G. A. 1983, *ApJ*, 271, 70

Behroozi, P., Wechsler, R., Hearin, A., & Conroy, C. 2018, arXiv e-prints, arXiv:1806.07893

Behroozi, P. S., Conroy, C., & Wechsler, R. H. 2010, *ApJ*, 717, 379

Behroozi, P. S., Wechsler, R. H., & Conroy, C. 2013, *ApJ*, 770, 57

Beifiori, A., Courteau, S., Corsini, E. M., & Zhu, Y. 2012, *MNRAS*, 419, 2497

Bell, E. F. 2003, *ApJ*, 586, 794

—. 2008, *ApJ*, 682, 355

Bell, E. F., & de Jong, R. S. 2001, *ApJ*, 550, 212

Bell, E. F., McIntosh, D. H., Katz, N., & Weinberg, M. D. 2003, *ApJS*, 149, 289

Bell, E. F., Wolf, C., Meisenheimer, K., et al. 2004, *ApJ*, 608, 752

Bell, E. F., van der Wel, A., Papovich, C., et al. 2012, *ApJ*, 753, 167

Benson, A. J. 2014, *MNRAS*, 444, 2599

Benson, A. J., & Bower, R. 2010, *MNRAS*, 405, 1573

Benson, A. J., Bower, R. G., Frenk, C. S., et al. 2003, *ApJ*, 599, 38

Bentz, M. C., & Katz, S. 2015, *PASP*, 127, 67

Berger, M. J., & Colella, P. 1989, Journal of Computational Physics, 82, 64

Berton, M., Foschini, L., Ciroi, S., et al. 2015, *A&A*, 578, A28

Berton, M., Congiu, E., Järvelä, E., et al. 2018, *A&A*, 614, A87

Binney, J. 1977, *ApJ*, 215, 483

Birnboim, Y., & Dekel, A. 2003, *MNRAS*, 345, 349

Birnboim, Y., Dekel, A., & Neistein, E. 2007, *MNRAS*, 380, 339

Birrer, S., Lilly, S., Amara, A., Paranjape, A., & Refregier, A. 2014, *ApJ*, 793, 12

Bîrzan, L., McNamara, B. R., Nulsen, P. E. J., Carilli, C. L., & Wise, M. W. 2008, *ApJ*, 686, 859

Bîrzan, L., Rafferty, D. A., McNamara, B. R., Wise, M. W., & Nulsen, P. E. J. 2004, *ApJ*, 607, 800

Blandford, R. D., & Begelman, M. C. 1999, *MNRAS*, 303, L1

Blandford, R. D., & McKee, C. F. 1982, *ApJ*, 255, 419

Blandford, R. D., & Znajek, R. L. 1977, *MNRAS*, 179, 433

Blanton, E. L., Randall, S. W., Douglass, E. M., et al. 2009, *ApJ*, 697, L95

Blanton, M. R., & Roweis, S. 2007, *AJ*, 133, 734

Bluck, A. F. L., Ellison, S. L., Patton, D. R., et al. 2014a, ArXiv e-prints, arXiv:1412.3862

Bluck, A. F. L., Mendel, J. T., Ellison, S. L., et al. 2014b, *MNRAS*, 441, 599

—. 2016, *MNRAS*, 462, 2559

Bluck, A. F. L., Bottrell, C., Teimoorinia, H., et al. 2019, *MNRAS*, 485, 666

Blumenthal, G. R., Faber, S. M., Primack, J. R., & Rees, M. J. 1984, *Nature*, 311, 517

Boehringer, H., Voges, W., Fabian, A. C., Edge, A. C., & Neumann, D. M. 1993, *MNRAS*, 264, L25

Böhringer, H., Matsushita, K., Churazov, E., Ikebe, Y., & Chen, Y. 2002, *A&A*, 382, 804

Bond, J. R., Cole, S., Efstathiou, G., & Kaiser, N. 1991, *ApJ*, 379, 440

Bondi, H. 1952, *MNRAS*, 112, 195

Bondi, H., & Hoyle, F. 1944, *MNRAS*, 104, 273

Booth, C. M., & Schaye, J. 2009, *MNRAS*, 398, 53

—. 2011, *MNRAS*, 413, 1158

Borch, A., Meisenheimer, K., Bell, E. F., et al. 2006, *A&A*, 453, 869

Bouché, N., Dekel, A., Genzel, R., et al. 2010, *ApJ*, 718, 1001

Bournaud, F., Jog, C. J., & Combes, F. 2007, *A&A*, 476, 1179

Bourne, M. A., & Sijacki, D. 2017, *MNRAS*, 472, 4707

Bower, R. G. 1991, *MNRAS*, 248, 332

Bower, R. G., Benson, A. J., & Crain, R. A. 2012, *MNRAS*, 422, 2816

Bower, R. G., Benson, A. J., Malbon, R., et al. 2006, *MNRAS*, 370, 645

Bower, R. G., Schaye, J., Frenk, C. S., et al. 2017, *MNRAS*, 465, 32

Bower, R. G., Vernon, I., Goldstein, M., et al. 2010, *MNRAS*, 407, 2017

Boylan-Kolchin, M., Springel, V., White, S. D. M., Jenkins, A., & Lemson, G. 2009, *MNRAS*, 398, 1150

Brammer, G. B., Whitaker, K. E., van Dokkum, P. G., et al. 2009, *ApJ*, 706, L173

—. 2011, *ApJ*, 739, 24

Brennan, R., Choi, E., Somerville, R. S., et al. 2018, *ApJ*, 860, 14

Bridge, C. R., Appleton, P. N., Conselice, C. J., et al. 2007, *ApJ*, 659, 931

Brinchmann, J., Charlot, S., White, S. D. M., et al. 2004, *MNRAS*, 351, 1151

Brinchmann, J., & Ellis, R. S. 2000, *ApJ*, 536, L77

Brown, M. J. I., Dey, A., Jannuzi, B. T., et al. 2007, *ApJ*, 654, 858

Brown, R. H., & Hazard, C. 1959, *MNRAS*, 119, 297

Brüggen, M., & Kaiser, C. R. 2002, *Nature*, 418, 301

Brüggen, M., Kaiser, C. R., Churazov, E., & Enßlin, T. A. 2002, *MNRAS*, 331, 545

Bryan, G. L., Norman, M. L., O'Shea, B. W., et al. 2014, *ApJS*, 211, 19

Burbidge, G. R., & Burbidge, E. M. 1969, *Nature*, 222, 735

Burbidge, G. R., & Hoyle, F. 1963, *ApJ*, 138, 57

Burbidge, G. R., & O'dell, S. L. 1972, *ApJ*, 178, 583

Cattaneo, A., Dekel, A., Devriendt, J., Guiderdoni, B., & Blaizot, J. 2006a, *MNRAS*, 370, 1651

—. 2006b, *MNRAS*, 370, 1651

Cattaneo, A., Faber, S. M., Binney, J., et al. 2009, *Nature*, 460, 213

Chabrier, G. 2003, *PASP*, 115, 763

Chang, Y.-Y., van der Wel, A., da Cunha, E., & Rix, H.-W. 2015, *ApJS*, 219, 8

Cheung, E., Faber, S. M., Koo, D. C., et al. 2012, *ApJ*, 760, 131

Cheung, E., Bundy, K., Cappellari, M., et al. 2016, *Nature*, 533, 504

Choi, E., Ostriker, J. P., Naab, T., & Johansson, P. H. 2012, *ApJ*, 754, 125

Choi, E., Ostriker, J. P., Naab, T., Oser, L., & Moster, B. P. 2015, *MNRAS*, 449, 4105

Choi, E., Ostriker, J. P., Naab, T., et al. 2017, *ApJ*, 844, 31

Choi, E., Somerville, R. S., Ostriker, J. P., Naab, T., & Hirschmann, M. 2018, *ApJ*, 866, 91

Christensen, C. G. 1975, *AJ*, 80, 282

Christensen, C. R., Davé, R., Governato, F., et al. 2016, *ApJ*, 824, 57

Churazov, E., Brüggen, M., Kaiser, C. R., Böhringer, H., & Forman, W. 2001, *ApJ*, 554, 261

Cicone, C., Maiolino, R., Sturm, E., et al. 2014, *A&A*, 562, A21

Ciotti, L., & Ostriker, J. P. 2001, *ApJ*, 551, 131

Cisternas, M., Jahnke, K., Bongiorno, A., et al. 2011, *ApJ*, 741, L11

Cole, S. 1991, *ApJ*, 367, 45

Cole, S., Norberg, P., Baugh, C. M., et al. 2001, *MNRAS*, 326, 255

Colless, M., Dalton, G., Maddox, S., et al. 2001, *MNRAS*, 328, 1039

Conroy, C., van Dokkum, P. G., & Kravtsov, A. 2015, *ApJ*, 803, 77

Conroy, C., & Wechsler, R. H. 2009, *ApJ*, 696, 620

Conroy, C., Wechsler, R. H., & Kravtsov, A. V. 2006, *ApJ*, 647, 201

Contreras, S., Baugh, C. M., Norberg, P., & Padilla, N. 2013, *MNRAS*, 432, 2717

—. 2015, *MNRAS*, 452, 1861

Cox, D. P. 1983, *ApJ*, 265, L61

Coziol, R., Andernach, H., Torres-Papaqui, J. P., Ortega-Minakata, R. A., & Moreno del Rio, F. 2017, *MNRAS*, 466, 921

Crenshaw, D. M., Schmitt, H. R., Kraemer, S. B., Mushotzky, R. F., & Dunn, J. P. 2010, *ApJ*, 708, 419

Crocker, A. F., Bureau, M., Young, L. M., & Combes, F. 2011, *MNRAS*, 410, 1197

Crommelin, A. C. D. 1918, Journal of the Royal Astronomical Society of Canada, 12, 33

Croton, D. J., Springel, V., White, S. D. M., et al. 2006, *MNRAS*, 365, 11

Curtis, H. D. 1920, Journal of the Royal Astronomical Society of Canada, 14, 317

Dale, D. A., Cohen, S. A., Johnson, L. C., et al. 2009, *ApJ*, 703, 517

Davé, R., Finlator, K., & Oppenheimer, B. D. 2012, *MNRAS*, 421, 98

David, L. P., Jones, C., Forman, W., et al. 2009, *ApJ*, 705, 624

Davies, J. J., Crain, R. A., McCarthy, I. G., et al. 2019, *MNRAS*, 485, 3783

Davis, B. L., Graham, A. W., & Cameron, E. 2018, *ApJ*, 869, 113

De Lucia, G., & Blaizot, J. 2007a, *MNRAS*, 375, 2

—. 2007b, *MNRAS*, 375, 2

De Lucia, G., Kauffmann, G., & White, S. D. M. 2004, *MNRAS*, 349, 1101

Dekel, A., & Birnboim, Y. 2006, *MNRAS*, 368, 2

Dekel, A., & Silk, J. 1986, *ApJ*, 303, 39

Dekel, A., Birnboim, Y., Engel, G., et al. 2009, *Nature*, 457, 451

Di Matteo, T., Khandai, N., DeGraf, C., et al. 2012, *ApJ*, 745, L29

Di Matteo, T., Springel, V., & Hernquist, L. 2005, *Nature*, 433, 604

Dickey, C., Geha, M., Wetzel, A., & El-Badry, K. 2019, arXiv e-prints, arXiv:1902.01401

Donahue, M., Mack, J., Voit, G. M., et al. 2000, *ApJ*, 545, 670

Donnari, M., Pillepich, A., Nelson, D., et al. 2019, *MNRAS*, 485, 4817

Dopita, M. A. 1985, *ApJ*, 295, L5

Dos Santos, P. M., & Lepine, J. R. D. 1979, *Nature*, 278, 34

Dressler, A. 1980, *ApJ*, 236, 351

—. 1984, *ApJ*, 286, 97

Dressler, A., & Richstone, D. O. 1988, *ApJ*, 324, 701

Driver, S. P., Norberg, P., Baldry, I. K., et al. 2009, Astronomy and Geophysics, 50, 5.12

Dubois, Y., Gavazzi, R., Peirani, S., & Silk, J. 2013, *MNRAS*, 433, 3297

Dubois, Y., Peirani, S., Pichon, C., et al. 2016, *MNRAS*, 463, 3948

Durkalec, A., Le Fèvre, O., de la Torre, S., et al. 2015, *A&A*, 576, L7

Dutton, A. A., van den Bosch, F. C., & Dekel, A. 2010, *MNRAS*, 405, 1690

Dye, S., Warren, S. J., Hambly, N. C., et al. 2006, *MNRAS*, 372, 1227

Eales, S., de Vis, P., W. L. Smith, M., et al. 2017, *MNRAS*, 465, 3125

Event Horizon Telescope Collaboration, Akiyama, K., Alberdi, A., et al. 2019, *ApJ*, 875, L1

Evrard, A. E. 1988, *MNRAS*, 235, 911

—. 1990, *ApJ*, 363, 349

Evrard, A. E., Summers, F. J., & Davis, M. 1994, *ApJ*, 422, 11

Faber, S. M., Willmer, C. N. A., Wolf, C., et al. 2007, *ApJ*, 665, 265

Fabian, A. C. 1994, *ARA&A*, 32, 277

—. 2012, *ARA&A*, 50, 455

Fabian, A. C., Nulsen, P. E. J., & Canizares, C. R. 1982, *MNRAS*, 201, 933

Fabian, A. C., Reynolds, C. S., Taylor, G. B., & Dunn, R. J. H. 2005, *MNRAS*, 363, 891

Fall, S. M., & Efstathiou, G. 1980, *MNRAS*, 193, 189

Fang, J. J., Faber, S. M., Koo, D. C., & Dekel, A. 2013, *ApJ*, 776, 63

Ferrarese, L., & Merritt, D. 2000, *ApJ*, 539, L9

Flynn, C., Holmberg, J., Portinari, L., Fuchs, B., & Jahreiß, H. 2006, *MNRAS*, 372, 1149

Ford, G. P., Gear, W. K., Smith, M. W. L., et al. 2013, *ApJ*, 769, 55

Forman, W., Kellogg, E., Gursky, H., Tananbaum, H., & Giacconi, R. 1972, *ApJ*, 178, 309

Franx, M., van Dokkum, P. G., Förster Schreiber, N. M., et al. 2008a, *ApJ*, 688, 770

Franx, M., van Dokkum, P. G., Schreiber, N. M. F., et al. 2008b, *ApJ*, 688, 770

Frenk, C. S., White, S. D. M., Efstathiou, G., & Davis, M. 1990, *ApJ*, 351, 10

Fryxell, B., Olson, K., Ricker, P., et al. 2000, *ApJS*, 131, 273

Furlong, M., Bower, R. G., Theuns, T., et al. 2015, *MNRAS*, 450, 4486

Gabor, J. M., & Davé, R. 2015, *MNRAS*, 447, 374

Gallo, E., Treu, T., Jacob, J., et al. 2008, *ApJ*, 680, 154

Gao, Y., & Solomon, P. M. 1999, *ApJ*, 512, L99

Gaspari, M., Brighenti, F., D'Ercole, A., & Melioli, C. 2011, *MNRAS*, 415, 1549

Gaspari, M., Brighenti, F., & Temi, P. 2012, *MNRAS*, 424, 190

Gebhardt, K., Bender, R., Bower, G., et al. 2000, *ApJ*, 539, L13

Geha, M., Blanton, M. R., Yan, R., & Tinker, J. L. 2012, *ApJ*, 757, 85

Genel, S., Vogelsberger, M., Springel, V., et al. 2014, *MNRAS*, 445, 175

Gerhard, O. E. 1981, *MNRAS*, 197, 179

Ghez, A. M., Klein, B. L., Morris, M., & Becklin, E. E. 1998, *ApJ*, 509, 678

Ghez, A. M., Salim, S., Weinberg, N. N., et al. 2008, *ApJ*, 689, 1044

Gingold, R. A., & Monaghan, J. J. 1977, *MNRAS*, 181, 375

Gitti, M., O'Sullivan, E., Giacintucci, S., et al. 2010, *ApJ*, 714, 758

Gladders, M. D., López-Cruz, O., Yee, H. K. C., & Kodama, T. 1998, *ApJ*, 501, 571

Gonçalves, T. S., Martin, D. C., Menéndez-Delmestre, K., Wyder, T. K., & Koekemoer, A. 2012, *ApJ*, 759, 67

Gott, III, J. R., & Turner, E. L. 1976, *ApJ*, 209, 1

Graham, A. W., Erwin, P., Caon, N., & Trujillo, I. 2001, *ApJ*, 563, L11

Greene, J. E., Peng, C. Y., Kim, M., et al. 2010, *ApJ*, 721, 26

Grogin, N. A., Kocevski, D. D., Faber, S. M., et al. 2011, *ApJS*, 197, 35

Gull, S. F., & Northover, K. J. E. 1973, *Nature*, 244, 80

Gültekin, K., Richstone, D. O., Gebhardt, K., et al. 2009, *ApJ*, 698, 198

Gunn, J. E., & Gott, J. Richard, I. 1972, *ApJ*, 176, 1

Guo, F., & Mathews, W. G. 2012, *ApJ*, 756, 181

Guo, F., & Oh, S. P. 2008, *MNRAS*, 384, 251

Guo, Q., Cooper, A. P., Frenk, C., Helly, J., & Hellwing, W. A. 2015, *MNRAS*, 454, 550

Guo, Q., White, S., Li, C., & Boylan-Kolchin, M. 2010, *MNRAS*, 404, 1111

Guo, Q., White, S., Boylan-Kolchin, M., et al. 2011, *MNRAS*, 413, 101

Gursky, H., Kellogg, E., Murray, S., et al. 1971, *ApJ*, 167, L81

Habouzit, M., Volonteri, M., & Dubois, Y. 2017, *MNRAS*, 468, 3935

Habouzit, M., Genel, S., Somerville, R. S., et al. 2019, *MNRAS*, 484, 4413

Häring, N., & Rix, H.-W. 2004, *ApJ*, 604, L89

Harrison, C. M., Alexander, D. M., Mullaney, J. R., & Swinbank, A. M. 2014, *MNRAS*, 441, 3306

Hatton, S., Devriendt, J. E. G., Ninin, S., et al. 2003, *MNRAS*, 343, 75

Hayward, C. C., & Hopkins, P. F. 2017, *MNRAS*, 465, 1682

Hearin, A. P., Watson, D. F., & van den Bosch, F. C. 2015, *MNRAS*, 452, 1958

Heckman, T. M., Armus, L., & Miley, G. K. 1990, *ApJS*, 74, 833

Heckman, T. M., & Best, P. N. 2014, *ARA&A*, 52, 589

Heckman, T. M., Miley, G. K., van Breugel, W. J. M., & Butcher, H. R. 1981, *ApJ*, 247, 403

Helly, J. C., Cole, S., Frenk, C. S., et al. 2003, *MNRAS*, 338, 903

Henriques, B. M. B., & Thomas, P. A. 2010, *MNRAS*, 403, 768

Henriques, B. M. B., Thomas, P. A., Oliver, S., & Roseboom, I. 2009, *MNRAS*, 396, 535

Henriques, B. M. B., White, S. D. M., Lilly, S. J., et al. 2019a, *MNRAS*, 485, 3446

—. 2019b, *MNRAS*, 485, 3446

Henriques, B. M. B., White, S. D. M., Thomas, P. A., et al. 2015, *MNRAS*, 451, 2663

—. 2013, *MNRAS*, 431, 3373

Hernquist, L. 1992, *ApJ*, 400, 460

Hernquist, L., & Katz, N. 1989, *ApJS*, 70, 419

Hernquist, L., & Quinn, P. J. 1988, *ApJ*, 331, 682

Hernquist, L., & Spergel, D. N. 1992, *ApJ*, 399, L117

Hlavacek-Larrondo, J., McDonald, M., Benson, B. A., et al. 2015, *ApJ*, 805, 35

Holden, B. P., Stanford, S. A., Eisenhardt, P., & Dickinson, M. 2004, *AJ*, 127, 2484

Hopkins, P. F. 2015, *MNRAS*, 450, 53

—. 2017, arXiv e-prints, arXiv:1712.01294

Hopkins, P. F., Hernquist, L., Cox, T. J., et al. 2006, *ApJS*, 163, 1

Hopkins, P. F., & Quataert, E. 2011, *MNRAS*, 415, 1027

Hopkins, P. F., Quataert, E., & Murray, N. 2011, *MNRAS*, 417, 950

—. 2012, *MNRAS*, 421, 3522

Hoyle, F., & Lyttleton, R. A. 1939, Proceedings of the Cambridge Philosophical Society, 35, 592

Hoyle, F., Wickramasinghe, N. C., & Reddish, V. C. 1968, *Nature*, 218, 1124

Hubble, E. 1936, *ApJ*, 84, 158

Hubble, E. P. 1925, The Observatory, 48, 139

—. 1926, *ApJ*, 64, doi:10.1086/143018

Huchra, J., & Sargent, W. L. W. 1973, *ApJ*, 186, 433

Huchra, J. P., Macri, L. M., Masters, K. L., et al. 2012, *ApJS*, 199, 26

Hudson, M. J., Harris, G. L., & Harris, W. E. 2014, *ApJ*, 787, L5

Ichimaru, S. 1977, *ApJ*, 214, 840

Icke, V. 1985, *A&A*, 144, 115

Ilbert, O., Salvato, M., Le Floc'h, E., et al. 2010, *ApJ*, 709, 644

Ilbert, O., McCracken, H. J., Le Fèvre, O., et al. 2013, *A&A*, 556, A55

Jennison, R. C., & Das Gupta, M. K. 1953, *Nature*, 172, 996

Johansson, P. H., Naab, T., & Ostriker, J. P. 2009, *ApJ*, 697, L38

Johnstone, R. M., Fabian, A. C., & Nulsen, P. E. J. 1987, *MNRAS*, 224, 75

Jones, D. H., Saunders, W., Colless, M., et al. 2004, *MNRAS*, 355, 747

Joseph, R. D., & Wright, G. S. 1985, *MNRAS*, 214, 87

Kampakoglou, M., Trotta, R., & Silk, J. 2008, *MNRAS*, 384, 1414

Kang, X., Jing, Y. P., Mo, H. J., & Börner, G. 2005, *ApJ*, 631, 21

Kang, Y., Bianchi, L., & Rey, S.-C. 2009, *ApJ*, 703, 614

Katz, N., & Gunn, J. E. 1991, *ApJ*, 377, 365

Katz, N., Hernquist, L., & Weinberg, D. H. 1992, *ApJ*, 399, L109

Katz, N., Weinberg, D. H., & Hernquist, L. 1996, *ApJS*, 105, 19

Katz, N., & White, S. D. M. 1993, *ApJ*, 412, 455

Kauffmann, G., Colberg, J. M., Diaferio, A., & White, S. D. M. 1999, *MNRAS*, 303, 188

Kauffmann, G., & Haehnelt, M. 2000, *MNRAS*, 311, 576

Kauffmann, G., Heckman, T. M., White, S. D. M., et al. 2003, *MNRAS*, 341, 33

Kennicutt, R. C., & Evans, N. J. 2012, *ARA&A*, 50, 531

Kennicutt, Jr., R. C. 1998, *ARA&A*, 36, 189

Kereš, D., Katz, N., Weinberg, D. H., & Davé, R. 2005, *MNRAS*, 363, 2

Khandai, N., Di Matteo, T., Croft, R., et al. 2015, *MNRAS*, 450, 1349

Kiang, T. 1961, *MNRAS*, 122, 263

King, A. 2003, *ApJ*, 596, L27

Klypin, A. A., Trujillo-Gomez, S., & Primack, J. 2011, *ApJ*, 740, 102

Knapp, G. R., Guhathakurta, P., Kim, D.-W., & Jura, M. A. 1989, *ApJS*, 70, 329

Knebe, A., Pearce, F. R., Thomas, P. A., et al. 2015, *MNRAS*, 451, 4029

Koekemoer, A. M., Faber, S. M., Ferguson, H. C., et al. 2011, *ApJS*, 197, 36

Komossa, S., Voges, W., Xu, D., et al. 2006, *AJ*, 132, 531

Kormendy, J. 1988, *ApJ*, 335, 40

Kormendy, J., & Ho, L. C. 2013, *ARA&A*, 51, 511

Kormendy, J., & Kennicutt, Jr., R. C. 2004, *ARA&A*, 42, 603

Kormendy, J., & Richstone, D. 1995, *ARA&A*, 33, 581

Krause, E., Hirata, C. M., Martin, C., Neill, J. D., & Wyder, T. K. 2013, *MNRAS*, 428, 2548

Kravtsov, A. V., Berlind, A. A., Wechsler, R. H., et al. 2004, *ApJ*, 609, 35

Kravtsov, A. V., Klypin, A. A., & Khokhlov, A. M. 1997, *ApJS*, 111, 73

Lambas, D. G., Tissera, P. B., Alonso, M. S., & Coldwell, G. 2003, *MNRAS*, 346, 1189

Lang, P., Wuyts, S., Somerville, R. S., et al. 2014, *ApJ*, 788, 11

Lanzetta, K. M., Wolfe, A. M., & Turnshek, D. A. 1995, *ApJ*, 440, 435

Lapi, A., Mancuso, C., Bressan, A., & Danese, L. 2017, *ApJ*, 847, 13

Larson, R. B., & Tinsley, B. M. 1978, *ApJ*, 219, 46

Leauthaud, A., Tinker, J., Bundy, K., et al. 2012, *ApJ*, 744, 159

Leavitt, H. S. 1908, Annals of Harvard College Observatory, 60, 87

Leavitt, H. S., & Pickering, E. C. 1912, Harvard College Observatory Circular, 173, 1

Leja, J., van Dokkum, P., & Franx, M. 2013, *ApJ*, 766, 33

Lemson, G., & Virgo Consortium, t. 2006, ArXiv Astrophysics e-prints, astro-ph/0608019

Lewis, A. R., Dolphin, A. E., Dalcanton, J. J., et al. 2015, *ApJ*, 805, 183

Li, C., & White, S. D. M. 2009, *MNRAS*, 398, 2177

Lian, J., Yan, R., Zhang, K., & Kong, X. 2016, *ApJ*, 832, 29

Lilly, S. J., Le Fevre, O., Crampton, D., Hammer, F., & Tresse, L. 1995, *ApJ*, 455, 50

Lin, Y.-T., Mohr, J. J., & Stanford, S. A. 2003, *ApJ*, 591, 749

Lu, Y., Mo, H. J., Katz, N., & Weinberg, M. D. 2012, *MNRAS*, 421, 1779

Lu, Y., Mo, H. J., Weinberg, M. D., & Katz, N. 2011, *MNRAS*, 416, 1949

Lynden-Bell, D. 1969, *Nature*, 223, 690

Lynden-Bell, D., & Rees, M. J. 1971, *MNRAS*, 152, 461

Madau, P., & Dickinson, M. 2014, *ARA&A*, 52, 415

Magorrian, J., Tremaine, S., Richstone, D., et al. 1998, *AJ*, 115, 2285

Maltby, P., & Moffet, A. T. 1962, *ApJS*, 7, 141

Man, A. W. S., Greve, T. R., Toft, S., et al. 2016, *ApJ*, 820, 11

Mandelbaum, R., Wang, W., Zu, Y., et al. 2016a, *MNRAS*, 457, 3200

—. 2016b, *MNRAS*, 457, 3200

Marchesini, D., van Dokkum, P. G., Förster Schreiber, N. M., et al. 2009, *ApJ*, 701, 1765

Marinacci, F., Vogelsberger, M., Pakmor, R., et al. 2018, *MNRAS*, 480, 5113

Martig, M., Bournaud, F., Teyssier, R., & Dekel, A. 2009, *ApJ*, 707, 250

Martin, D. C., Fanson, J., Schiminovich, D., et al. 2005, *ApJ*, 619, L1

Martin, D. C., Wyder, T. K., Schiminovich, D., et al. 2007, *ApJS*, 173, 342

Martín-Navarro, I., Brodie, J. P., Romanowsky, A. J., Ruiz-Lara, T., & van de Ven, G. 2018, *Nature*, 553, 307

Martín-Navarro, I., Brodie, J. P., van den Bosch, R. C. E., Romanowsky, A. J., & Forbes, D. A. 2016, ArXiv e-prints, arXiv:1609.05899

Mathews, W. G., & Baker, J. C. 1971, *ApJ*, 170, 241

Mathews, W. G., & Brighenti, F. 2003, *ARA&A*, 41, 191

McAlpine, S., Bower, R. G., Harrison, C. M., et al. 2017, *MNRAS*, 468, 3395

McCarthy, I. G., Schaye, J., Bird, S., & Le Brun, A. M. C. 2017, *MNRAS*, 465, 2936

McCarthy, I. G., Schaye, J., Ponman, T. J., et al. 2010, *MNRAS*, 406, 822

McConnell, N. J., & Ma, C.-P. 2013, *ApJ*, 764, 184

McCracken, H. J., Milvang-Jensen, B., Dunlop, J., et al. 2012, *A&A*, 544, A156

McDonald, M., Gaspari, M., McNamara, B. R., & Tremblay, G. R. 2018, *ApJ*, 858, 45

McGlynn, T. A. 1984, *ApJ*, 281, 13

McKee, C. F., & Ostriker, J. P. 1977, *ApJ*, 218, 148

McMillan, P. J. 2011, *MNRAS*, 414, 2446

McNamara, B. R., & Nulsen, P. E. J. 2007, *ARA&A*, 45, 117

Mendez, A. J., Coil, A. L., Lotz, J., et al. 2011, *ApJ*, 736, 110

Mihos, J. C., & Hernquist, L. 1996, *ApJ*, 464, 641

Miley, G. 1980, *ARA&A*, 18, 165

Miyoshi, M., Moran, J., Herrnstein, J., et al. 1995, *Nature*, 373, 127

Moore, B., Ghigna, S., Governato, F., et al. 1999, *ApJ*, 524, L19

Morishita, T., Ichikawa, T., Noguchi, M., et al. 2015, *ApJ*, 805, 34

Morris, S. L., Weymann, R. J., Dressler, A., et al. 1993, *ApJ*, 419, 524

Mortlock, A., Conselice, C. J., Bluck, A. F. L., et al. 2011, *MNRAS*, 413, 2845

Mortlock, A., Conselice, C. J., Hartley, W. G., et al. 2015, *MNRAS*, 447, 2

Moshir, M., & et al. 1990, in IRAS Faint Source Catalogue, version 2.0 (1990)

Moster, B. P., Naab, T., & White, S. D. M. 2013, *MNRAS*, 428, 3121

Moster, B. P., Somerville, R. S., Maulbetsch, C., et al. 2010, *ApJ*, 710, 903

Moustakas, J., Coil, A. L., Aird, J., et al. 2013, *ApJ*, 767, 50

Mukherjee, D., Bicknell, G. V., Wagner, A. Y., Sutherland, R. S., & Silk, J. 2018, *MNRAS*, 479, 5544

Muratov, A. L., Kereš, D., Faucher-Giguère, C.-A., et al. 2015, *MNRAS*, 454, 2691

Mutch, S. J., Poole, G. B., & Croton, D. J. 2013, *MNRAS*, 428, 2001

Muzzin, A., Marchesini, D., Stefanon, M., et al. 2013, *ApJ*, 777, 18

Naab, T., & Burkert, A. 2003, *ApJ*, 597, 893

Naiman, J. P., Pillepich, A., Springel, V., et al. 2018, *MNRAS*, 477, 1206

Navarro, J. F., & White, S. D. M. 1993, *MNRAS*, 265, 271

Negroponte, J., & White, S. D. M. 1983, *MNRAS*, 205, 1009

Nelson, D., Pillepich, A., Springel, V., et al. 2018a, *MNRAS*, 475, 624

Nelson, D., Kauffmann, G., Pillepich, A., et al. 2018b, *MNRAS*, 477, 450

Nelson, D., Pillepich, A., Springel, V., et al. 2019, arXiv e-prints, arXiv:1902.05554

Newman, J. A., Cooper, M. C., Davis, M., et al. 2013, *ApJS*, 208, 5

Norman, M. L., Wilson, J. R., & Barton, R. T. 1980, *ApJ*, 239, 968

O'Dea, C. P., Baum, S. A., Mack, J., Koekemoer, A. M., & Laor, A. 2004, *ApJ*, 612, 131

Oemler, Jr., A. 1974, *ApJ*, 194, 1

Oemler, Jr, A., Abramson, L. E., Gladders, M. D., et al. 2016, ArXiv e-prints, arXiv:1611.05932

Oppenheimer, B. D., & Davé, R. 2008, *MNRAS*, 387, 577

Oppenheimer, B. D., Davé, R., Kereš, D., et al. 2010, *MNRAS*, 406, 2325

Oppenheimer, B. D., Davies, J. J., Crain, R. A., et al. 2019, arXiv e-prints, arXiv:1904.05904

O'Shea, B. W., Bryan, G., Bordner, J., et al. 2004, ArXiv Astrophysics e-prints, astro-ph/0403044

Ostriker, J. P., & Tremaine, S. D. 1975, *ApJ*, 202, L113

Page, M. J., Symeonidis, M., Vieira, J. D., et al. 2012, *Nature*, 485, 213

Pakmor, R., Bauer, A., & Springel, V. 2011, *MNRAS*, 418, 1392

Pakmor, R., Springel, V., Bauer, A., et al. 2016, *MNRAS*, 455, 1134

Pan, Z., Li, J., Lin, W., Wang, J., & Kong, X. 2014, *ApJ*, 792, L4

Pandya, V., Brennan, R., Somerville, R. S., et al. 2016, ArXiv e-prints, arXiv:1611.03869

Papovich, C., Finkelstein, S. L., Ferguson, H. C., Lotz, J. M., & Giavalisco, M. 2011, *MNRAS*, 412, 1123

Papovich, C., Labbé, I., Quadri, R., et al. 2015, *ApJ*, 803, 26

Patel, S. G., van Dokkum, P. G., Franx, M., et al. 2013a, *ApJ*, 766, 15

Patel, S. G., Fumagalli, M., Franx, M., et al. 2013b, *ApJ*, 778, 115

Peebles, P. J. E. 1970, *AJ*, 75, 13

—. 1982, *ApJ*, 263, L1

Peng, Y.-j., & Maiolino, R. 2014, *MNRAS*, 443, 3643

Peng, Y.-j., Lilly, S. J., Kovač, K., et al. 2010, *ApJ*, 721, 193

Penny, S. J., Masters, K. L., Smethurst, R., et al. 2018, *MNRAS*, 476, 979

Pillepich, A., Springel, V., Nelson, D., et al. 2018, *MNRAS*, 473, 4077

Planck Collaboration, Ade, P. A. R., Aghanim, N., et al. 2014, *A&A*, 571, A16

—. 2016, *A&A*, 594, A13

Pontzen, A., Tremmel, M., Roth, N., et al. 2017, *MNRAS*, 465, 547

Porter, L. A., Somerville, R. S., Primack, J. R., & Johansson, P. H. 2014, *MNRAS*, 444, 942

Prochaska, J. X., Chen, H.-W., Howk, J. C., Weiner, B. J., & Mulchaey, J. 2004, *ApJ*, 617, 718

Pujol, A., & Gaztañaga, E. 2014, *MNRAS*, 442, 1930

Rafferty, D. A., McNamara, B. R., Nulsen, P. E. J., & Wise, M. W. 2006, *ApJ*, 652, 216

Randall, S. W., Forman, W. R., Giacintucci, S., et al. 2011, *ApJ*, 726, 86

Reddish, V. C. 1969, *MNRAS*, 145, 357

Rees, M. J., & Ostriker, J. P. 1977, *MNRAS*, 179, 541

Reines, A. E., Greene, J. E., & Geha, M. 2013, *ApJ*, 775, 116

Reines, A. E., & Volonteri, M. 2015, *ApJ*, 813, 82

Rice, W., Lonsdale, C. J., Soifer, B. T., et al. 1988, *ApJS*, 68, 91

Rieke, G. H., & Rieke, M. J. 1988, *ApJ*, 330, L33

Rix, H.-W., & Rieke, M. J. 1993, *ApJ*, 418, 123

Roos, O., Juneau, S., Bournaud, F., & Gabor, J. M. 2015, *ApJ*, 800, 19

Roychowdhury, S., Ruszkowski, M., Nath, B. B., & Begelman, M. C. 2004, *ApJ*, 615, 681

Rubin, V. C., Ford, Jr., W. K., & Thonnard, N. 1978, *ApJ*, 225, L107

—. 1980, *ApJ*, 238, 471

Ruiz, A. N., Cora, S. A., Padilla, N. D., et al. 2015, *ApJ*, 801, 139

Rupke, D. S. N., Gültekin, K., & Veilleux, S. 2017, *ApJ*, 850, 40

Saglia, R. P., Opitsch, M., Erwin, P., et al. 2016, *ApJ*, 818, 47

Sahu, N., Graham, A. W., & Davis, B. L. 2019, arXiv e-prints, arXiv:1903.04738

Salim, S., Rich, R. M., Charlot, S., et al. 2007, *ApJS*, 173, 267

Salpeter, E. E. 1964, *ApJ*, 140, 796

Sanders, D. B., Soifer, B. T., Elias, J. H., et al. 1988, *ApJ*, 325, 74

Sanders, R. H. 1981, *ApJ*, 244, 820

Sargent, W. L. W., Young, P. J., Boksenberg, A., et al. 1978, *ApJ*, 221, 731

Savorgnan, G. A. D., Graham, A. W., Marconi, A., & Sani, E. 2015, ArXiv e-prints, arXiv:1511.07437

Schawinski, K., Urry, C. M., Simmons, B. D., et al. 2014, *MNRAS*, 440, 889

Schaye, J., & Dalla Vecchia, C. 2008, *MNRAS*, 383, 1210

Schaye, J., Dalla Vecchia, C., Booth, C. M., et al. 2010, *MNRAS*, 402, 1536

Schaye, J., Crain, R. A., Bower, R. G., et al. 2015, *MNRAS*, 446, 521

Schechter, P. 1976, *ApJ*, 203, 297

Schiminovich, D., Wyder, T. K., Martin, D. C., et al. 2007, *ApJS*, 173, 315

Schiminovich, D., Catinella, B., Kauffmann, G., et al. 2010, *MNRAS*, 408, 919

Schmidt, M. 1959, *ApJ*, 129, 243

—. 1963, *Nature*, 197, 1040

Scoville, N., Aussel, H., Brusa, M., et al. 2007, *ApJS*, 172, 1

Searle, L., Sargent, W. L. W., & Bagnuolo, W. G. 1973, *ApJ*, 179, 427

Sellgren, K., Hall, D. N. B., Kleinmann, S. G., & Scoville, N. Z. 1987, *ApJ*, 317, 881

Serjeant, S., & Hatziminaoglou, E. 2009, *MNRAS*, 397, 265

Sérsic, J. L. 1963, Boletin de la Asociacion Argentina de Astronomia La Plata Argentina, 6, 41

Shakura, N. I., & Sunyaev, R. A. 1973, *A&A*, 24, 337

Shankar, F., Bernardi, M., Sheth, R. K., et al. 2016, *MNRAS*, 460, 3119

Shapiro, S. L. 1971, *AJ*, 76, 291

Shapley, H. 1919, Journal of the Royal Astronomical Society of Canada, 13, 438

Shapley, H., & Curtis, H. D. 1921, Bulletin of the National Research Council, 2, 171

Shin, J., Woo, J.-H., & Mulchaey, J. S. 2016, ArXiv e-prints, arXiv:1610.03487

Shlosman, I., Vitello, P. A., & Shaviv, G. 1985, *ApJ*, 294, 96

Sijacki, D., Pfrommer, C., Springel, V., & Enßlin, T. A. 2008, *MNRAS*, 387, 1403

Sijacki, D., Springel, V., Di Matteo, T., & Hernquist, L. 2007, *MNRAS*, 380, 877

Sijacki, D., Vogelsberger, M., Genel, S., et al. 2015, *MNRAS*, 452, 575

Silk, J. 1977, *ApJ*, 211, 638

—. 2003, *MNRAS*, 343, 249

Silk, J., & Rees, M. J. 1998, *A&A*, 331, L1

Skrutskie, M. F., Cutri, R. M., Stiening, R., et al. 2006, *AJ*, 131, 1163

Smethurst, R. J., Lintott, C. J., Simmons, B. D., et al. 2015, *MNRAS*, 450, 435

Soltan, A. 1982, *MNRAS*, 200, 115

Somerville, R. S., & Davé, R. 2015, *ARA&A*, 53, 51

Somerville, R. S., Gilmore, R. C., Primack, J. R., & Domínguez, A. 2012, *MNRAS*, 423, 1992

Somerville, R. S., Hopkins, P. F., Cox, T. J., Robertson, B. E., & Hernquist, L. 2008, *MNRAS*, 391, 481

Somerville, R. S., & Primack, J. R. 1999, *MNRAS*, 310, 1087

Somerville, R. S., Primack, J. R., & Faber, S. M. 2001, *MNRAS*, 320, 504

Spergel, D. N., Verde, L., Peiris, H. V., et al. 2003, *ApJS*, 148, 175

Spitzer, Lyman, J. 1956, *ApJ*, 124, 20

Springel, V. 2005, *MNRAS*, 364, 1105

—. 2010, *MNRAS*, 401, 791

Springel, V., & Hernquist, L. 2002, *MNRAS*, 333, 649

—. 2003, *MNRAS*, 339, 289

Springel, V., White, S. D. M., Tormen, G., & Kauffmann, G. 2001a, *MNRAS*, 328, 726

Springel, V., Yoshida, N., & White, S. D. M. 2001b, New Astronomy, 6, 79

Springel, V., White, S. D. M., Jenkins, A., et al. 2005, *Nature*, 435, 629

Springel, V., Pakmor, R., Pillepich, A., et al. 2018, *MNRAS*, 475, 676

Stanford, S. A., Eisenhardt, P. R., & Dickinson, M. 1998, *ApJ*, 492, 461

Strateva, I., Ivezić, Ž., Knapp, G. R., et al. 2001, *AJ*, 122, 1861

Sturm, E., González-Alfonso, E., Veilleux, S., et al. 2011, *ApJ*, 733, L16

Su, K.-Y., Hopkins, P. F., Hayward, C. C., et al. 2018, arXiv e-prints, arXiv:1809.09120

Su, M., Slatyer, T. R., & Finkbeiner, D. P. 2010, *ApJ*, 724, 1044

Suginohara, T., & Ostriker, J. P. 1998, *ApJ*, 507, 16

Surace, J. A., Sanders, D. B., & Mazzarella, J. M. 2004, *AJ*, 127, 3235

Sutherland, R. S., & Dopita, M. A. 1993, *ApJS*, 88, 253

Tabor, G., & Binney, J. 1993, *MNRAS*, 263, 323

Tang, S., & Wang, Q. D. 2005, *ApJ*, 628, 205

Tasitsiomi, A., Kravtsov, A. V., Wechsler, R. H., & Primack, J. R. 2004, *ApJ*, 614, 533

Taylor, E. N., Hopkins, A. M., Baldry, I. K., et al. 2015, *MNRAS*, 446, 2144

Temi, P., Brighenti, F., & Mathews, W. G. 2009, *ApJ*, 707, 890

Terrazas, B. A., Bell, E. F., Henriques, B. M. B., & White, S. D. M. 2016a, *MNRAS*, 459, 1929

Terrazas, B. A., Bell, E. F., Henriques, B. M. B., et al. 2016b, ArXiv e-prints, arXiv:1609.07141

Terrazas, B. A., Bell, E. F., Woo, J., & Henriques, B. M. B. 2017, *ApJ*, 844, 170

Teyssier, R. 2002, *A&A*, 385, 337

Thomas, D., Maraston, C., Bender, R., & Mendes de Oliveira, C. 2005, *ApJ*, 621, 673

Tinker, J. L., Leauthaud, A., Bundy, K., et al. 2013, *ApJ*, 778, 93

Tinsley, B. M. 1968, *ApJ*, 151, 547

Tomczak, A. R., Quadri, R. F., Tran, K.-V. H., et al. 2014, *ApJ*, 783, 85

Tonry, J. L. 1984, *ApJ*, 283, 27

—. 1987, *ApJ*, 322, 632

Toomre, A. 1964, *ApJ*, 139, 1217

Toomre, A. 1977, in Evolution of Galaxies and Stellar Populations, ed. B. M. Tinsley & R. B. G. Larson, D. Campbell, 401

Toomre, A., & Toomre, J. 1972, *ApJ*, 178, 623

Torrey, P., Wellons, S., Machado, F., et al. 2015, *MNRAS*, 454, 2770

Trayford, J. W., Theuns, T., Bower, R. G., et al. 2016, ArXiv e-prints, arXiv:1601.07907

Tremmel, M., Karcher, M., Governato, F., et al. 2017, *MNRAS*, 470, 1121

Trujillo-Gomez, S., Klypin, A., Primack, J., & Romanowsky, A. J. 2011, *ApJ*, 742, 16

Tumlinson, J., Thom, C., Werk, J. K., et al. 2011, Science, 334, 948

Vale, A., & Ostriker, J. P. 2004, *MNRAS*, 353, 189

van den Bergh, S. 1961, *ZAp*, 53, 219

—. 1990, *QJRAS*, 31, 153

van den Bosch, R. 2016, ArXiv e-prints, arXiv:1606.01246

van Dokkum, P. G., & Franx, M. 1996, *MNRAS*, 281, 985

van Dokkum, P. G., Whitaker, K. E., Brammer, G., et al. 2010, *ApJ*, 709, 1018

van Dokkum, P. G., Leja, J., Nelson, E. J., et al. 2013, *ApJ*, 771, L35

van Haarlem, M. P., Wise, M. W., Gunst, A. W., et al. 2013, *A&A*, 556, A2

Velander, M., van Uitert, E., Hoekstra, H., et al. 2014, *MNRAS*, 437, 2111

Vikhlinin, A., Kravtsov, A., Forman, W., et al. 2006, *ApJ*, 640, 691

Villar-Martín, M., Humphrey, A., Delgado, R. G., Colina, L., & Arribas, S. 2011, *MNRAS*, 418, 2032

Vogelsberger, M., Genel, S., Springel, V., et al. 2014a, *MNRAS*, 444, 1518

—. 2014b, *Nature*, 509, 177

Voit, G. M., & Donahue, M. 2005, *ApJ*, 634, 955

Volonteri, M., Dubois, Y., Pichon, C., & Devriendt, J. 2016, *MNRAS*, 460, 2979

von Hoerner, S. 1960, *ZAp*, 50

Wandel, A., Peterson, B. M., & Malkan, M. A. 1999, *ApJ*, 526, 579

Wang, E. X., Taylor, P., Federrath, C., & Kobayashi, C. 2019, *MNRAS*, 483, 4640

Wang, H., Mo, H. J., Chen, S., et al. 2018, *ApJ*, 852, 31

Wang, W., & White, S. D. M. 2012, *MNRAS*, 424, 2574

Watson, D. F., Hearin, A. P., Berlind, A. A., et al. 2015, *MNRAS*, 446, 651

Wechsler, R. H., & Tinker, J. L. 2018, *ARA&A*, 56, 435

Weinberger, R., Springel, V., Hernquist, L., et al. 2017, *MNRAS*, 465, 3291

Weinberger, R., Springel, V., Pakmor, R., et al. 2018, *MNRAS*, arXiv:1710.04659

Weinmann, S. M., Pasquali, A., Oppenheimer, B. D., et al. 2012, *MNRAS*, 426, 2797

Werk, J. K., Prochaska, J. X., Tumlinson, J., et al. 2014, *ApJ*, 792, 8

Werner, N., McNamara, B. R., Churazov, E., & Scannapieco, E. 2019, *Space Sci. Rev.*, 215, 5

Wetzel, A. R., Tinker, J. L., & Conroy, C. 2012, *MNRAS*, 424, 232

White, S. D. M. 1976, *MNRAS*, 177, 717

White, S. D. M. 1983, in IAU Symposium, Vol. 100, Internal Kinematics and Dynamics of Galaxies, ed. E. Athanassoula, 337–344

White, S. D. M., & Frenk, C. S. 1991, *ApJ*, 379, 52

White, S. D. M., & Rees, M. J. 1978, *MNRAS*, 183, 341

Williams, C. C., Giavalisco, M., Cassata, P., et al. 2014, *ApJ*, 780, 1

Williams, R. J., Quadri, R. F., Franx, M., van Dokkum, P., & Labbé, I. 2009, *ApJ*, 691, 1879

Woo, J., Dekel, A., Faber, S. M., & Koo, D. C. 2015, *MNRAS*, 448, 237

Woo, J.-H., Bae, H.-J., Son, D., & Karouzos, M. 2016, *ApJ*, 817, 108

Woods, D. F., Geller, M. J., & Barton, E. J. 2006, *AJ*, 132, 197

Wuyts, S., Förster Schreiber, N. M., van der Wel, A., et al. 2011, *ApJ*, 742, 96

Wylezalek, D., Schnorr Müller, A., Zakamska, N. L., et al. 2017, *MNRAS*, 467, 2612

Yang, X., Mo, H. J., & van den Bosch, F. C. 2009, *ApJ*, 695, 900

Yepes, G., Kates, R., Khokhlov, A., & Klypin, A. 1997, *MNRAS*, 284, 235

York, D. G., Adelman, J., Anderson, Jr., J. E., et al. 2000, *AJ*, 120, 1579

Yu, Q., & Tremaine, S. 2002, *MNRAS*, 335, 965

Yuan, W., Zhou, H. Y., Komossa, S., et al. 2008, *ApJ*, 685, 801

Zhang, C., Churazov, E., & Schekochihin, A. A. 2018, *MNRAS*, 478, 4785

Zhuravleva, I., Churazov, E., Schekochihin, A. A., et al. 2014, *Nature*, 515, 85

Zubovas, K., & King, A. 2012, *ApJ*, 745, L34

Zwicky, F. 1933, Helvetica Physica Acta, 6, 110

—. 1948, The Observatory, 68, 121